REDOX PROPERTIES AND CHEMICAL STABILITY OF SOLUBLE CONDUCTING MATERIALS: THE μ-OXO-(TETRA-t-BUTYLPHTHALO CYANINATO)GERMANIUM AND POLY(3,4-DIBUTYLTHIOPHENE)

By

Line Francoise Le Blevenec

A DISSERTATION

Submitted to

Michigan State University

in partial fulfillement of the requirements

for the degree of

DOCTOR OF PHILOSOPHY

Department of Chemistry

1990

ABSTRACT

REDOX PROPERTIES AND CHEMICAL STABILITY OF SOLUBLE CONDUCTING MATERIALS: THE μ-OXO-(TETRA-t-BUTYLPHTHALO CYANINATO)GERMANIUM AND POLY(3,4-DIBUTYLTHIOPHENE)

By

Line Francoise Le Blevenec

The redox chemistry and chemical stability of soluble conducting materials such as the already existing μ-oxo-(tetra-t-butylphthalocyaninato) germanium and the newly synthesized poly(3,4-dibutylthiophene) were characterized using a variety of conventional electrochemical and spectroscopic techniques.

Controlled potential coulometry (CPC), cyclic (CV), rotating disk (RDE), rotating ring-disk (RRDE), and differential pulse (DPV) voltammetry data show that the germanium polymer can be reduced to any fractional oxidation state ranging from 0 to 1- and remains chemically stable. The redox response occurring over a 1500 mV range is indicative of a broad continuous process. The observed voltammograms are relatively featureless compared to conventional electroactive compounds but have the characteristics of a Nernstian process. At a degree of reduction greater than 100% (i.e. one electron added per phthalocyanine site), the polymer quantitatively breaks into electroactive monomer units. The decomposition was easily monitored using modified RRDE

technique. Digital simulations of voltammetric responses prove that the decomposition of the germanium polymer follows an ECEE-type mechanism. A rate of 20 sec^{-1} was obtained for the decomposition.

The other soluble conducting polymer under investigation, the poly(3,4-dibutylthiophene), was synthesized by oxidative polymerization of the corresponding monomer using CV technique. CPC, CV, and DPV data show that this polythiophene derivative can be oxidized to any degree in the 0-0.34 range both in solution and as thin film coated on an electrode surface. In any form or state, it is chemically stable. Again a broad, continuous redox response is observed in solution over a 1000 mV range, resulting in the formation of a smooth doping profile. The conductivity profile as function of band-filling parallels the doping profile. A maximum value of 1 S cm^{-1} was obtained for a 34% oxidized film using standard four-probe method. Optical absorption measurements performed on solutions of poly(3,4-dibutylthiophene) oxidized to various degrees indicate that the nature of the charge carriers is mainly bipolaron in character. No polaron state was detected, even at low oxidizing levels.

To my father

ACKNOWLEDGMENTS

First, I would like to express my gratitude to my advisors Dr. Eugene Legoff and Dr. John G. Gaudiello who helped to guide me during the course of this study. Their principles of independence might have resulted in a little bit of a frustration sometimes but in the long run it is the best way of obtaining scientific integrity. I also would like to thank Dr. Alexander I. Popov for his encouragement, help, and friendship towards a foreigner.

I also wish to thank the members of my group in particular Dave and Evaldo for their useful comments and discussions as well as Mike (Benz) for having provided me some thiophene derivative compounds for my study.

I also would like to thank Anne and Marina for their unforgettable friendships.

A special thank goes to my parents for their guidance, unconditional support, and love throughout my all life.

Finally, I would like to thank my husband for his friendship, understanding, and love all along these years.

TABLE OF CONTENTS

LIST OF TABLES

LIST OF SCHEMES

page #

LIST OF FIGURES

1. INTRODUCTION

Organic materials that become electrically conducting upon oxidation or reduction (doping) have been a field of great interest over the past two decades[1]. This interest really started with the discovery in the 1970s that oxidized polyacetylene exhibits a conductivity value in the metallic regime[2]. It was reinforced with the possible use of these materials in numerous technological applications. Such applications include batteries, sensors, electrochromic displays, solar energy devices, electromagnetic shieldings, antistatic charge devices, and microelectronic components for computer industry[3]. These conducting materials are generally classified into two groups: charge-transfer salts[1,4] and conducting polymers[1,5]. Charge-transfer salts are comprised of discrete molecular components which have been condensed into a segregated, stacked framework. A typical example is TTF-TCNQ (tetrathiafulvalene tetracyanoquinodimethane) complex. Conducting polymers are covalently linked assemblies based on covalently bonded conjugated hydrocarbons or heterocycles arranged in a linear network. Among the most studied conducting polymers are polyacetylene, polypyrrole, and polythiophene.

Based on the electrical conductivity, any common material can be viewed as belonging to one of the three groups: metal, semiconductor, or insulator (Figure 1)[4a]. The conductivity of typical metals such as copper is 10^6 S cm^{-1} at room temperature. The conductivity is generally expressed in S cm^{-1} which is equivalent to ohm^{-1} cm^{-1}. In terms of band theory, metal is associated with a partially filled valence band and an empty conduction band. Conduction arises from the availability of a large number of electrons in the valence band which can

serve as charge carriers and move easily to the close empty band. In metals, the conductivity increases as temperature decreases; this phenomenon is explained by the fact that, at low temperatures, few electrons are scattered by lattice vibrations (called phonons) and, thus, are not perturbed in their conductive movement.

The conductivity of semiconductors ranges between 10^{-5} S cm^{-1} and 10^{2} S cm^{-1}. The valence band is completely filled, the conduction band is completely empty, and the band gap between them is relatively small. In this case, there are fewer electrons around to serve as charge carriers and the number of available carriers is strongly dependent on temperature. At higher temperatures, more electrons can be promoted into the conduction band and hence conductivity increases with increasing temperature.

Insulators such as Teflon and polystyrene have conductivity less than 10^{-6} S cm^{-1}. The only difference between insulators and semiconductors is that the band gap between the valence and the conduction band is larger in the insulator group preventing the movement of the electrons from the valence band to the conduction band.

Neutral or undoped polymers are usually classified as insulators due to their very low conductivity. However, when they become partially oxidized or reduced, their conductivity extends over a wide range from insulators all the way to metals. Usually, the conductivity increases by several orders of magnitude upon doping. Recently, a group of researchers at BASF, West Germany, reported the synthesis of oxidized polyacetylene which exhibits a conductivity of $2.5\ 10^{5}$ S cm^{-1}, comparable to that of copper.

Figure 1. Room temperature electrical conductivity (S cm^{-1}) of common materials. The vertical axis represents the conductivity scale.

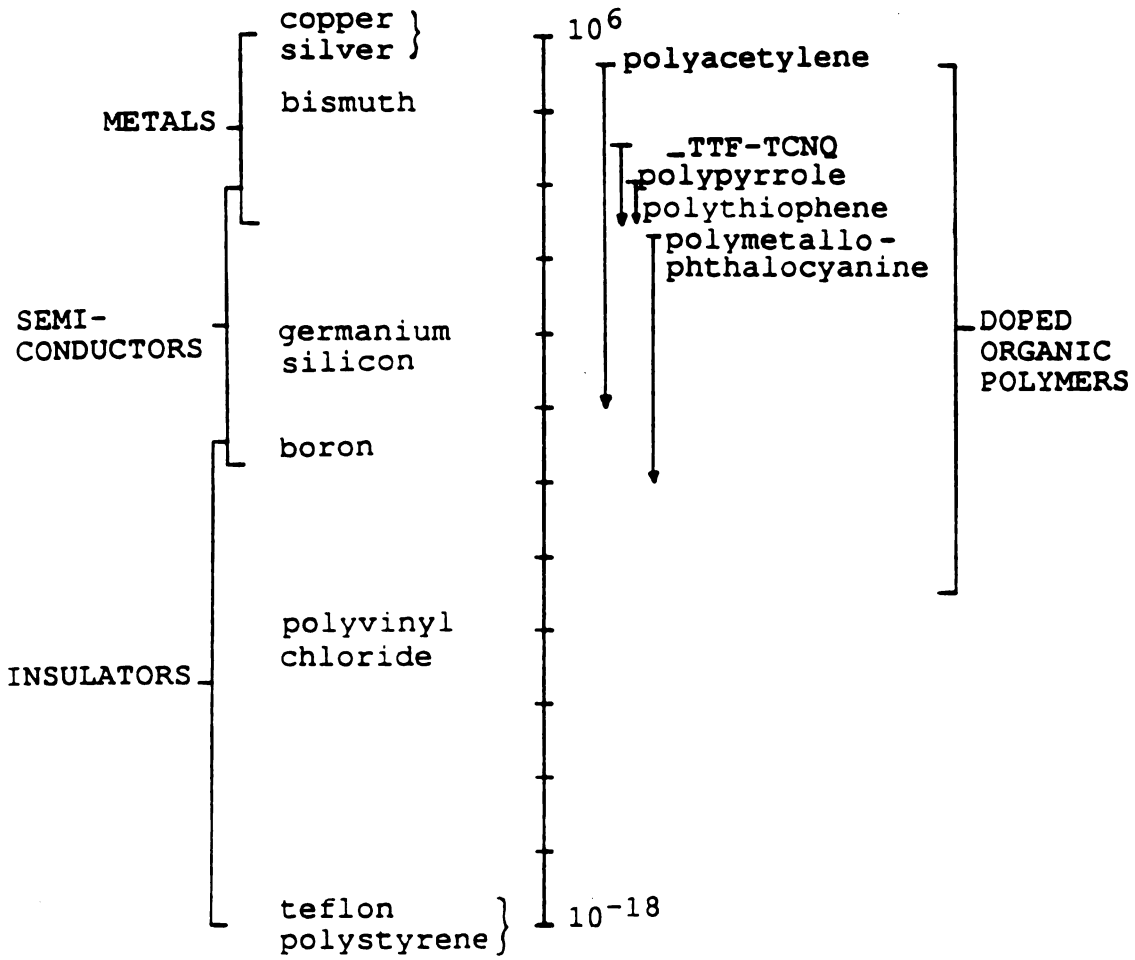
copper
silver
bismuth
METALS
SEMI-
CONDUCTORS
germanium
silicon
boron
polyvinyl
chloride
INSULATORS
teflon
polystyrene
10^{6}
10^{-18}
polyacetylene
TTF-TCNQ
polypyrrole
polythiophene
polymetallo-
phthalocyanine
DOPED
ORGANIC
POLYMERS

FIGURE 1

Charge-transfer salts have typical conductivity ranging from 10^1 S cm^{-1} to 10^5 S cm^{-1} which is the conductivity in the semiconducting and metallic regime. Both charge-transfer salts and conducting polymers undergo a metal insulator transition. Conductivity reaches a maximum at some temperature usually less than room temperature. Above this point, the temperature dependence is metallic, that is, the conductivity increases as temperature decreases. Below it, the temperature dependence is that of a semiconductor, that is, the conductivity increases with increasing temperature.

The charge-transfer salts and the conducting polymers have several features in common. They both exhibit anisotropic or quasi-one-dimensional properties[6]. Electrical conductivity is much greater in one direction than in the others. In charge-transfer salts, the conductivity is greatest along the stacking axis of the molecule whereas in conducting polymers the conductivity is greatest along the chain direction of the polymer. Another common feature of these materials is that they are ionic in the conducting state. In the case of charge-transfer salts, charge is transferred between the donor and acceptor components of the complex and in the case of conducting polymers, charge is transferred between the polymer chain and a dopant (chemical oxidizing or reducing agent, or electrode). Along with fractional or partial oxidation state, the polymers must possess a band-type electronic structure formed by closely arranged adjacent molecules which interact with each other in order to be electrically conducting.

The band formation is described by the tight binding theory analysis analogous to the Huckel theory for an infinite linear polyene[1e,4a,7]. When two singly occupied π atomic orbitals are allowed to interact in a single molecule, two

molecular orbitals are formed: a π-bonding orbital, completely filled, of lower energy and a π^*-antibonding orbital, completely empty, of higher energy (Figure 2). If the π-bonding and π^*-antibonding orbitals of two molecules, stacked directly one above the other, are allowed to interact, two sets of two molecular orbitals are formed and separated in energy by 2t, where t is the transfer integral (analogous to β in the Huckel theory). If N molecules are allowed to interact, there will be Nπ states in the highest occupied molecular orbital (HOMO) band and Nπ^* states in the lowest unoccupied molecular orbital (LUMO) band. A band is formed when the energy difference between the states remains small. The HOMO band, usually called the valence band, is entirely filled and the LUMO band, or conduction band, is entirely empty. Into each of these bands 2N electrons can be placed. A material with a full valence band and an empty conduction band will be an insulator, or possibly a semiconductor depending on the size of the gap separating the two bands. The bandwidth of a band, represented by 4t, describes the extent of interaction between adjacent molecules in the stack. The second property that the charge-transfer salts and the conducting polymers must have is a fractional oxidation state[6,8]. In other words, they must have depleted bands. This is analogous to the requirement that the highest occupied molecular orbital of a metal be partially filled. The partial band-filling can be achieved in several ways. In charge-transfer salts, charge (electrons) is transferred between the donor and the acceptor molecules. Conducting polymers can be doped either chemically or electrochemically. Theoretical and experimental studies dealing with electronic structure have provided information on band formation and energy[7a,9]. However, few studies have dealt with the formation of a fractional oxidation state. The success of a partial oxidation state formation depends on a complex and largely uncontrollable

Figure 2. Process leading to the formation of an energetic band.

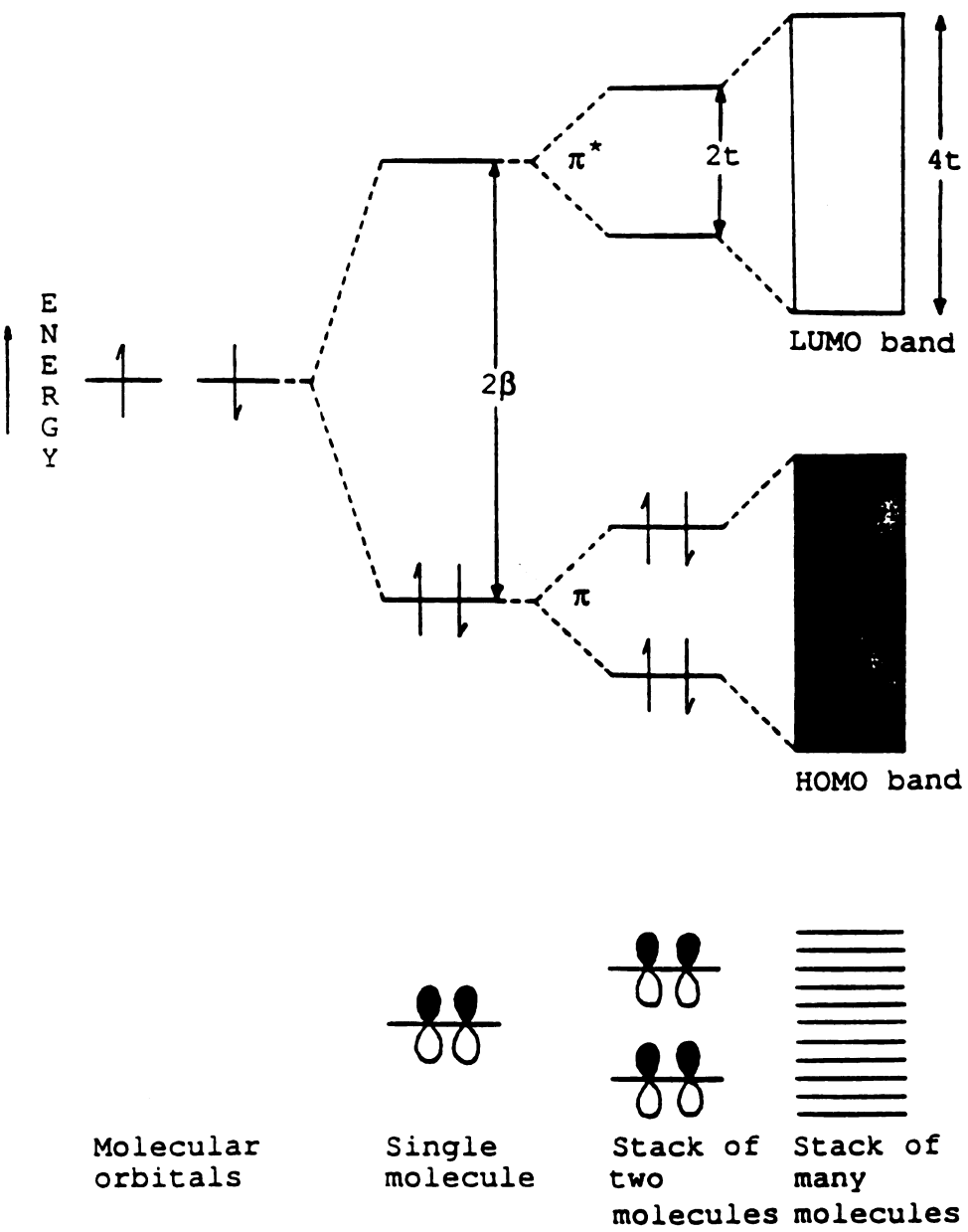
ENERGY
π*
2t
4t
LUMO band
2β
π
HOMO band
Molecular orbitals
Single molecule
Stack of two molecules
Stack of many molecules

FIGURE 2

variety of factors such as Van der Waals forces, repulsion interactions, ionization potential-electron affinity, and the kinetics of crystallization.

Charge-transfer salts are usually obtained by induced charge-transfer between donor and acceptor molecules[4]. The donors and acceptors are usually large planar molecules that can stack on top of each other in a segregated arrangement. The band formation is due to the overlap of π orbitals of the molecules in the stack. The segregated arrangement allows the transferred charge to move easily along the separate donor and acceptor stacks. Charge-transfer salts must crystallize in a segregated array without any defect to be highly conducting. Structure defects or distortions can lead to a metal insulator phase transition, resulting in insulating properties at low temperatures. The band-filling is determined by the extent of charge-transfer from donor to acceptor molecules. The degree of band-filling depends on the properties of both donors and acceptors. The fractional oxidation state can be achieved using chemical or electrochemical dopants.

Conducting polymers differ from charge-transfer salts in several ways[10,11]. They are chemically more stable and easy to process. In general, conducting polymers refer to conjugated unsaturated hydrocarbon and heterocycle systems. They are usually obtained by a chemical coupling reaction or by electrochemically initiated polymerization of the corresponding monomer. Most of them possess a band-type electronic structure due to the overlap of π molecular orbitals on adjacent molecules. However, they do not have a fractional oxidation state in the neutral form. Insulators or semiconductors in the neutral form, they become electrically conducting upon doping. Doping can be performed by chemical or electrochemical techniques. In both cases, charge is

transferred between the polymeric cation (anion) and a counterion which is the oxidizing (reducing) form of the reducing (oxidizing) agent[6]. π-Conjugated polymers are widely used because they can be easily oxidized (reduced) and form a stable cation (anion) rather than undergoing other chemistry. Besides, in their systems, the π-electrons can be easily removed or added without breaking the σ bonds which are primarily responsible for holding the polymer together. Mild oxidizing and reducing agents such as iodine and lithium are utilized to ensure that only a charge-transfer reaction occurs and no other chemical reaction[12]. The dopant usually perturbs the polymer extensively. Because of its large size which does allow it to fit into the polymer lattice and because of the extensive charge-transfer with the polymer chains, the dopant can cause geometrical changes in the chain. The doping level is small and limited to the concentration and strength of the chemical dopant. The chemically doped polymers are generally insoluble which prevents their direct physicochemical characterization and their electronic properties from being studied[13]. Doping also can be performed electrochemically. With electrochemical techniques, synthesis and doping occur simultaneously. The monomer undergoes polymerization by applying an oxidation potential at the electrode surface. The resulting polymer is in its oxidized (cationic) form with counterion derived from the electrolyte solution. Compared with chemical doping, electrochemical doping is cleaner with fewer interferring chemical reactions. It is also more precise, enabling the conductivity of systems to be switched between the conducting and insulating state by simply applying the appropriate voltage. Finally, electrochemical doping is more informative. It has been used to study primarily thin films of material coated on an electrode surface[14]. Thermodynamic and kinetic data can be obtained from these studies. However, the redox behavior of modified electrodes can be influenced by counterion diffusion within the film, as well as material discontinuities and

nonuniformities[15]. Also, it is possible to separate Faradaic and capacitive components of current. Electrochemical doping performed on slurries of insoluble materials are time consuming, do not provide any information on the time dependent-doping process, and yield only macroscopic data regarding the charge-transfer. The observed response is complicated by variations in particle size and structural changes accompanying the doping process[16]. To eliminate such complications regarding the redox process of these materials, it is desirable to have soluble materials whose redox properties can be studied in solution by conventional electrochemical and spectroscopic techniques.

The synthesis of such soluble, conducting materials is currently an area of great interest. It is motivated by the processibility properties required in technological applications. Recently, soluble polymeric metallophthalo cyanines[17p-r] and soluble polythiophene derivatives[17a-o] have been prepared. In both cases, solubility is insured by the addition of organic functionalities to the polymer backbone.

Hanack and coworkers at the University of Tubingen, West Germany, have recently synthesized soluble tetraalkylsubstituted cofacially joined, Group IV B phthalocyaninato macromolecules $[R_4PcMO]_n$ where M = Si, Ge, Sn Pc = phthalocyaninato, and R = tetra-t-butyl or tetramethylsilyl (Figure 3)[17p,q]. The presence of the bulky substituents give rise to high solubilities in common organic solvents such as methylene chloride, benzene, acetone, and tetrahydrofuran. Metallophthalocyanine polymers are very interesting materials because they combine the characteristics of both charge-transfer salts and conducting polymers. Similar to charge-transfer salts, the large planar

Figure 3. Schematic structure of peripherally-alkylated μ-oxopolymers $[R_4PcMo]_n$ M = Si, Ge, Sn; Pc = phthalocyaninato; R = t-Bu_4, Tms.

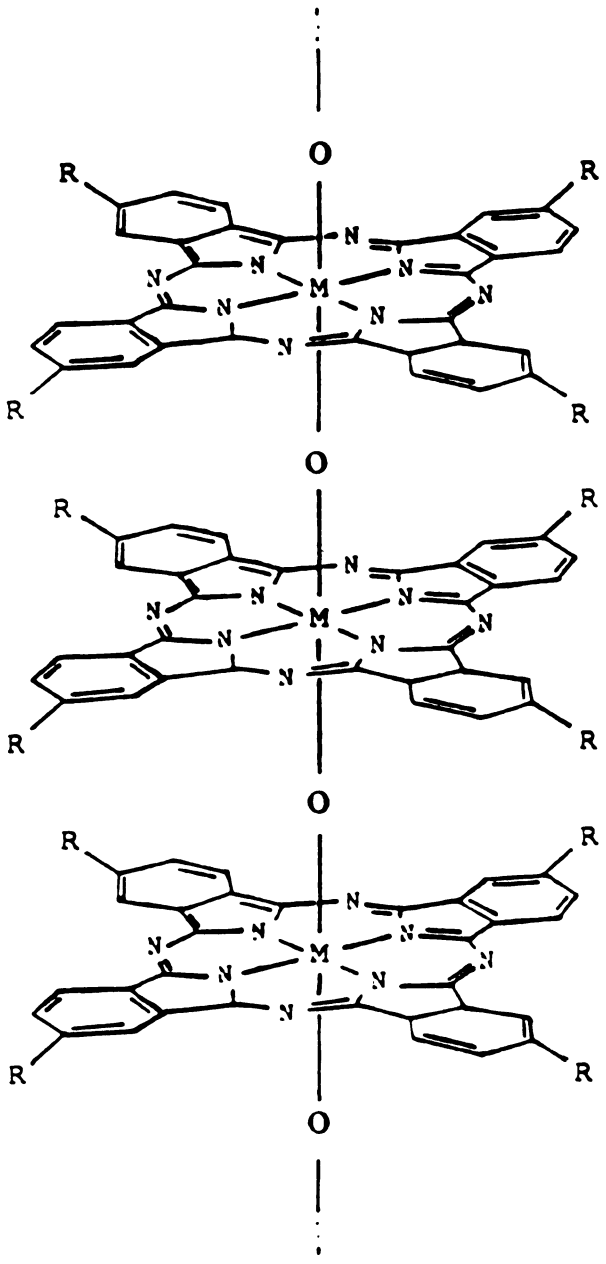

FIGURE 3

phthalocyanine molecules are stacked on top of each other with small Pc-Pc interspacing distance allowing interactions between molecular orbitals which leads to the formation of a band-type electronic structure. Similar to conducting polymers, the phthalocyanine rings are held together in a rigid cofacial orientation. These macrocyclic metal complexes have been bridged to a large variety of ligands[17q,18]. Pyrazine, tetrazine, cyanide, and isothiocyanate groups have been used to bridge Fe, Ru, Co, and Rh macrocyclic transition metal complexes. Other ligands such as oxygen, sulfur, alkylnyl have been used to bridge Si, Ge, and Sn phthalocyanines.

The particular substituted peripherally alkylated μ-oxopolymers (oxygen-metal bridging) are essentially identical to the unsubstituted analogs whose electric, optical, and magnetic properties have been extensively studied in the solid state by Marks and his group[16,19]. Unsubstituted and substituted μ-oxopolymers with M = Si, Ge have been chemically oxidized using halogens such as iodine and bromine[17p-r,19a-e]. For example, the partial oxidation of unsubstituted Si and Ge phthalocyanines was accomplished by stirring a mixture of polymer and the halogen in benzene for two days. In contrast for M = Sn, doping resulted in destruction of the tin-oxygen bond. This different behavior towards doping could be explained because tin is significantly larger than Si and Ge, and did not fit without distortion into the hole of the phthalocyanine molecule, thus weakening the tin-oxygen bond. Unsubstituted and substituted Si phthalocyanine polymers also can be oxidized with nitrosonium salts NO^+X^- where X^- = BF_4^-, PF_6^-, and SbF_6^-[19e]. X-ray diffraction studies suggested that the chemical doping was largely inhomogeneous and that there was a change in crystal structure from orthorhombic to tetragonal upon doping. The nature of the iodine-doped μ-oxopolymer's electronic structure was probed by electron spin

resonance (ESR). The symmetry of the lineshapes and the g-values were consistent with π-radical cations, i.e., the unpaired spin density was located in the molecular orbitals which is predominantly ligand in character. The broad electronic absorption spectra were also indicative of an oxidation process occurring at the macrocycle level and the formation of a radical cation. Four probe Van der Pawl electrical conductivity measurements on the unsubstituted $[MPcO]_n$ powders showed them to be insulators. However, iodine or bromine doping resulted in substantial increase in conductivity, an increase of several orders of magnitude leading to the semiconducting or even metallic state. For example, the conductivity of $[PcSiO]_n$ doped to its maximum with iodine increased from 5.5 10^{-6} S cm^{-1} to 1.4 S cm^{-1}. Conductivity of $[PcGeO]_n$ and $[PcSnO]_n$ doped with iodine also increased, respectively, from 2.2 10^{-10} S cm^{-1} to 1.1 S cm^{-1} and from 1.2 10^{-9} S cm^{-1} to 6.5 10^{-7} S cm^{-1}. Substituted μ-oxopolymers follow the same trend of increasing conductivity upon chemical doping (Figure 5). The conductivity of substituted Si, Ge, and Sn phthalocyanine polymers doped with iodine increased for M = Si from 8.0 S cm^{-1} to 2.0 S cm^{-1}, for M = Ge from 6.0 10^{-11} S cm^{-1} to 1.0 10^{-3} S cm^{-1} and from 4.0 10^{-12} S cm^{-1} to 1.0 10^{-6} S cm^{-1} for M = Sn. Compared with unsubstituted polymers, the electrical conductivity values of substituted polymer analogs were very similar before doping and slightly lower upon doping. The general trend in conductivity as function of metal is $\sigma_{Si} \geq \sigma_{Ge} > \sigma_{Sn}$. Since the doping process was largely ligand dominated and relatively insensitive to the identity of the metal, the metal dependence of the conductivity observed in these polymers was logically ascribed to structural differences such as how the interplanar separation was influenced by metal ionic radius. The conductivity of these materials increased continuously as the iodine content increased indicating that, at higher partial oxidation of the polymer, the number of charge carriers increased. However,

Table 1. Pressed power room temperature electrical conductivity data for doped and undoped μ-oxopolymers.

Table 2. Pressed powder room temperature electrical conductivity data for doped and undoped alkyl substituted μ-oxopolymers.

TABLE 1

COMPOUND	σ_{RT} (S cm^{-1})
$[PcSiO]_n$	$5.5\ 10^{-6}$
$[(PcSiO)I_{0.31}]_n$	1.4
$[PcGeO]_n$	$2.2\ 10^{-10}$
$[(PcGeO)I_{1.08}]_n$	$1.1\ 10^{-1}$
$[PcSnO]_n$	$1.2\ 10^{-9}$
$[(PcSnO)I_{0.35}]_n$	$6.5\ 10^{-7}$

TABLE 2

COMPOUND	σ_{RT} (S cm^{-1})
$[t\text{-}Bu_4PcSiO]_n$	$8.0\ 10^{-8}$
$[(t\text{-}Bu_4PcSiO)I_{0.4}]_n$	$2.0\ 10^{-3}$
$[t\text{-}Bu_4PcGeO]_n$	$6.0\ 10^{-11}$
$[(t\text{-}Bu_4PcGeO)I_{0.4}]_n$	$1.0\ 10^{-3}$
$[t\text{-}Bu_4PcSnO]_n$	$4.0\ 10^{-12}$
$[(t\text{-}Bu_4PcSnO)I_{0.9}]_n$	$1.0\ 10^{-6}$

independent of the metal and the chemical oxidizing power, and the amount of oxidizing agent added in large excess, the band-filling of these polymers did not exceed 35%. In other words, it was possible to vary the amount of band-filling up to 35% by adjusting the amount of single dopant, but it was not possible to chemically oxidize a polymer from 0 to 100% and tune its properties as function of band-filling.

To get better control over band-filling and to eliminate the problems associated with solid state discussed earlier, unsubstituted Si μ-oxophthalocyaninatopolymers have been doped electrochemically[16]. Electrochemical doping was performed as slurries. The finely ground polymer was oxidized in a three-compartment electrochemical cell (Figure 4) while suspended in a stirred electrochemical solution. Contrary to chemical doping, electrochemical doping is homogeneous. Initially, the crystal structure of the Si polymer was orthorhombic. After partial oxidation at 50%, the crystal structure changed from orthorhombic to tetragonal. Once it was in tetragonal structure, the polymer can be further oxidized, reversibly reduced, and cycled a number of times between oxidized and reduced states with no decomposition and no structural change. It was noted that the oxidation of the tetragonal phase required less energy than the initial orthorhombic phase. However, attempt of electrochemical doping of $[GePcO]_n$ oxidatively was unsuccessful. As for chemical doping, electrochemical doping was also accompanied by an increase in conductivity. The magnitude in conductivity observed at a given doping level was roughly comparable for the electrochemically and chemically doped Si polymers. The principal difference was that the level of partial oxidation accessible for the electrochemically doped polymer was larger. The highest degree of partial oxidation level, 67%, was obtained with p-toluenesulfonate

counterion (TOS^-)[16d]. The highest degree of partial oxidation achieved in this electrochemically doped polymer appeared to be a beneficial consequence of the unlimited oxidizing power of the potentiostat. Electronic, optical, and magnetic studies of $[SiPcO(BF_4)_y]_n$ material revealed an evolution in properties from insulator/semiconductor to metal-like with increasing doping level. With electrochemical doping, it was thus proven that band-filling could be varied over a broad range of compositions and although all complications associated with solid state remained, the results on these systems were very encouraging because it was the first time that such band-filling tunability has been achieved to a major extent for a conventional conductor. Along with substituted peripherally-alkylated μ-oxopolymers previously described in detail, other soluble phthalocyanine polymers such as substituted peripherally-alkylated phthalocyaninato transition metal complexes $[t\text{-}Bu_4PcRudib]_n$ and $[t\text{-}Bu_4PcRuMe_4dib]_n$, where dib = p diisocyanobenzene and Me_4dib = tetramethyldiisocyanobenzene, have been synthesized recently and characterized by spectroscopic techniques; but up to now, no doping has yet been performed on either these substituted or unsubstituted analog materials.

Recently, several groups have synthesized soluble polythiophenes[17a-o]. Like polyphthalocyanines, significant interactions exist between the redox sites of the polymers. However, these are primarily through-bond overlap of the π systems instead of through-space orbital overlap as in polyphthalocyanines. In all these soluble thiophene polymers, solubility was achieved through addition of long linear alkyl chains ranging from butyl to dodecyl, at the 3-position. Blocking the 3-position prevents crosslinking polymerization and leads to a more structurally regular polymer by increasing the amount of α α' coupling in the polymer. Poly(3-alkylthiophenes) can be synthesized chemically or

electrochemically. Chemical synthesis is accomplished by oxidative polymerization of appropriately 3-substituted thiophene using transition metal halides such as $FeCl_3$ or $MoCl_5$[20a]. Another synthetic route involves the preparation of 3-substituted 2,5-diiodothiophene followed by Ni-catalyzed Grignard coupling[17d,20b-d]. More often, these polymers are synthesized through oxidative electrochemical polymerization of their corresponding monomers by applying a constant current or potential at the anode, leading to the formation of a film at the electrode surface[13a,17f,20,21]. Polymerization occurs via a cation-radical coupling mechanism that involves dehydrogenation on the 2- and 5-positions of thiophene oligomers. The resulting film is obtained in its oxidized form and the overall charge balance is achieved by incorporating an anion derived from the electrolyte. Because the anions are directly incorporated into the film, the choice of the anion is important in determining the quality of the film. Best results were found with the inert, small anions PF_6^- and BF_4^-[13a]. The oxidized polymer can then be reversibly undoped (and subsequently re-doped) by electrochemical or chemical reduction (re-oxidation). In contrast, the chemically synthesized polymers are produced in their undoped insulating state and can be doped chemically or electrochemically to their conducting states. These polymers are chemically stable in both their neutral and doped states. The maximum doping level encountered in these polymers was 36% which could be achieved either by chemical or electrochemical methods[22]. Upon doping, soluble poly(3-hexylthiophene) exhibits relatively high conductivity compared with the insoluble parent polythiophene[23]. The electrical conductivity can be as high as 95 S cm^{-1} for PF_6^- doped poly(3-hexylthiophene). To obtain such value, the polymer must be synthesized in a three-compartment oxygen- and moisture-free electrochemical cell. Lower conductivity was obtained for chemically synthesized polymers. The presence of β-substituent has little influence on the conductivity

but allows the polymer to remain soluble in its doped form. Since these polythiophene derivatives are soluble in common organic solvents in both their neutral and conducting forms, the electronic, optical, and magnetic properties of these polymers in the undoped and doped states as well as during the doping process have been studied. In particular, ESR measurements and optical data on the oxidized polymer in solution helped in elucidating the nature of the charge storage configurations. The results indicated that doping induced charged kinks or excitations (polarons and bipolarons). This situation is mainly due to a large coupling between the lattice deformation and the electronic excitations. The charges transferred from the dopant molecule produce a local deformation of the polymer chain which varies the bond lengths. As a result, this distortion affects the electronic structure of the polymer and leads to the formation of bipolarons (dications) which are spinless species. In the formation of bipolarons, the valence band remains full while the conduction band remains empty and low energy states are created in the gap between the two bands. Another important feature of poly(3-alkylthiophenes) is that the electronic, optical, and magnetic properties of these conducting systems can be studied both in solution and in the solid state on chemically modified electrodes. Thus, the influence of the medium on such properties resulting from doping can be determined.

It has been already shown that, by adding an alkyl substituent at the 3-position, the amount of α α' coupling in the polymer increases thereby producing a better film quality without significant decrease in conductivity. Another way to enhance the selectivity of α α' coupling consists in using chemically synthesized oligomers (dimer, trimer, etc) instead of a thiophene monomer as starting materials for the electropolymerization. Studies on electrochemically synthesized polymers derived from thiophene, bithiophene and

terthiophene revealed that it is easier to oxidize the material as the chain length of the starting oligomers increased, but unexpectedly the ease of oxidation was accompanied by a large decrease in conductivity[24]. These results were interpreted by the decreasing reactivity of the radical cations derived from these three substrates. No result has yet been reported on the study of the soluble alkyl substituted analogs, probably due to difficulties encountered in synthesizing these oligomers.

Following a different approach to force polymerization of thiophene in the 2- and 5-position, Elsenbauer and coworkers have used dialkyl thiophenes to chemically synthesize soluble polydialkylthiophenes. The alkyl groups in position 3 and 4 serve two important functions. They increase greatly the solubility of these materials and they eliminate all future sites for polymerization ($\alpha\,\beta$ linkages). These materials should be able to undergo oxidation and reduction with minimum interference from side reactions. All studies conducted on doped polydialkylthiophenes should then be the result of the doping process only.

In this study we will take advantage of the good solubility and chemical stability of the polyalkylated phthalocyanines and thiophenes to study the redox and physicochemical properties of conducting materials by a variety of conventional analytical techniques. These methods will allow us to provide information concerning the properties of these materials as function of band-filling. These conducting materials will be characterized to a sophisticated level, never attempted before. This will greatly help in searching for a rational preparation of materials with specific, predictable, and tunable properties.

2. EXPERIMENTAL

2.1 Glassware

2.1.1 Vacuum lines

High vacuum line

Prior to begining of the electrochemical experiments, the solvents were transferred into the electrochemical cells via high vacuum line (10^{-5} torr). The cells were then backfilled with argon (Matheson 99.95%) to maintain an air- and moisture-free atmosphere throughout the experiments. The argon was previously passed through a drying column (magnesium on silica) to remove residual oxygen and moisture. Between experiments, the solvents were stored under high vacuum to preserve their high quality.

Schlenk line

Reactions requiring an air- and moisture-free environment were performed using standard Schlenk line techniques[25].

2.1.2 Electrochemical cells

Different glass, electrochemical cells that are connected directly to a high vacuum line were constructed and used in this study. Controlled potential coulometry (Bulk electrolysis) was carried out in a three-compartment cell[26]. The counter electrode, a platinum gauze, was isolated from the working electrode compartment by two fine porosity glass frits. The reference electrode, a silver wire, was separated from the working electrode by a fine porosity glass frit. The working electrode was an 8 cm^2 platinum gauze electrode. A 0.018 cm^2 platinum disk working electrode (Bioanalytical Systems Inc) also was placed in the working

electrode compartment to allow voltammetric measurements to be performed under the same conditions as controlled potential coulometry experiments. The platinum disk electrode was polished with 0.05 μm Al_2O_3 before use (Buekler). Diffusional voltammetry experiments (cyclic and differential pulse voltammetry) were carried out in a single compartment cell. A 0.018 cm^2 platinum disk working electrode, a platinum wire counter electrode, and a silver wire reference electrode were used in these cells. Arrays of 5 individually platinum wire working electrodes (0.5 cm long) separated from each other by 80 μm Teflon insulating spacer were used in the conductivity measuring experiment.

An indium-tin oxide (ITO) conducting glass working electrode, a platinum flag reference electrode, and a platinum wire counter electrode were used in the optical characterization experiment.

Hydrodynamic voltammetry experiments (rotating disk and rotating ring-disk voltammetry) were performed in a three-compartment cell carefully designed to reduce the formation of a vortex[27]. A silver wire reference electrode and a platinum gauze counter electrode were placed in sidearm compartments separated from the working electrode compartment by fine porosity glass frits. The working electrodes (Pine instruments) were either the platinum rotating disk electrode with a radius of 0.256 cm or the rotating ring-disk electrode comprising a platinum disk and a platinum ring with disk radius=0.228 cm, inner ring radius=0.246 cm, and outer ring radius=0.269 cm, and a collection efficiency (N) of 23%. This collection efficiency value was determined from the rotating ring-disk voltammogram of the standard $Fe(CN)_6^{3-}/Fe(CN)_6^{4-}$ redox couple and confirmed by digital simulation.

2.2 Methods of purification

2.2.1 Solvents

Acetic anhydride and pyridine were dried over calcium hydride and purified by distillation under nitrogen. Methanol was dried with magnesium turnings and purified by distillation under nitrogen. Quinoline was dried over barium oxide for two days and then decanted. The decanted quinoline was vacuum distilled and stored over activated 3A molecular sieves.

Nitromethane (EM Science) was dried over phosphorous pentoxide and purified by distillation under nitrogen. The resulting solution was then degassed on the vacuum line by employing several freeze-pump-thaw cycles and then vacuum-transferred to a greaseless round bottom flask containing activated 3A molecular sieves and stored on the high vacuum line. Tetrahydrofuran (HPLC grade, Burdick and Jackson) was dried by addition of a sodium-potassium alloy and the same procedure as for nitromethane was used to degas, transfer and store the solvent on the high vacuum line. Acetonitrile (HPLC grade, Burdick and Jackson) was dried over calcium hydride and then decanted. The decanted solution was degassed, vacuum-transferred, and stored on the high vacuum line as above.

2.2.2 Supporting electrolyte

Tetrabutylammonium fluoroborate (electrometric grade, Southwestern Analytical Chemicals) was recrystallized from ethyl acetate/diethyl ether (5:1 volume ratio, 80 ^{0}C) and vacuum dried for three days.

2.3 Instrumentation

2.3.1 Chromatographic

The molecular weight of the soluble poly(3,4-dibutylthiophene) was determined by gel permeation chromatography (GPC) using a Waters 840 instrument equipped with an exclusion column in which polystyrene-linked material was loaded. The elution time was measured using 10^{-2} M polymer solution in tetrahydrofuran by monitoring the refractive index difference between the polymer solution and the solvent itself. The molecular weight was determined from the retention time calibration using polystyrene standards whose molecular weights ranged from 2 10^3 to 2 10^6.

2.3.2 Spectroscopic

Proton nuclear magnetic resonance spectra were obtained on either a Bruker WM-250 (250 MHz), Varian Gemini (300 MHz) or Varian VXR-300 (300 MHz) spectrometers. Chemical shifts are reported in parts per million (δ) using the proton resonance of the residual solvent as the internal reference (acetone, δ=2.04; chloroform, δ=7.24; tetrahydrofuran, δ=1.73). Fourier-transformed infrared spectra were obtained on a Nicolet 740 spectrophotometer either as Nujol mulls using KBr plates or KBr pressed pellets. Routine UV-Vis absorption spectra were recorded on a Cary 17 using 1-cm matched quartz cells. For in-situ spectroelectrochemical experiments, in the solid state, a 1*1*4 cm^3 quartz cuvette was fitted with an indium-tin oxide transparent electrode which functioned as the working electrode, a platinum flag as counter electrode, and a silver wire as reference electrode. The cell was fitted with a tight Teflon top and maintained under positive argon pressure during the measurements. In solution, a simple 1-cm matched quartz cell was used. All UV-Vis NIR spectra were performed on a Cary 2300.

2.3.3 Electrochemical

A Princeton Applied Research (PAR) 273 potentiostat/galvanostat interfaced to a Zenith 248AT computer with a National Instrument PC 2A IEEE-48 card for instrument control and data acquisition was used for the bulk electrolysis and CV and DPV voltammetry experiments. Experimental results were recorded on a Hewlett-Packard 7475A plotter. A bioanalytical system 100A potentiostat, interfaced to a Zenith 158XT computer and a Hewlett-Packard Colorpro plotter was alternatively used for bulk electrolysis and voltammetry experiments. A Pine Instrument AFRDE4 bipotentiostat coupled with a AFMSR rotator was used for rotating disk voltammetry experiments. A platinum/Teflon rotating disk and ring-disk electrode, also constructed by Pine Instrument company, served as working electrode. The voltammograms were recorded on a Soltec X-Y or X-Y_1-Y_2 recorders. The film thicknesses were determined with a Dektak 11A profiler, and dc electrical conductivities (σ) were measured in-situ by a standard four probe technique at room temperature[28]. Values of σ (S cm^{-1}) were calculated from the relation :

$$\sigma = P / L R e \qquad (1)$$

where :

L = length of a platinum stripping (0.5 cm)

P = gap between two consecutive strippings (80 μm)

e = film thickness in μm

R = measured resistance in ohm

All electrochemical experiments were performed either in oxygen- and moisture-free specially designed cells (as described in section 2.1.2) or inside a vacuum drybox.

2.4 Electrochemical techniques

2.4.1 Controlled potential coulometry

Bulk electrolysis or controlled potential coulometry (CPC) was used to convert compounds from one oxidation state to another[29]. In a CPC experiment, the potential of the working electrode is applied to a value such that complete electrolysis of the desired species occurs. The total charge passed during the electrolysis is obtained by integrating current over time. Rapid stirring of the solution was maintained during the course of the experiment to ensure efficient mass transfer of material to the working electrode. A large surface area of the working electrode as well as minimum solvent were employed to minimize electrolysis time. Supporting electrolyte (0.1-0.2 M $TBABF_4$) was placed in each compartment of the CPC cell (Figure 4) and 0.04-1 mM of the polymer or 0.9-25 mM of the corresponding repeat unit (monomer or oligomer) were added only to the working electrode compartment. The cell was then connected to a high vacuum line and evacuated (10^{-5} torr). After cooling it with an isopropanol/dry ice bath, a known amount of solvent was vacuum transferred. The cell was then backfilled with argon and allowed to warm up to room temperature prior to use. Usually CPC is employed to determine the number of moles of material electrolyzed (N) or the number of electrons involved in the electrolysis process (n) from the amount of charge passed through an electrochemical cell during electrolysis (Q). Faraday's law correlates these three variables by the equation :

$$Q = n F N \qquad (2)$$

where :

Q = charge transferred

n = number of electrons

N = moles of material electrolyzed

Figure 4. Electrochemical cell used in controlled potential coulometry experiment.

A = platinum gauze counter electrode

B = fine porosity glass frits

C = silver wire reference electrode

D = platinum gauze working electrode for CPC

E = platinum disk working electrode for CV and DPV

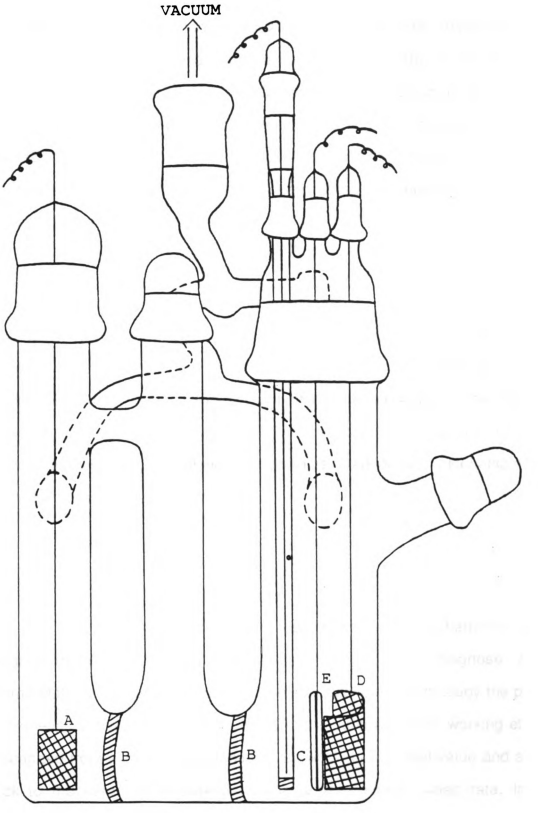

FIGURE 4

The amount of charge used in equation (2) is the total measured charge subtracted from the charge due to the background current. In this study, CPC was used mainly to determine the degree of partial reduction as function of potential. This technique was employed since it is an absolute method for determining oxidation states which depend only on the potential of the working electrode. The degree of partial charge transfer (partial oxidation or reduction) is calculated from the equation:

$$\%\ \text{of charge transfer} = \frac{\text{charge}}{\text{mass of polymer/gfw of repeat unit})*F} * 100 \qquad (3)$$

A value of 100% represents the addition of one electron per repeat unit. In this expression no particular degree of polymerization is assumed, but a simple relationship exists between the amount of charge passed and the number of moles of redox sites or repeat units. From the shape of the plots of normalized currents versus time, information on chemical stability and mechanism during electrolysis was also obtained.

2.4.2 Voltammetry

Cyclic voltammetry

One of the most widely used techniques in electrochemistry is cyclic voltammetry (CV)[29]. It is attractive for its ability to diagnose reaction intermediates which undergo further chemical reactions and to study the products and kinetics of these reactions. During CV, the potential of the working electrode is scanned from some initial potential to a switching potential value and scanned back to the same initial potential value at a constant sweep rate. In a CV experiment, for the study of the μ-oxo-(tetra-t-butylphthalocyaninato)germanium, 0.1-0.2 M of the supporting electrolyte, $TBABF_4$, was placed in a single

compartment cell. The polymer (10-40 μM) was placed in a "dumpster", a rotatable reservoir allowing the addition of the polymer in the cell at any time. With the dumpster, voltammograms of only the blank solution could be obtained and were subtracted from the sample voltammograms to obtain background-corrected voltammograms. The background voltammograms also served in determining the potential range from the solvent which also was used for the entire experiment. From the current-potential curve response, several variables of the system studied can be determined. The number of electrons (n) transferred during the electrode reaction, for a reversible couple, can be calculated from the separation between anodic and cathodic peak potentials[29]. In the study of the polydialkylthiophenes, cyclic voltammetry was used to prepare the polymers. Polymerizaton was carried out at 5 ^{0}C in electrolytic solutions of nitromethane or acetonitrile containing 0.2 M supporting electrolyte ($TBABF_4$). Under these conditions, a polymer film was deposited on the ITO electrode surface. Good film quality and high conductivity were achieved by sweeping the electrode potential for a few minutes at a sweep rate of 50 mV sec^{-1} which corresponds to few micron thickness. As synthesized, the polymer was in its oxidized form. Neutral (or undoped) polymer was easily obtained by reversing the direction of the potential sweep. In order to increase the amount of polymer formed, polymerization was performed in the CPC cell using big platinum gauze electrode (10 cm^2) as working and counter electrodes. The chemical stability of reactants and products and kinetic information regarding the electron transfer reaction also can be evaluated by changing the sweep rate. In the study of the μ-oxo-(tetra-t-butylphthalocyaninato)germanium, CV was mainly used to probe the products of the redox-induced reaction and to study their chemical stability. CV also was used to determine n.

Rotating disk and rotating ring-disk voltammetry

Rotating disk (RDE) and rotating ring-disk (RRDE) voltammetry are among the most useful techniques for studying electrode reactions. In RDE, the working electrode is connected to a motor which spins the electrode and causes the solution to move to the electrode surface by convective mass transport. Unlike most voltammetric techniques, which are performed in motionless solution and where diffusion is the main mode of mass transport, RDE is performed in a continuously stirred solution and convection is favoured over diffusion due to a greater mass transport rate[29]. Because the electrode moves constantly with respect to the solution and at a rapid rotation rate, fresh solution is continuously brought up to the electrode surface. The rotation of the working electrode and a slow potential scan rate (10 mV sec^{-1}) allow these experiments to be performed under steady state. In a steady state experiment, the current at a given potential is independent of both the scan direction and time. Consequently, preelectrolysis, which is a problem encountered when using the DPV technique, does not occur. In this study, the current-potential response of the RDE voltammograms for the μ-Oxo-(tetra-t-butylphthalocyaninato)germanium was used to obtain the doping profile of the germanium polymer as function of potential. In RDE voltammetry, the current at any potential is given by the equation :

$$i = 0.62\, n\, F\, A\, D_O^{2/3}\, \nu^{-1/6}\, \omega^{1/2}\, [C_O^{*} - C_O(y=0)] \qquad (4)$$

where :

ω = angular velocity of the disk electrode
($\omega = 2\,\pi\, f$ with f = rotation rate)

ν = kinematic viscosity of the solvent
($\nu = h / d$ with d = density)

C_O^{*} = bulk concentration of the electroactive material

$C_o(y=0)$ = concentration of the electroactive material at the electrode surface

D_o = diffusion coefficient of the material

A = area of the disk electrode (0.163 cm^2)

n = number of electrons

Using equation (4), the current at the potential corresponding to 100% reduction, i_l, is given by the equation :

$$i_l = 0.62\ F\ A\ D_o^{2/3}\ \nu^{-1/6}\ \omega^{1/2}\ C_o^{*} \qquad (5)$$

Dividing equation (4) by equation (5) yields to equation (6) which gives rise to the expression of the fractional concentration of the material undergoing electron transfer reaction.

$$\frac{i}{i_l} = \frac{C_o^{*} - C_o(y=0)}{C_o^{*}} \qquad (6)$$

Derived from equation (6), the percent reduction at any potential is given by the equation:

$$\%\ \text{reduction} = i / i_l * 100 \qquad (7)$$

The RDE technique also was used to determine if there was any kinetic limitation accompanying the doping process. For a totally reversible system, the plot of i vs $\omega^{1/2}$ is predicted to be linear with zero intercept as expected from the current-potential curve at the rotating disk electrode. Any deviation from linearity suggests some kinetic step involved in the electron transfer reaction. Such behavior is observed for an electrode reaction with slow kinetics, i.e., the rate of electron transfer is sufficiently slow to act as a limiting factor.

Diffusion coefficients of both the neutral germanium polymer and the monomer were also estimated from the current-potential curves of the RDE

voltammogram and used in the calculation of the degree of polymerization of the μ-oxo-(tetra-t-butylphthalocyaninato)germanium material. The relationship between molecular weight (M) and diffusion coefficient (D) for macromolecules is well known[30]. For coil-shaped polymers, the diffusion coefficient is predicted to vary with (molecular weight)$^{-0.55}$. For thin rod-shaped polymers, D is proportional to $M^{-0.88}$. Spectroscopic data of the short length oligomeric silicon and germanium phthalocyanines (n = 1 to 4) prove conclusively that these compounds have a stacked ring rod-like structure in solution. Assuming that the μ-oxo-(tetra-t-butylphthalocyaninato)germanium polymer maintains this rod-like structure in solution, the molecular weight of the polymer can be calculated from the equation :

$$D_p = (M_m / M_p)^{0.81} D_m \qquad (8)$$

where :

D_p, D_m = diffusion of the polymer and corresponding monomer

M_p, Mm = molecular weight of the polymer and monomer

(987.90 g mole^{-1})

Knowing the molecular weight of the polymer and of its repeat unit, the degree of polymerization for the soluble germanium polymer can be easily determined. The RDE technique is very attractive because it provides the information contained in a series of CPC experiments in a few minutes instead of few hours and without degradation of the solution.

The rotating ring-disk voltammetry is an extension of the previously discussed rotating disk voltammetry in that the disk electrode is encircled by a ring which functions as a second working electrode. The well defined steady state response of the technique along with the ability to control and examine two independent electrode processes permitted the quantitative characterization of

multi-site redox systems. The stability of electroactive compounds as a function of potential was easily followed via RRDE by performing continuous shielding-collection experiments. In RRDE, the disk electrode is poised at a potential where polymer reduction (oxidation) occurs and the potential of the ring is scanned from the disk potential towards more positive (negative) values. Initially, the flux of neutral polymer to the ring is decreased by its consumption at the disk and the current observed at the ring (i_{Rc}, a cathodic current) (i_{Ra}, an anodic current) is reduced compared to that observed when no reaction is occurring at the disk (i_{Rc}^0)(i_{Ra}^0). This experimental configuration is the conventional shielding in RRDE experiment. At ring potentials sufficiently positive (negative) relative to the disk value, where only oxidation (reduction) of the reduced (oxidized) polymer back to neutral polymer can occur, the ring current arises from the collection of disk generated material (an anodic current) (a cathodic current). Under these conditions, the conventional RRDE experiment can be conducted. At ring potentials between these two limiting cases,the new current observed at the ring is composed of both anodic and cathodic components (both shielding and collection type processes).

For a chemically stable system, the relation between i_R, i_R^0, and i_d is given by the equation :

$$N = \frac{i_R^0 - i_R}{i_d} \qquad (9)$$

i_R, i_R^0 = ring current observed at a specific potential with and without a reaction occurring at the ring

i_d = current observed at the disk

N = collection efficiency of the electrode assembly, a constant dependent only on electrode geometry.

Hence, $(i_R^0 - i_R) / i_d$ will be a constant value regardless of the values of i_d and i_R. Deviations from N imply chemical complications and can be used to monitor the potential required to initiate the process. In both RDE and RRDE experiments, 0.2 M supporting electrolyte $TBABF_4$ was placed in a three-compartment cell (Figure 5). A known amount of the germanium polymer (30-35 μM) was added to the working electrode compartment. The solvent used in these experiments was vacuum transferred in a tube following regular procedure described previously and then pipetted into the cell which is already inside an inert atmosphere drybox. The rotator along with the bipotentiostat were also placed in drybox allowing the experiment to be performed in an inert atmosphere.

Differential pulse voltammetry

Differential pulse voltammetry (DPV) is used to characterize the redox response of the polymer. In this technique, a small amplitude potential step pulse is applied to the system and the derivative current is recorded as a function of potential. The derivative current is comprised of the current measured at the end of the pulse subtracted from that just before the pulse. The cell and procedure used in the DPV experiment were identical to the one used for CV studies. Due to its high sensitivity and very good resolution, DPV has often been used in the detection of very low concentrations of analyte. In this study, DPV was used for the fine characterization of the redox response of the germanium polymer and corresponding monomer because unlike the featureless response observed for most voltammetric techniques, DPV is extremely sensitive to small changes in the doping profile[29]. DPV, taken after each CPC cycle, i.e., oxidation (reduction) followed by reduction back (re-oxidation) provided information on the stability of the material on the CPC timescale. The shape and magnitude of the DPV voltammogram along with other parameters specific to the technique and system

Figure 5. Electrochemical cell used in rotating disk and rotating ring-disk voltammetry

A = platinum gauze counter electrode

B = fine porosity glass frits

C = platinum disk and ring-disk working electrodes

D = silver wire reference electrode

E = brush contact

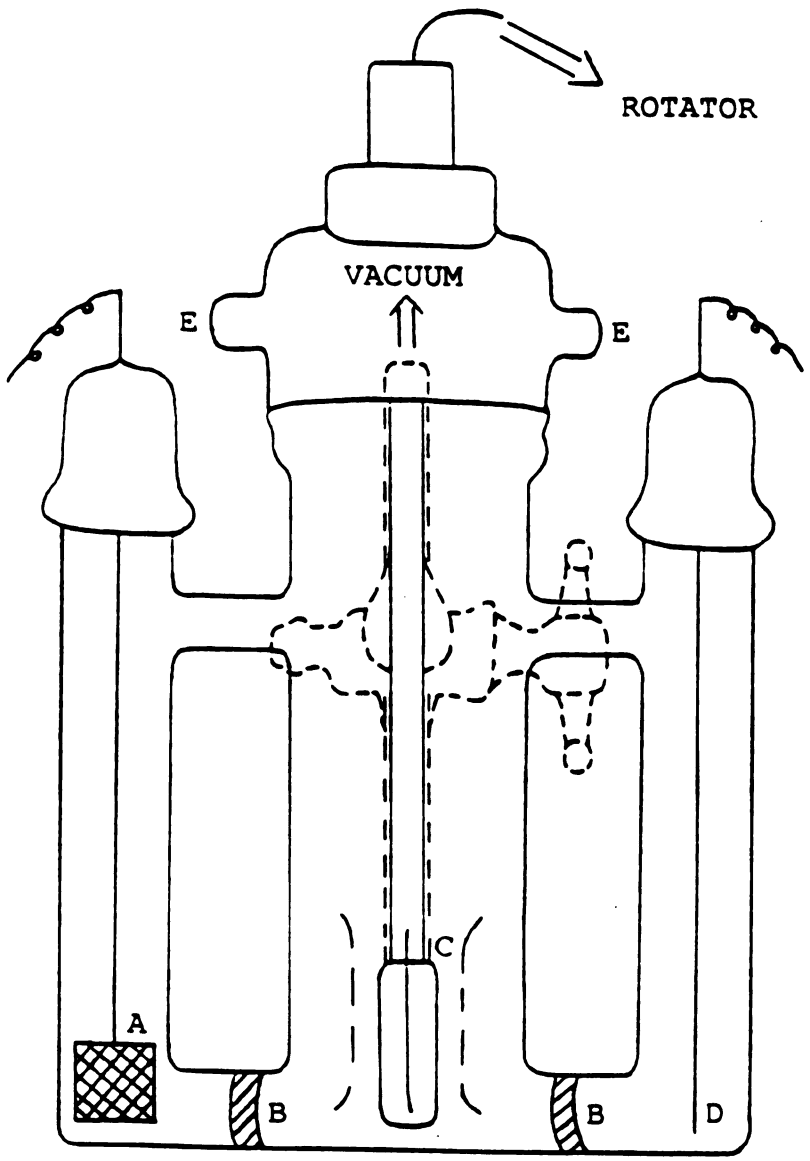

FIGURE 5

employed were finally used in modelling the current-potential DPV response of the germanium providing information on the electronic interactions between redox sites within the polymer.

2.4.3 Digital simulation

Digital simulations are numerical methods which have been found very useful in elucidating the mechanism of complicated redox events. In this study, digital simulation of differential pulse and rotating ring-disk voltammetry experiments were undertaken to model the current-potential response of the germanium polymer. Information on the electronic interactions of the redox sites within the polymer was provided by estimating the standard potential of each site. The current-potential response also provided information on the chain length of the polymer. The ultimate goal of digital simulation will be to predict the electrochemical behavior of any conducting polymer from corresponding oligomers (few unit long). In this model, the polymer can be viewed as an array of multiple redox sites undergoing sequential reversible Nernstian electron transfer in equilibrium with one another (see Appendix 1). Both the DPV and RRDE simulation programs are based on the method of finite differences[32]. The solution near the electrode surface is divided into a number of volumes of equal size. A flow chart illustrating the general procedure employed to simulate DPV voltammogram is shown in Figure 6. The first step consists in setting up the bulk concentration of the solution prior the experiment. Initially, the solution is assumed to contain only one species in a particular reduction state in the first volume element. The initial bulk concentration value was chosen to be identical to the experimental one of Figure 22a. Next, steps were taken to set up the apparent bulk concentration of the solution for the base potential value and the surface boundary conditions at the working electrode for the pulse potential

Figure 6. Flow chart explaining the DPV simulation program.

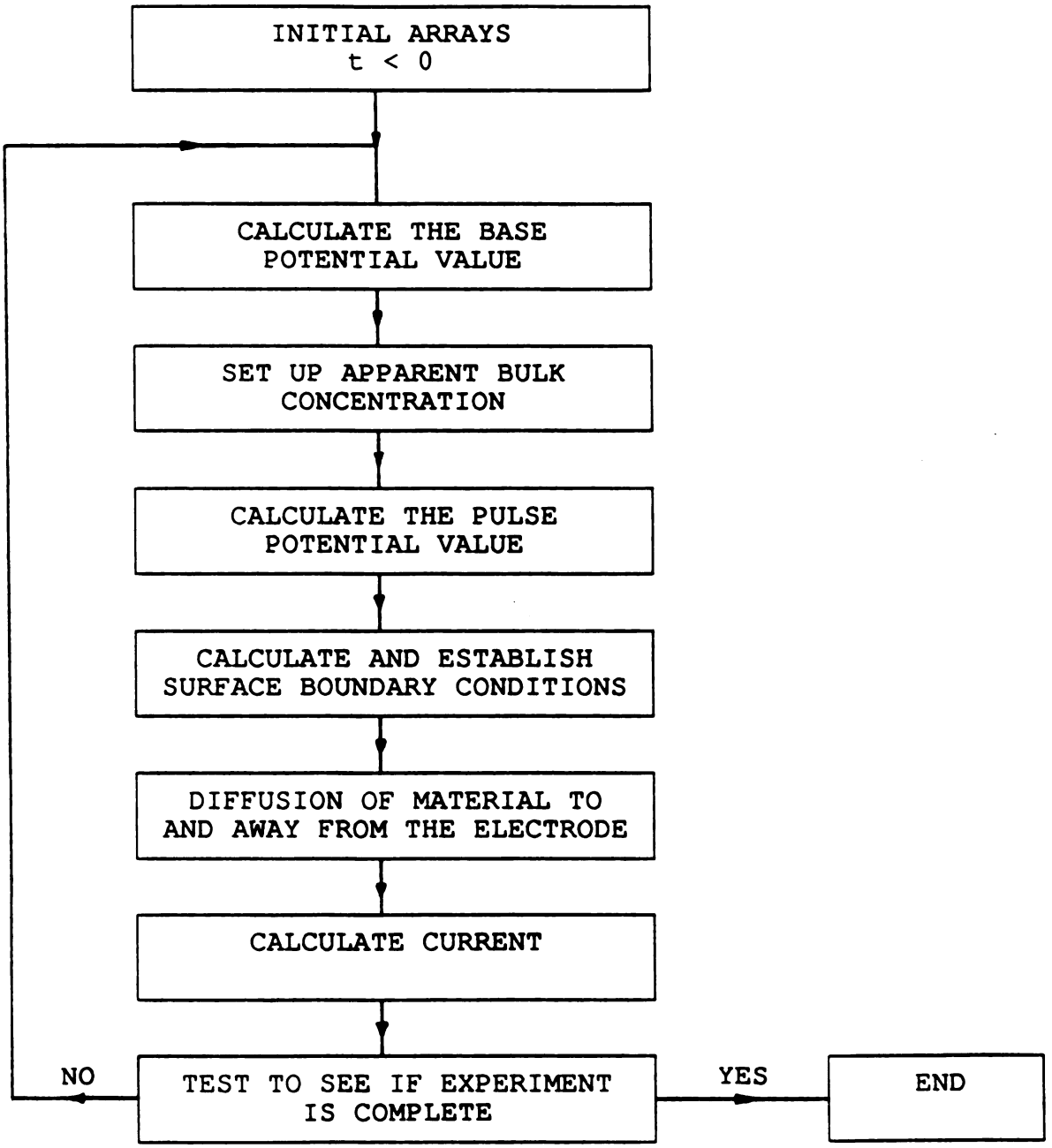
INITIAL ARRAYS
t < 0
CALCULATE THE BASE POTENTIAL VALUE
SET UP APPARENT BULK CONCENTRATION
CALCULATE THE PULSE POTENTIAL VALUE
CALCULATE AND ESTABLISH SURFACE BOUNDARY CONDITIONS
DIFFUSION OF MATERIAL TO AND AWAY FROM THE ELECTRODE
CALCULATE CURRENT
TEST TO SEE IF EXPERIMENT IS COMPLETE
NO
YES
END

FIGURE 6

value. The ratio of the concentration of reactant over product at the electrode surface follows the Nernst equation and is a function of electrode potential. The number of sites in the polymer that are oxidized or reduced depends only on the standard potential of each site and the potential of the working electrode. From the diffusion of material to and from the electrode and the number of sites of polymer being oxidized or reduced, a dimensionless current was calculated that ends the first interaction. The current is derived from the first Fick's law of diffusion which relates flux of species to concentration gradient. The program then goes back to the calculation of the next base potential value and calculates the new dimensionless current. Continuing the process generates the current profile of the solution as function of time. The program ends when the final potential of the experiment is reached. The procedure employed for the RDE simulation is similar to the DPV one with the difference that the mass transport equation is comprised of a diffusion and a convection term. These procedures are essentially identical to those used to model single charge transfer systems. The main difference between the models employed for these multicomponent systems and the others described in the literature were the equations used to describe the initial and surface boundary conditions and the dimensionless current. Several parameters of the system studied are necessary for the simulation. The standard potential of each redox site, the dimensionless diffusion coefficient of each site, the diffusion coefficient, and the concentration of the bulk solution along with parameters specific to the technique were entered as input in the computer program. In addition, the doping profile of the germanium polymer was easily determined from the simulated DPV voltammogram. From the RRDE simulation, the chemical stability of this polymer was monitored as function of potential. Both the mechanism and rate accompanying homogeneous reactions were accurately determined.

2.5 Spectroelectrochemical technique

Experimental and theoretical studies have shown that the doping of organic conducting polymers induces a charge transfer along the polymer chain which results in significant local modifications of the chain geometry[1a,4a,6,33]. These modifications markedly affect the electronic structure of the polymer by inducing localized electronic states in the gap between the valence and the conduction band. They also lead to the possible formation of solitons, polarons, and/or bipolarons, depending on the nature and/or the doping level of the polymer[10a,17k,33]. For conducting polymers possessing a degenerate ground state such as polyacetylene, solitons are the most important charge defects encountered in these polymers[33c]. For those without a degenerate ground state such as polypyrrole or polythiophene, polarons and/or bipolarons are the dominant charge-storage configurations[33i-k]. From this point and below, the discussion focusses on the polaron and bipolaron concepts. A common way to study the existence of polarons and bipolaron is by investigating the optical absorption spectra of conducting polymers. Shown in Figure 7 are the energy level diagrams and the transitions expected for these two types of excitations. In the case of a hole polaron, four transitions can be expected from the valence band and the gap level to the conduction band and the upper level. For a chain with a bipolaron, transitions from the lower gap state are not possible because it is empty and only two transitions remain between the valence band and the two levels in the gap for a total of three transitions with the interband transition. All these features appear in the absorption spectra of conducting polymers because the number and energy of the transitions are different according to whether polaron or bipolaron are present or not. Optical studies on polythiophene and poly(3-alkylthiophene) have provided evidence that, upon doping, the majority of

Figure 7. Energy level diagrams showing allowed optical transitions for polythiophene chain with hole polaron and bipolaron.

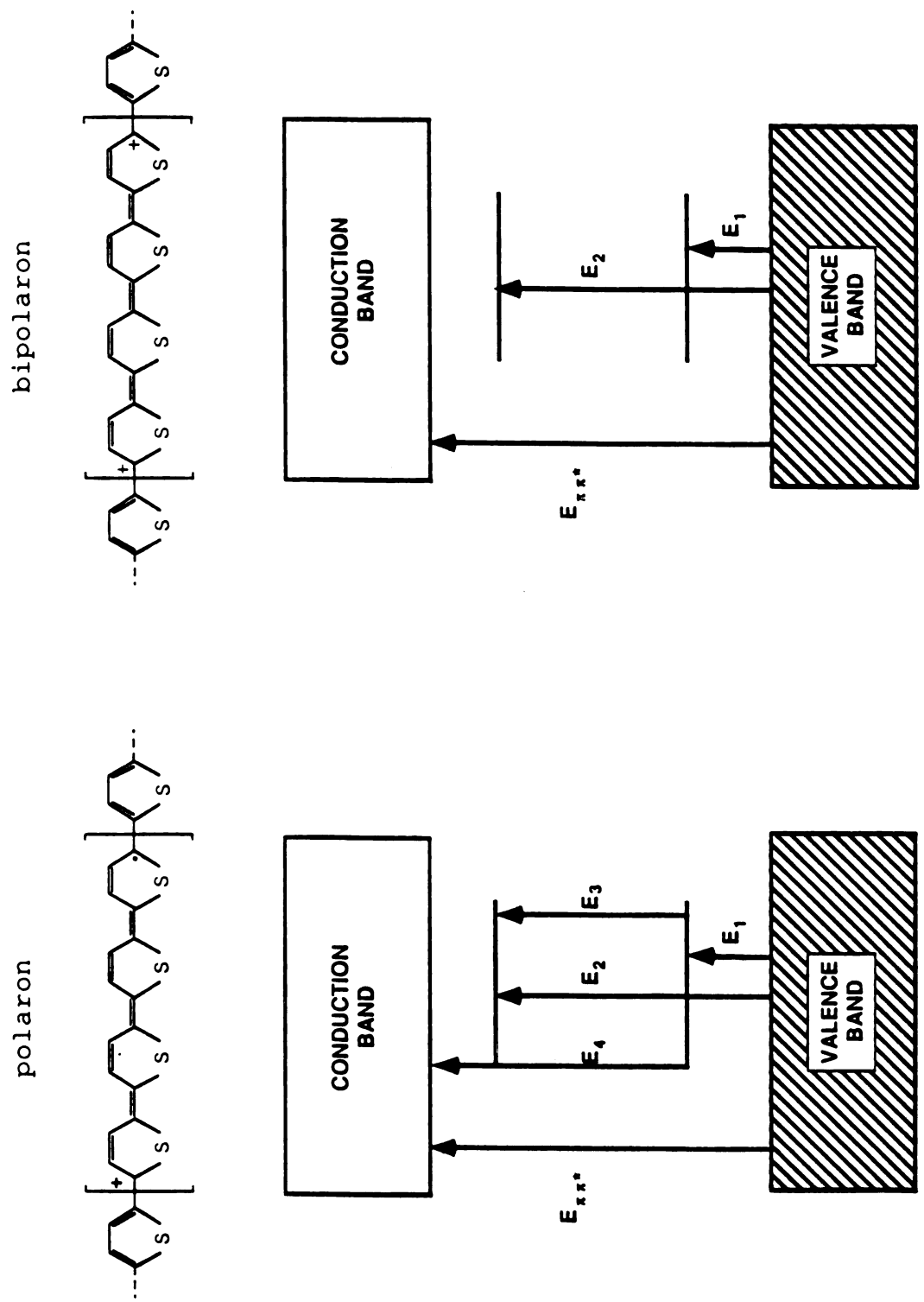
polaron
bipolaron
CONDUCTION BAND
VALENCE BAND
E_1
E_2
E_3
E_4
$E_{\pi\pi^*}$

FIGURE 7

the charge is stored in bipolaron[33i,j]. In this study, absorption spectroscopy was primary used to characterize the electronic processes that occur in the poly(3,4-dibutylthiophene) in the undoped and doped states as well as during doping. Since this polythiophene derivative is soluble in common organic solvents, in both neutral and conducting forms, optical properties, as well as charge-storage configurations of the polymer, were studied in solution and correlated with the ones obtained in the solid state. The changes observed in the optical spectra of such conducting polymers will serve in elucidating the mechanism of doping and the nature of the charge-storage species in the polythiophene chain. Finally, comparison of the optical absorption spectra of several similar polydialkylthiophenes using oligomers of different chain lengths for the polymerization process will provide information on the amount of conjugation within the polymer chain in our search for optimized polymerization conditions in order to synthesize the best conducting polymers.

3. PROBING THE CHEMICAL STABILITY AS FUNCTION OF BAND-FILLING FOR THE SOLUBLE CONDUCTING μ-OXO-(TETRA-t-BUTYLPHTHALOCYANINATO)GERMANIUM

3.1 Introduction

In our group, we are interested in the study of materials containing multiple interacting redox centers[31,34]. Understanding the factors that govern the redox properties of these interacting centers is of importance in many chemical systems. The inability to accurately control and determine such factors as composition, structure, chain length, and degree of band-filling have slowed down the construction of new conducting materials for specific applications. Our efforts in understanding how the properties of conducting materials can be tuned for specific applications have let us to study the soluble, already existing μ-oxo-(tetra-t-butylphthalocyaninato)germanium system. As previously described, this material consists of covalently linked assemblies arranged in a stacked architecture. It has been shown that upon chemical doping this material becomes electrically conducting suggesting a large amount of electronic interaction between the adjacent redox centers[30a,35]. In this study, the redox electrochemistry and chemical stability of the soluble μ-oxo-(tetra-t-butylphthalocyaninato)germanium will be investigated using a large variety of conventional electrochemical and analytical techniques. Particular efforts will focus on band-filling and the changes in the electrochemical properties of such a system that occur upon variations in band-filling. Electrochemical techniques will be employed to quickly and easily determine the degree of band-filling-potential profile. It will be the first time that a wide range in degree of band-filling is obtained for the doping of any conducting system. With the addition of

spectrochemical techniques, the chemical stability at any degree of band-filling will be determined. Modified conventional electrochemical techniques also will be developed to probe quickly and easily the chemical stability of such a system as function of band-filling without degrading the solution used for the measurements. These in-depth and novel probings of the redox stability of conducting materials is unobtainable in solid state using either chemical or electrochemical techniques. Electrochemical studies also will be performed to obtain information on the energetics (potentials required to reach the different oxidation states) and kinetics (rate of the electron transfer) for the doping of this material. The ease and rate at which a material donates or accepts charge is an important consideration in designing systems for specific applications. Computer simulations of electrochemical techniques will be developed to observe the amount of interaction between the redox sites. For example, the standard potential of each individual redox center will be estimated by these methods. Digital simulations of electrochemical techniques also will be used to prove the type of mechanism occurring at the electrode surface during the doping process. The rate constants of the homogeneous reactions resulting from the doping process of the system also will be estimated by simulation. Redox information obtained from this study will allow one to predict the electrochemical properties of conducting materials as band-filling is systematically altered. This will aid greatly in the characterization and design of new conducting systems.

3.2 Synthesis

Both the dihydroxy(tetra-t-butylphthalocyaninato)germanium monomer and the μ-oxo-(tetra-t-butylphthalocyaninato)germanium polymer were prepared according to the method described by Hanack et al[17q,r,36]. The synthetic route leading to the formation of the polymer is outlined in scheme I. Ten steps

Scheme I. Synthesis of the μ-oxo-(tetra-t-butylphthalocyaninato)germanium polymer.

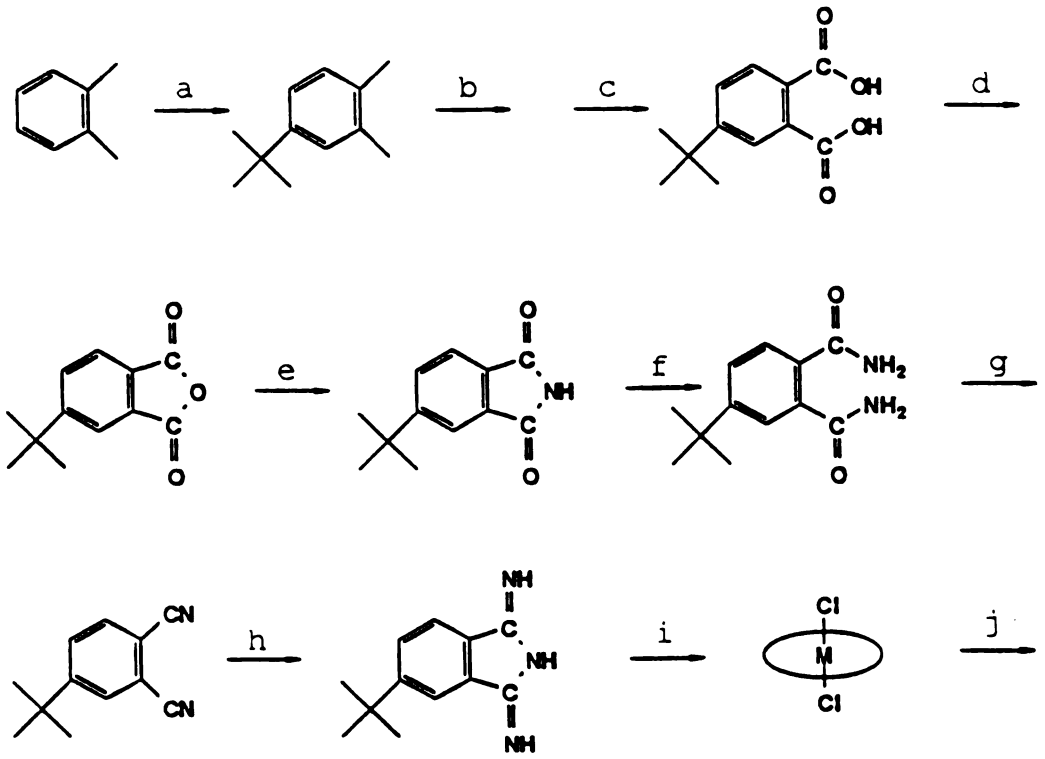

$t\text{-}Bu_4PcGe$ =

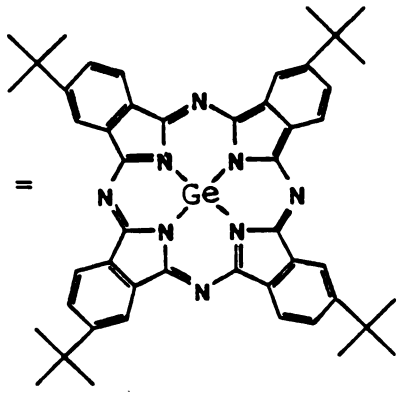

$[t\text{-}Bu_4PcGeO]_n$

a. $(CH_3)_3CCl$ / $FeCl_3$

b. $KMnO_4$ / aq. pyridine

c. EtOH

d. acetic anhydride / heat

e. urea

f. aq. NH_3

g. $POCl_3$ / pyridine

h. anhydrous NH_3 / MeOH

i. $GeCl_4$

j. NaOH / H_2O / pyridine

k. 340 ^oC / 10 hours / 10^{-5} torr

SCHEME I

were needed from the commercially available o-xylene. The key step involves the formation of the Pc macrocycle from the reaction of the substituted 1,3-diiminoisoindoline with germanium tetrachloride. The product of this reaction, the trans-dichloro(tetra-t-butylphthalocyaninato)germanium, t-$Bu_4PcGeCl_2$, was then easily hydrolyzed in basic medium to form the dihydroxy(tetra-t-butylphthalocyaninato)germanium t-$Bu_4PcGe(OH)_2$. Dehydration of t-$Bu_4PcGe(OH)_2$ carried out in a tube furnace at 340 ^oC for 10 hours under high vacuum yielded the μ-oxo-(tetra-t-butylphthalocyaninato)germanium polymer. The polymer backbone consists of Pc macrocycle subunits held together via linear Ge-O-Ge covalent bonds in a stacking arrangement. The polymer was characterized by IR, UV-Vis and elemental analysis. Data for the μ-oxo-(tetra-t-butylphthalocyaninato)germanium polymer and the corresponding monomeric dihydroxide are summarized in Table 3. The IR spectrum of the polymer in comparison with the spectrum of the monomeric dihydroxide shows the absence of the symmetric Ge-O stretch at 646 cm^{-1} and the appearance of the antisymmetric O-Ge-O stretch at 893 cm^{-1} (Figure 8). The absorption bands observed in the 600 nm and 300 nm region for both the polymer and the monomeric dihydroxide can be assigned to the Q-like and B-like π - π^* electronic transitions, respectively (Figure 9). Good agreement was observed between the experimental and calculated elemental composition for both the polymer and monomer. Good agreement also was observed for data presented in this study and those reported in the literature[17q,r]. The degree of polymerization (n) for the germanium polymer was taken as 15 based on the analysis of diffusion coefficient data (vida infra) from RDE voltammograms of both the polymer and monomer, and confirmed by the simulated voltammetric results of the polymer. Hanack and coworkers estimated the degree of polymerization for the corresponding silicon polymer to be 25[17r]. Marks et al

Table 3. Infra-red spectral, optical absorption spectral, and elemental analytical data for the $[t\text{-}Bu_4PcGeO]_n$ and $t\text{-}Bu_4PcGe(OH)_2$ materials.

TABLE 3

compound	IR (Nujol) (cm^{-1}) ν(Ge-O)	ν(O-Ge-O)	UV-Vis (THF) (nm) Q-band	B-band	Elemental analysis (%) C,H,N(found)
Polymer		893	620	330	68.74, 5.81, 13.42
Monomer	646		680	360	69.11, 6.41, 13.78

Figure 8. Fourier-transformed infra-red spectra of $[t\text{-}Bu_4PcGeO]_n$ and $t\text{-}Bu_4PcGe(OH)_2$ as Nujol mulls.

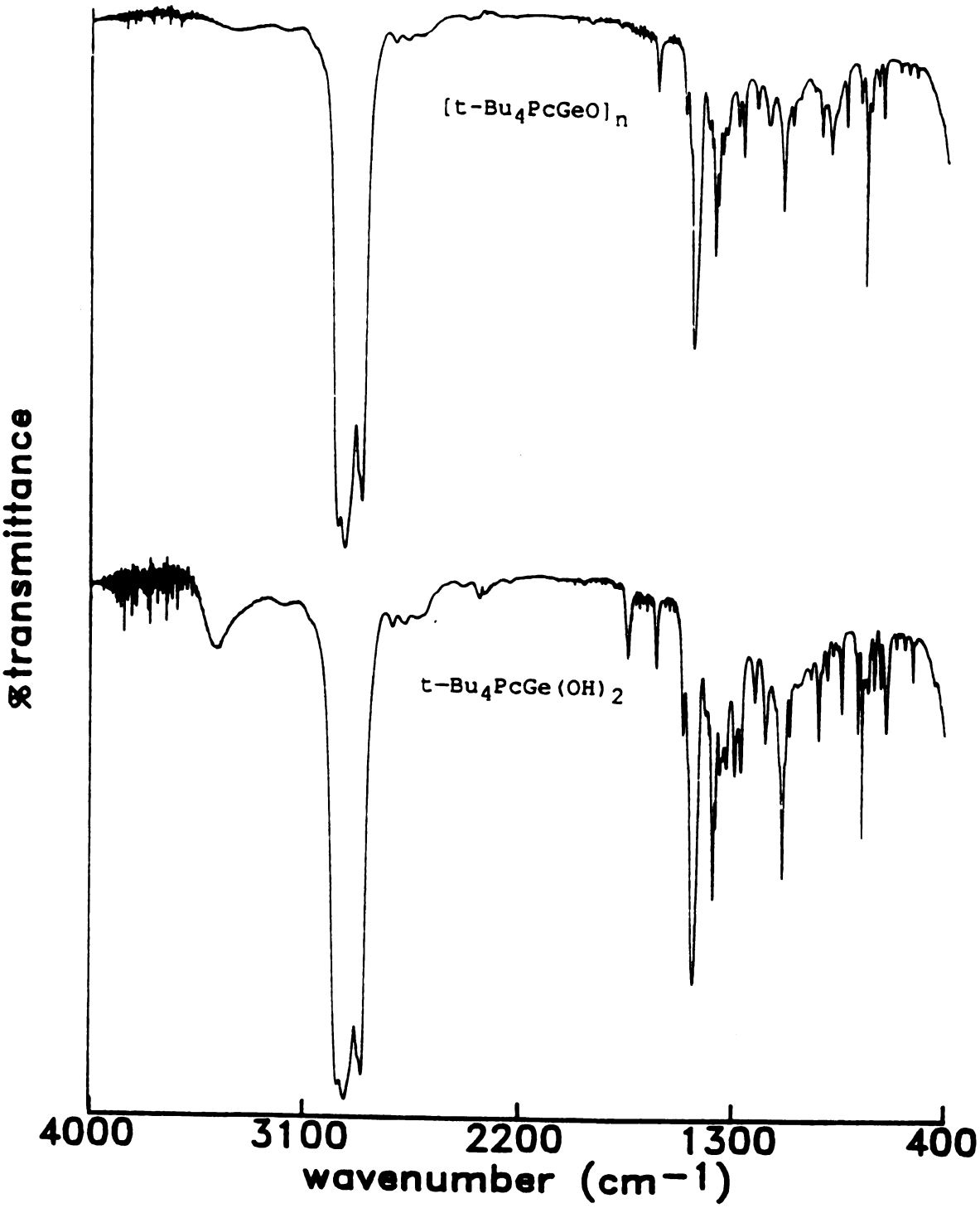
[t-Bu4PcGeO]n
t-Bu4PcGe(OH)2
%transmittance
4000
3100
2200
1300
400
wavenumber (cm-1)

FIGURE 8

Figure 9. Optical absorption spectra of $[t\text{-}Bu_4PcGeO]_n$ and $t\text{-}Bu_4PcGe(OH)_2$ as solutions in THF.

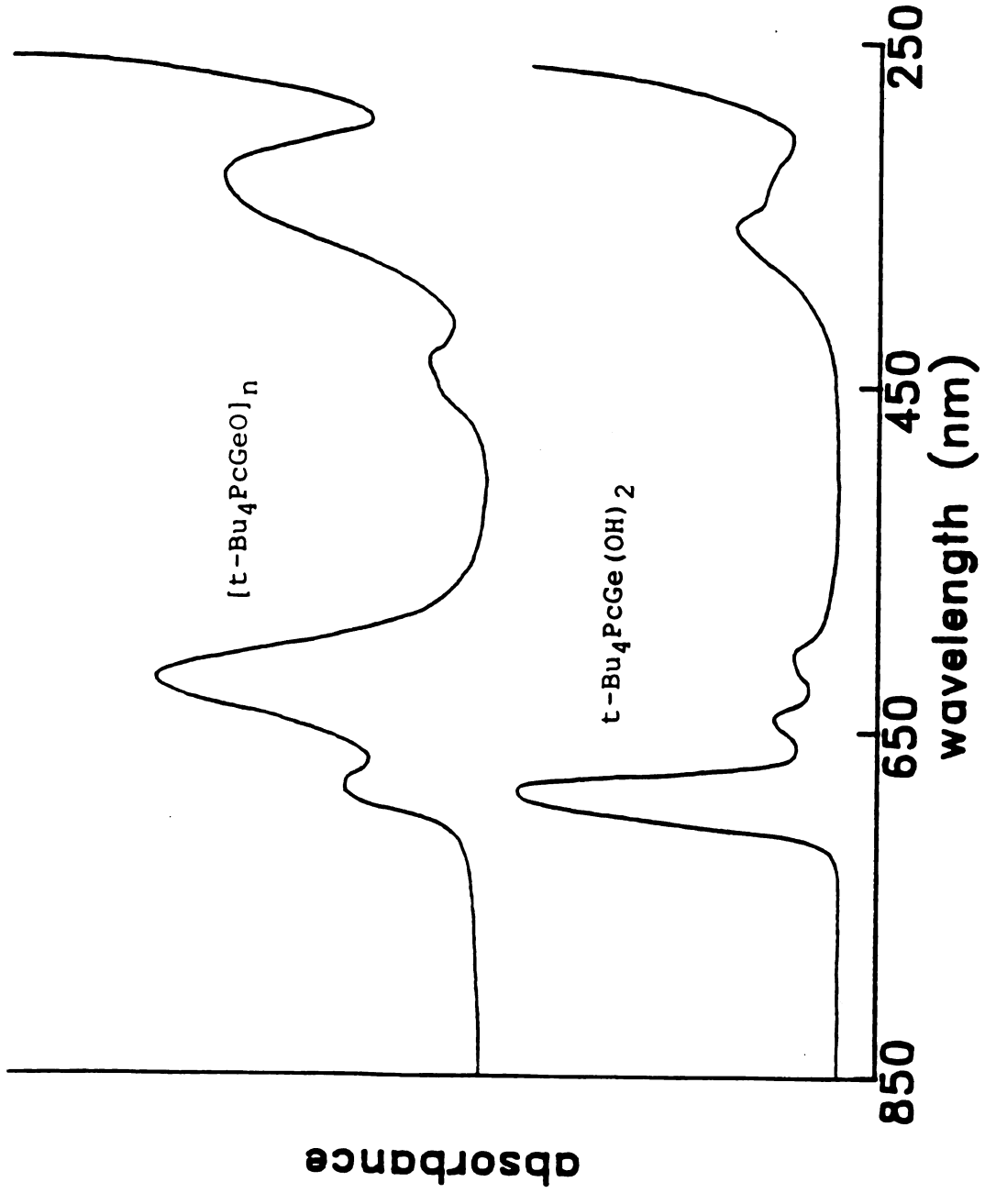
absorbance
850
650
450
250
wavelength (nm)
[t-Bu4PcGeO]n
t-Bu4PcGe(OH)2

FIGURE 9

characterized the analogous unsubstituted silicon and germanium polymer $[MPcO]_n$, and found that the germanium polymer has a n value approximatively 40% that of the silicon one[36]. Thus, a value of 15 for the soluble germanium polymer seemed probable and was used to calculate the concentration of the solutions. The μ-oxo-(tetra-t-butylphthalocyaninato)germanium is soluble in benzene, methylene chloride, and tetrahydrofuran. The good solubility arises from the presence of the tetra-t-butyl substituents. As a consequence, the reductive properties and chemical stability of the μ-oxo-(tetra-t-butylphthalocyaninato)germanium were investigated in solution, thus facilitating the study over that in the solid state.

3.3 Electrochemical studies

Stacked phthalocyanine systems are unique in that both types of doping (p and n) are theoretically possible. For example, extensive studies on the metallophthalocyanine polymer $[SiPcO]_n$ have shown that this material can be reversibly oxidized by electrochemical means as a slurry[16]. Reductive studies, even if not so conclusive, have been shown to be possible[19e,36]. In this study, only the reductive redox properties of the substituted metallophthalocyanine polymer $[t\text{-}Bu_4PcGeO]_n$ will be investigated in details. Attempts to electrochemically oxidize solutions of this material have been unsuccessful due to the degradation of this material in the electrochemical solvents used (chlorinated solvents). A solute-solvent interaction occurs resulting in the partial fragmentation of the O-Ge-O bond. In contrast, the reduction of the polymer solutions were stable in the electrochemical experiment timescale. All electrochemical experiments dealing with the reduction of the μ-oxo-(tetra-t-

butylphthalocyaninato)germanium polymer will be performed in tetrahydrofuran (THF). The working potential range in THF with 0.2 M TBABF4 is 2.2 V starting at +0.05 V vs SSCE.

3.3.1 Cyclic voltammetry

Shown in Figure 10 is a series of cyclic voltammograms of a 33.4 μM solution of the $[t\text{-}Bu_4PcGeO]_n$ polymer (0.413 mg ml^{-1}) at 100 mV sec^{-1}. Curve 10a is the CV response observed when the potential of the working electrode is scanned between +0.05 V and -1.45 V. A broad rather featureless response is obtained comparable to the featureless capacitive charging current of a blank solution containing only supporting electrolyte. This broad featureless response of the polymer was expected. It can be explained by the small potential difference between successive reductions resulting in incompletely resolved reduction waves and causing coalescence into one, multiple electron wave. This type of response is characteristic of a material with a lot of interactions between the redox sites[34]. For a redox system comprised of non-interacting redox centers, the shape of the current-potential response would be identical with the one of the monomer, and the standard potentials for both systems would be the same[30a,37]. However, the magnitude of the current would depend on the total number of redox centers. The shape of the response is independent of sweep rate (v) but its magnitude, the current, is proportional to $v^{1/2}$ in the 10-200 mV sec^{-1} range investigated. The response also remains unchanged upon repeated cycling suggesting that the products resulting of the reduction and re-oxidation of the polymer are chemically stable in the CV timescale. As described below, controlled potential coulometry data prove that the polymer is being cycled between the neutral and 1-state (one electron added per Pc site) over this 1500 mV potential range. For comparison, the cyclic voltammogram of

Figure 10. Cyclic voltammograms for the reduction of a 33.4 μM solution of $[t\text{-}Bu_4PcGeO]_n$/0.2 M $TBABF_4$ in THF at a sweep rate of 100 mV sec^{-1}.

a. virgin polymer solution

b. two successive scans of the virgin polymer solution

c. polymer solution after controlled potential coulometry (CPC) reduction at -1.65 V (decomposition into monomeric type units) and oxidation back to its neutral form

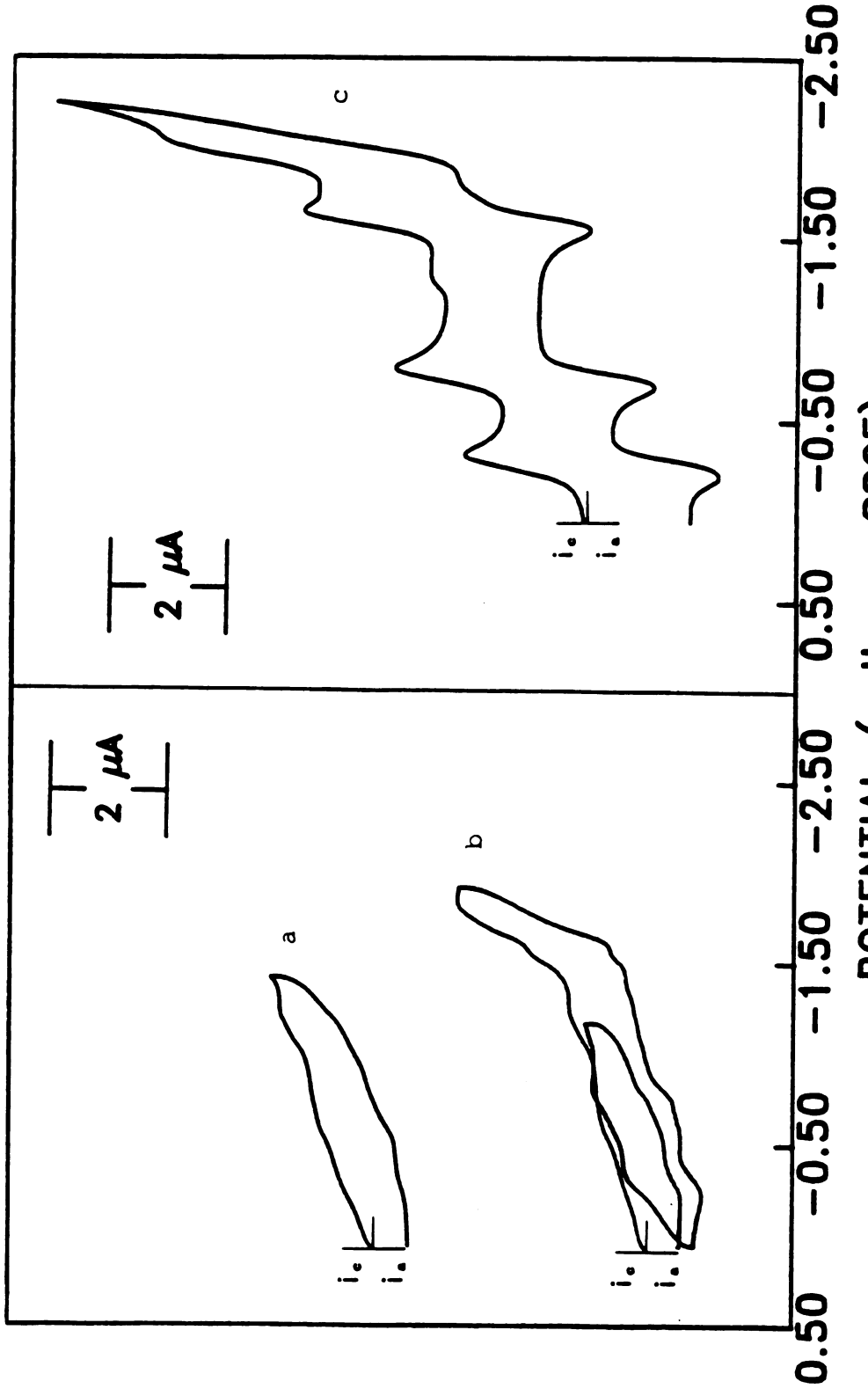
2 μA
2 μA
a
b
c
i_a
i_c
0.50
-0.50
-1.50
-2.50
0.50
-0.50
-1.50
-2.50
POTENTIAL (volts vs SSCE)

FIGURE 10

conventional Nernstian one-electron redox couples (including electroactive polymers having little or no interactions between the redox sites) exhibits a change in oxidation state over only 200 mV potential range. Shown in Figure 10b are the consecutive voltammograms observed when scanned between +0.05 V and -1.95 V. On the first scan, a broad featureless response is again initially seen. At approximatively -1.70 V, a huge increase in current occurs and upon potential reversal, two small oxidations waves appear near -0.65 V and -0.25 V. On the second scan, two new small reduction waves that are the corresponding of the oxidation waves are seen. Upon potential reversal at -1.20 V, the two oxidation waves are again observed. These two processes are not independent, they are part of the large process occurring at -1.70 V because they do not appear when reversing the scan before reaching this potential. This behavior suggests that the polymer is unstable if reduced at potentials more negative than -1.45 V. The polymer appears to be decomposing into an electroactive species at more negative potentials.

3.3.2 Controlled potential coulometry

To accurately determine the percent reduction vs potential profile for the μ-oxo-(tetra-t-butylphthalocyaninato)germanium, a series of CPC experiments were performed at various potentials. The current-time responses of the polymer reduced at different potentials and oxidized back at 0.20 V are shown in Figures 11 and 12. The potential of re-oxidation was set up to 50 mV beyond the rest potential to ensure that the polymer was back in its neutral form. The current was monitored until it decayed to a constant limiting background value, less than 1% of the initial current (10^{-6} A cm^{-2}). Electrolysis times were typically 1 h to $1^{1/2}$ h. The current was then integrated over time to obtain the total amount of charge transferred during the CPC process. The net amount of charge used in

Figure 11. Current-time curves for the reduction of a 33.4 μM solution of $[t\text{-}Bu_4PcGeO]_n$/0.2 M $TBABF_4$ in THF during controlled potential electrolysis (CPC).

a. polymer solution reduced at -0.55 V

b. polymer solution reduced at -1.05 V

c polymer solution reduced at -1.25 V

d. polymer solution reduced at -1.45 V

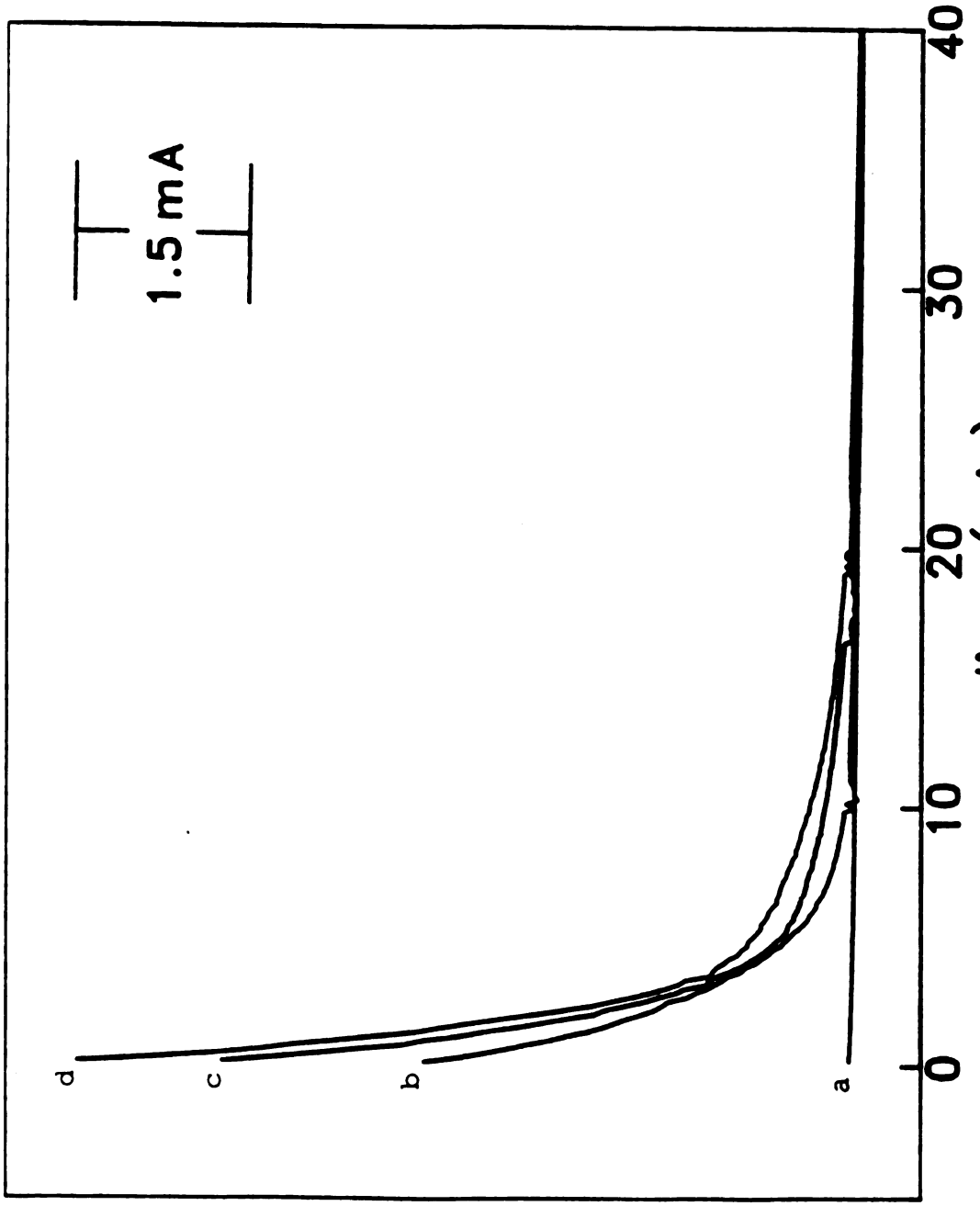

FIGURE 11

Figure 12. Current-time curves for the oxidation of reduced $[t\text{-}Bu_4PcGeO]_n/TBABF_4$ in THF resulting of Figure 11.

a'. polymer solution (a) re-oxidized at 0.20 V

b'. polymer solution (b) re-oxidized at 0.20 V

c'. polymer solution (c) re-oxidized at 0.20 V

d'. polymer solution (d) re-oxidized at 0.20 V

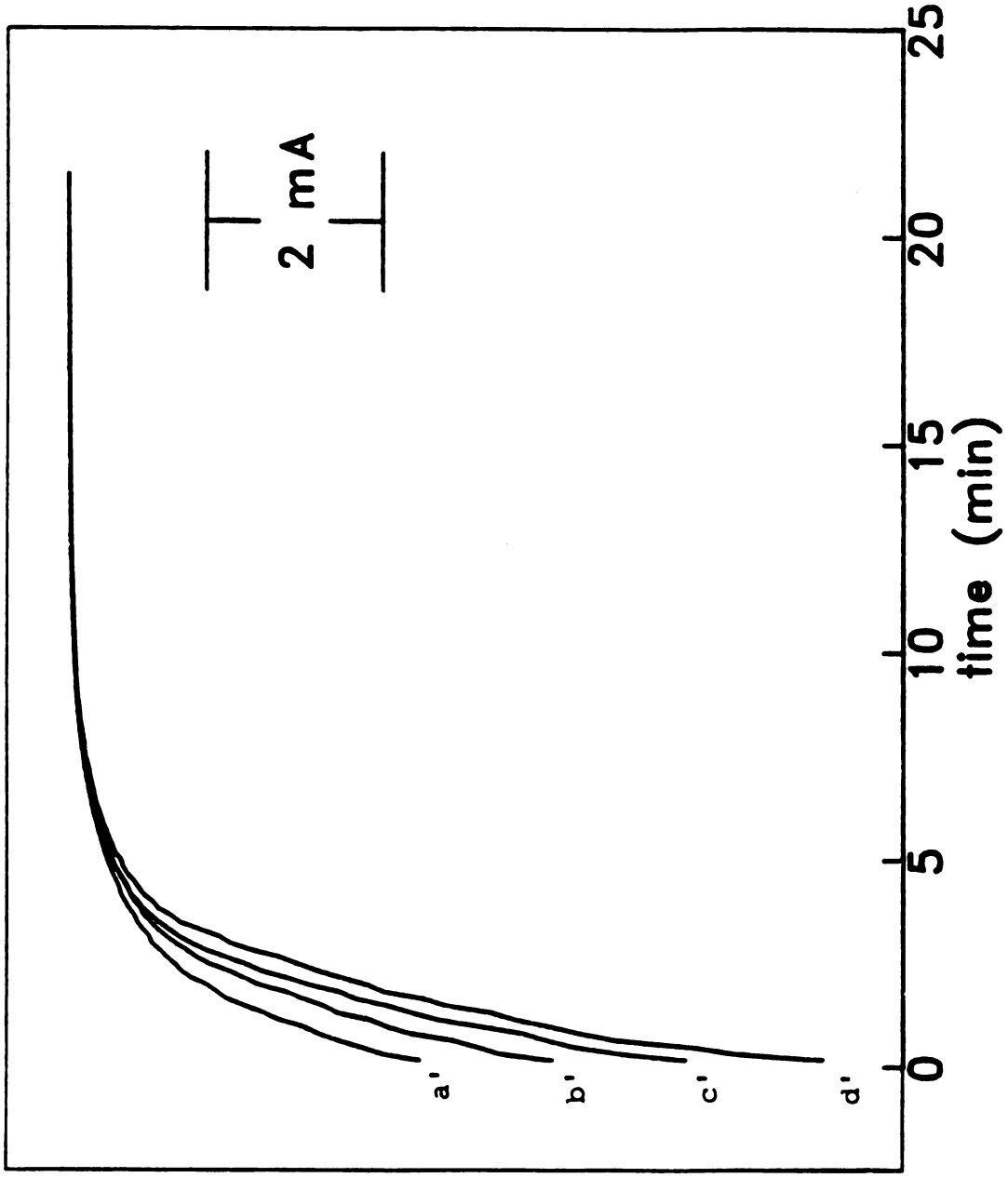

FIGURE 12

the determination of the percent reduction (equation 3) was calculated by subtracting the product of the steady state background current and time of the experiment from the total amount of charge measured. Shown in Figure 13 is a plot of the percent reduction of the germanium polymer as function of potential. The percent reduction, at a given potential, is determined by averaging the amount of charge passed for the initial reduction of the neutral polymer and oxidation back to the neutral form at 0.20 V. The error bars represent the difference between these two values. The small difference between the two values can be attributed to the variation in potential of the quasi-reference electrode in the course of the experiment. This small difference suggests that the reduced form of the polymer at all degrees of partial reduction is stable on the CPC timescale, i.e., several hours. Electrochemical and spectroscopic characterization of the cycled neutral polymer also support this assumption. The CV and DPV voltammograms of the polymer obtained after each reduction/re-oxidation cycle appear identical to that of the virgin material (Figures 10a and 22c). The UV-Vis absorption spectra of the neutral polymer taken after each cycle are very similar to those of the virgin polymer (Figure 9). Figure 14 represents the UV-Vis absorption spectrum of the neutral polymer after being reduced at 100% and oxidized back to its neutral form. The presence of intense peaks at 621 nm and 334 nm proves that the phthalocyanine ring remains intact and the absence of new peaks confirms the good stability of the cycled polymer. The corresponding infra-red spectrum (Figure 15) exhibits the asymmetric O-Ge-O band at 904 cm^{-1}, but does not show the symmetric Ge-O band in the 600 cm^{-1} region characteristic of the monomer dihydroxide. This suggests that the cycled polymer does not decompose into monomeric type units. If the polymer was degrading into molecular species or small oligomers, the smooth doping profile would not be observed. Instead, a sharp change in the percent

Figure 13. Degree of partial reduction vs potential determined by controlled potential coulometry for the reduction of $[t\text{-}Bu_4PcGeO]_n/TBABF_4$ in THF. Each point (□) corresponds to the mean value for a reduction/re-oxidation cycle. The error bars represent the difference between the reduction and re-oxidation.

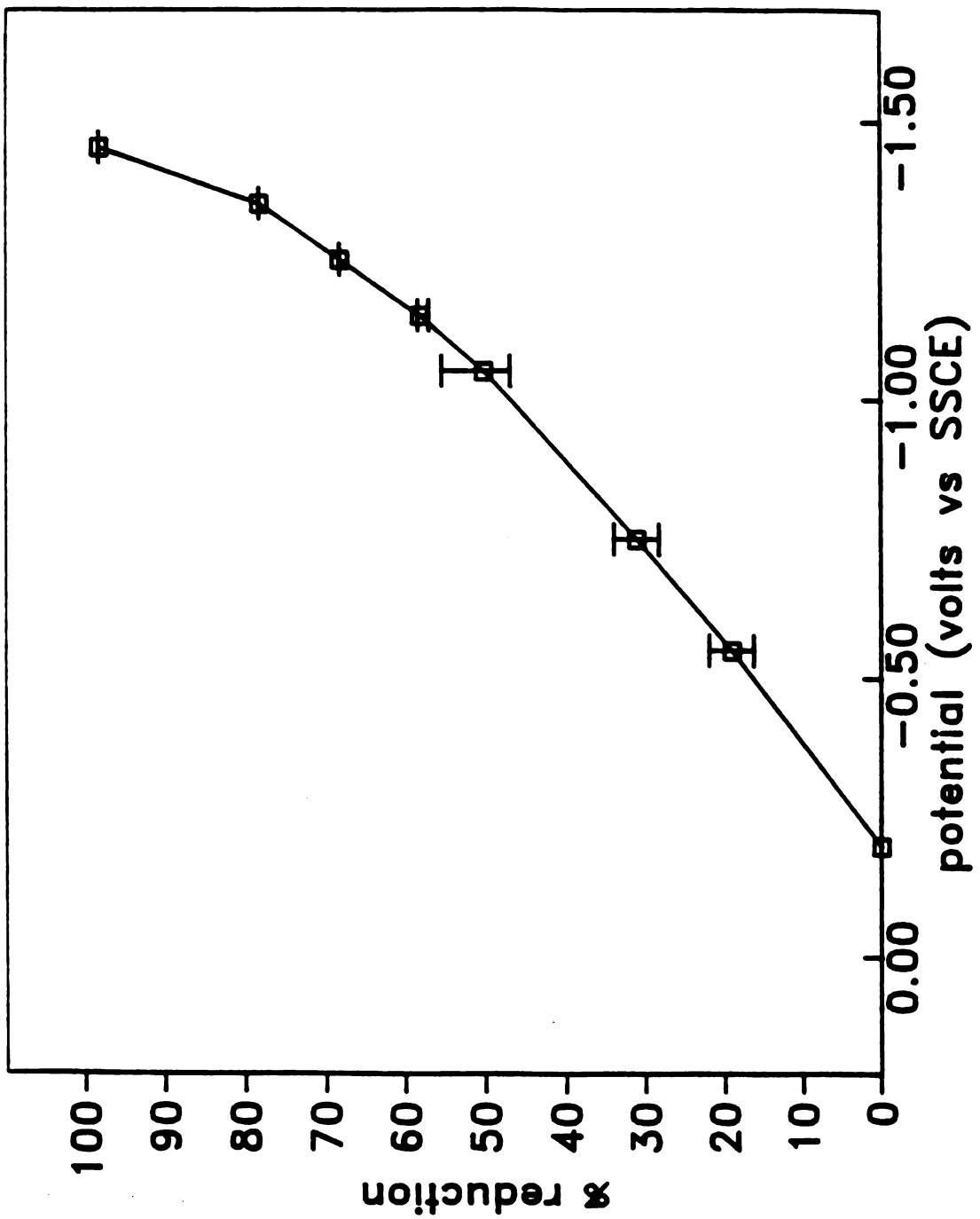
% reduction
100
90
80
70
60
50
40
30
20
10
0
0.00
-0.50
-1.00
-1.50
potential (volts vs SSCE)

FIGURE 13

Figure 14. Optical absorption spectra of $[t\text{-}Bu_4PcGeO]_n$ in THF after CPC at -1.44 V (98 % reduction) and oxidation back to its neutral form at 0.20 V. The spectrum is very similar to the one obtained for the virgin polymer (Figure 9).

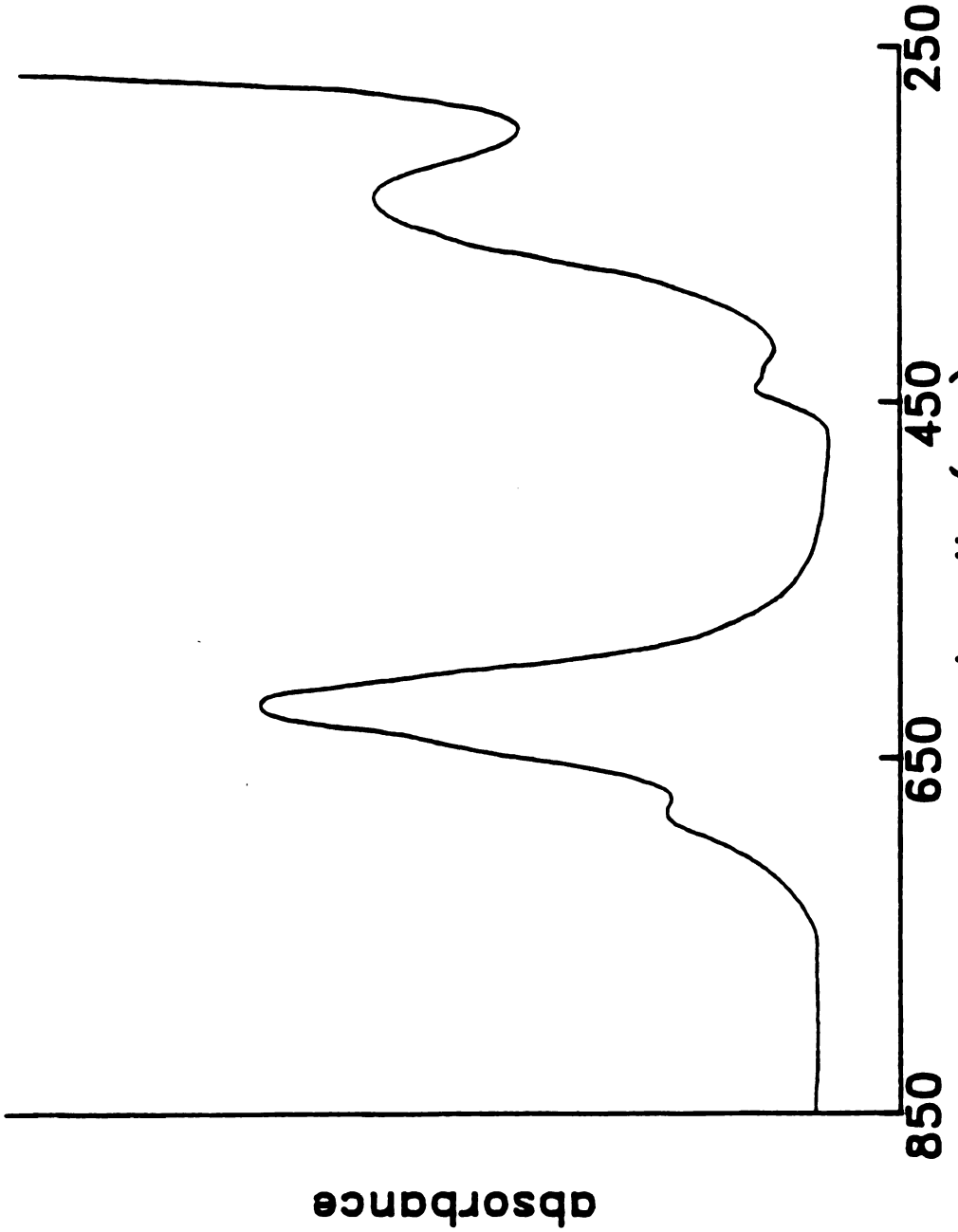

FIGURE 14

Figure 15. Fourier-transformed infra-red spectra of $[t\text{-}Bu_4PcGeO]_n$/Nujol after CPC at -1.44 V (98 % reduction) and oxidation back to its neutral form at 0.20 V. The band at 904 cm^{-1} is assigned to the asymmetric O-Ge-O strech.

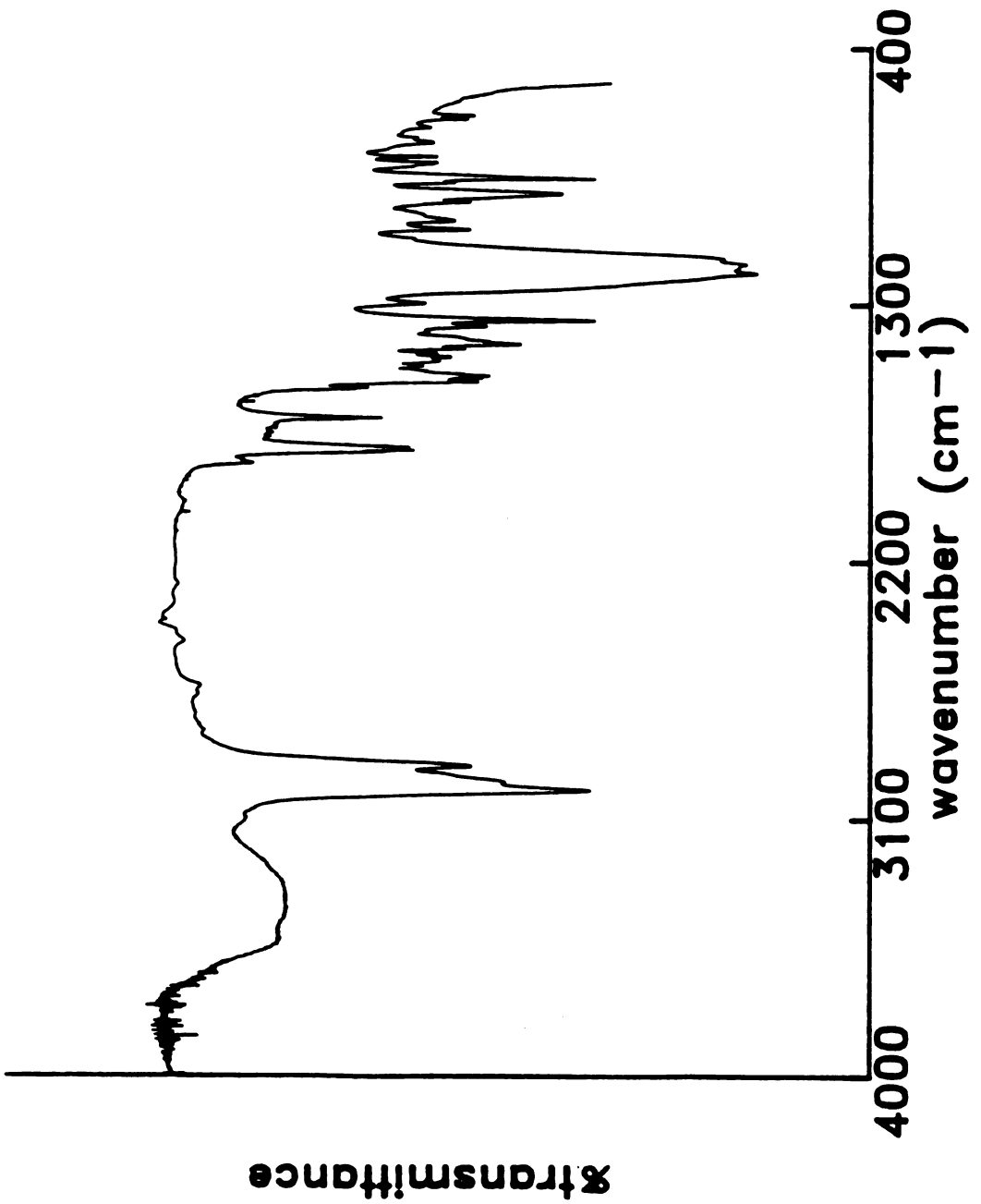

FIGURE 15

reduction would be seen. The smooth doping profile suggests the formation of an energetic band from which charge can be continuously and cyclicly added. It is the first time that such behavior has been observed in the solution redox chemistry. Additional proof of chemical stability was obtained from a series of plots of normalized currents vs time at different potentials. The current during a CPC experiment is expected to decay exponentially[29]. Shown in Figure 16 is a series of log(i(t)/i(0)) vs time plots for the reduction of the polymer. In each CPC experiment, the current, at any time, is normalized to the initial current value. The data obtained at -1.02 V (50% reduction) and -1.44 V (98% reduction) exhibit the linear behavior of a chemically stable redox system. When bulk electrolysis is performed at -1.65 V, a potential corresponding to halfway through the large reduction wave of the CV in Figure 9b, the data clearly deviate from linearity. At this potential, the polymer is 227% reduced with a collection efficiency of 102%. This increase in potential of only 200 mV results in more than doubling of the degree of reduction. Although no electroactivity is gained or lost, the nature of the electroactive species has changed. Shown in Figure 10c is the cyclic voltammogram of a solution after being reduced at -1.65 V and oxidized back at 0.20 V. The response is no longer the broad featureless wave initially observed for the virgin polymer (Figure 10a) but is similar to the one usually obtained for a conventional redox couple. The first three reduction waves at E_{pc1} = -0.35 V, E_{pc2} = -0.83 V and E_{pc3} = -1.68 V are characteristic of consecutive Nernstian one-electron reduction processes resulting in the formation of a chemically stable product[38]. The difference between the cathodic and anodic peak potentials for each wave (ΔEp) is approximatively 75 mV, close to the 60 mV expected for such a process. Deviations of ΔEp from the Nernstian value of 60 mV probably can be attributed to effects of uncompensated resistance in this highly resistive solvent. Further information about the electrochemical process was obtained by

Figure 16. Variations of log (i(t)/i(0)) with time at different potentials determined from controlled potential coulometry curves for the reduction of $[t\text{-}Bu_4PcGeO]_n/TBABF_4$ in THF. i(0) represents the initial current value for each CPC experiment. The ordinate scale pertains only to the data obtained at -1.02 V. Each successive curve is shifted upwards by 1 unit. The % reduction of the listed potentials are as follows: -1.02 V: 50% reduction, -1.44 V: 98% reduction, and -1.65 V: 227% reduction.

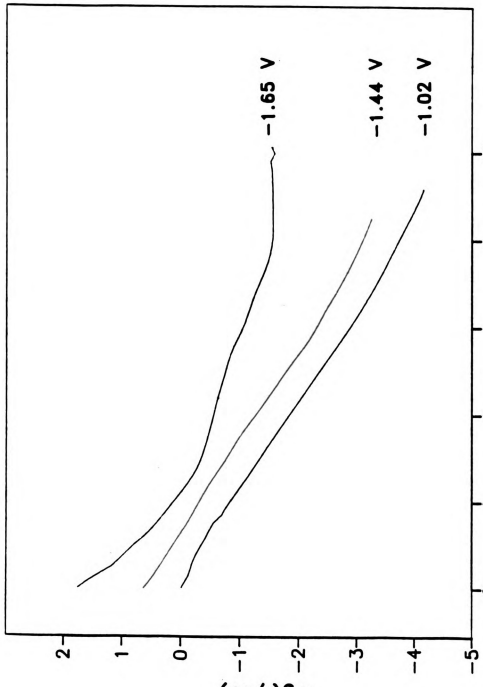

FIGURE 16

investigating the dependence of peak currents and potentials on scan rate. The peak potentials are invariant with the scan rate (v), and the magnitude of the anodic and cathodic peak currents are the same in the 10-200 mV range and increase as $v^{1/2}$. These results demonstrate that the cycled polymer is stable in this potential range and the waves are diffusion-limited. The fourth reduction wave at E_{pc4} = -2.09 V, near the background limit of the solvent, is well defined and lacks the corresponding oxidation wave upon potential reversal is unstable on the CV timescale, i.e., a few minutes. Sequential CPC measurements performed at potentials 200 mV more negative than each of the first three reduction waves also suggest that the first three processes are consecutive one-electron reductions to form stable products. For each CPC experiment performed at these three reduction/oxidation processes, the same amount of charge was passed (reduction) and collected (oxidation back to the neutral material) as expected for 100% reduction of the polymer. These results are summarized in Table 4 and suggest that the polymer has fragmented into a mixture of monomeric or oligomeric species without any loss in electroactivity. As will be shown later via the redox characterization of dihydroxy(tetra-t-butylphthalocyaninato)germanium , the corresponding polymer, when it is more than 100% reduced, quantitatively decomposes into monomeric type units that are electrochemically and spectroscopically identical to it.

The plots of log(i(t)/i(0)) vs time at different potentials also serve in elucidating the type of reactive mechanism occurring at the electrode during the CPC process. In the late 1970s, Dr. Louis Meites and his group at the Polytechnic Institute of Brooklyn reported a theoretical description of the current-time curves obtained during a controlled potential electrolysis for different reactions such as EC (electron transfer at the electrode surface followed by

Table 4. Controlled potential coulometry data for μ-oxo-(tetra-t-butyl phthalocyaninato)germanium.

TABLE 4

Potential for reduction/oxidation cycle (V)	Percent reduction	Percent oxidation
-1.45 /0.20	98	99
-1.65[b]/0.20	227	229
-0.50 /0.20	97	98
-1.10 /0.20	208	200
-1.85 /0.20	298	293

b Decomposition of the polymer occurs following reduction at -1.65 V .

homogeneous chemical reaction) and ECE (EC reaction followed by another electron transfer reaction)[39]. By comparing the log(i(t)/i(0)) vs time plots in this study with the ones discussed in Meites' work, it appears that the type of reaction occurring during the electrolysis of the germanium polymer can be described as an ECE-type mechanism :

$$O_1 + n_1\, e \iff R_1$$

$$R_1 \longrightarrow O_2$$

$$O_2 + n_2\, e \iff R_2$$

where :

O_1, O_2 = oxidized species

R_1, R_2 = reduced species

n_1, n_2 = number of electrons transferred in the process

The plots of log (i(t)/i(0)) vs time at -1.02 V and -1.44 V are concave-downward curves and according to Meites results, the chemical step can be identified with certainty in this case. In contrast, the plot at -1.65 V is a concave-upward curve. Meites explained that the small and slowly decreasing current observed was probably due to a very slow transformation of R_1 into O_2. By including additional voltammetry results for the polymer and the corresponding monomer, the mechanism was refined into an E_nCEE mechanism:

$$O_{n-j}\, R_j + e^- \iff O_{n-1-j}\, R_{j+1} \qquad (1 \le j \le n-1)$$

$$[t\text{-}Bu_4PcGeO]_n + n\, e^- \longrightarrow n\ t\text{-}Bu_4PcGeO^-$$

$$n\ t\text{-}Bu_4PcGeO^- + n\, e^- \longrightarrow n\ t\text{-}Bu_4PcGeO_2^-$$

$$n\ t\text{-}Bu_4PcGeO_2^- + n\, e^- \longrightarrow n\ t\text{-}Bu_4PcGeO_3^-$$

For the first series of electron transfer processes, 15 different E^0 values are needed to respond for the complete reduction of the germanium polymer. During the chemical step, the polymer breaks into n number of monomeric units in the anion form. These anions can then be further reduced into dianions and trianions.

3.3.3 Rotating disk and rotating ring-disk voltammetry

The complex nature of the redox response for the polymer and its chemical stability as a function of the degree of reduction was investigated in details through the use of rotating disk and rotating ring-disk electrode voltammetry. Shown in Figure 17 is a series of RDE voltammograms at different rotation rates for the reduction of the germanium polymer. For comparison, the RDE voltammogram of the blank solution containing only the supporting electrolyte at a rate of 700 rpm over the same potential range is included. The results correlate well with the CV data set out in Figure 10. The onset of current begins near -0.40 V and steadily increases to near -1.65 V where a large increase in current is again observed. Based on the CPC and CV results discussed above, this increase is believed to be due to the reduction of the decomposition product of the polymer following 100% reduction. The 1.25 V range observed before the onset of the large increase in current is nearly identical to the potential increment seen in the CPC results (Figure 13). Thus the current response between -0.40 V and -1.65 V is believed to arise from the one-electron reduction of the polymer. The slope of the RDE response in this region is independent of angular velocity (ω) and the current magnitude at any potential within this range increases with $\omega^{1/2}$. Levich plots, i.e., i(E) vs $\omega^{1/2}$, obtained for several potentials within the same range as above, yield straight lines with intersect close to zero (Figure 18) suggesting that there is no kinetic limitation towards the reduction process[32a,40]. The small deviation from zero intercept can be attributed to higher background currents at high potentials. This behavior implies that the reduction process of the polymer within this potential range is mass-transfer limited and that there are no surface effects (adsorption) influencing the electron transfer process. The reduction of the polymer is simply a

Figure 17. Rotating disk electrode voltammograms for the reduction of a 33.4 μM solution of $[t\text{-}Bu_4PcGeO]_n$/0.2 M $TBABF_4$ in THF at various rotation rates. The current of the blank solution does not change with increasing rotation rate.

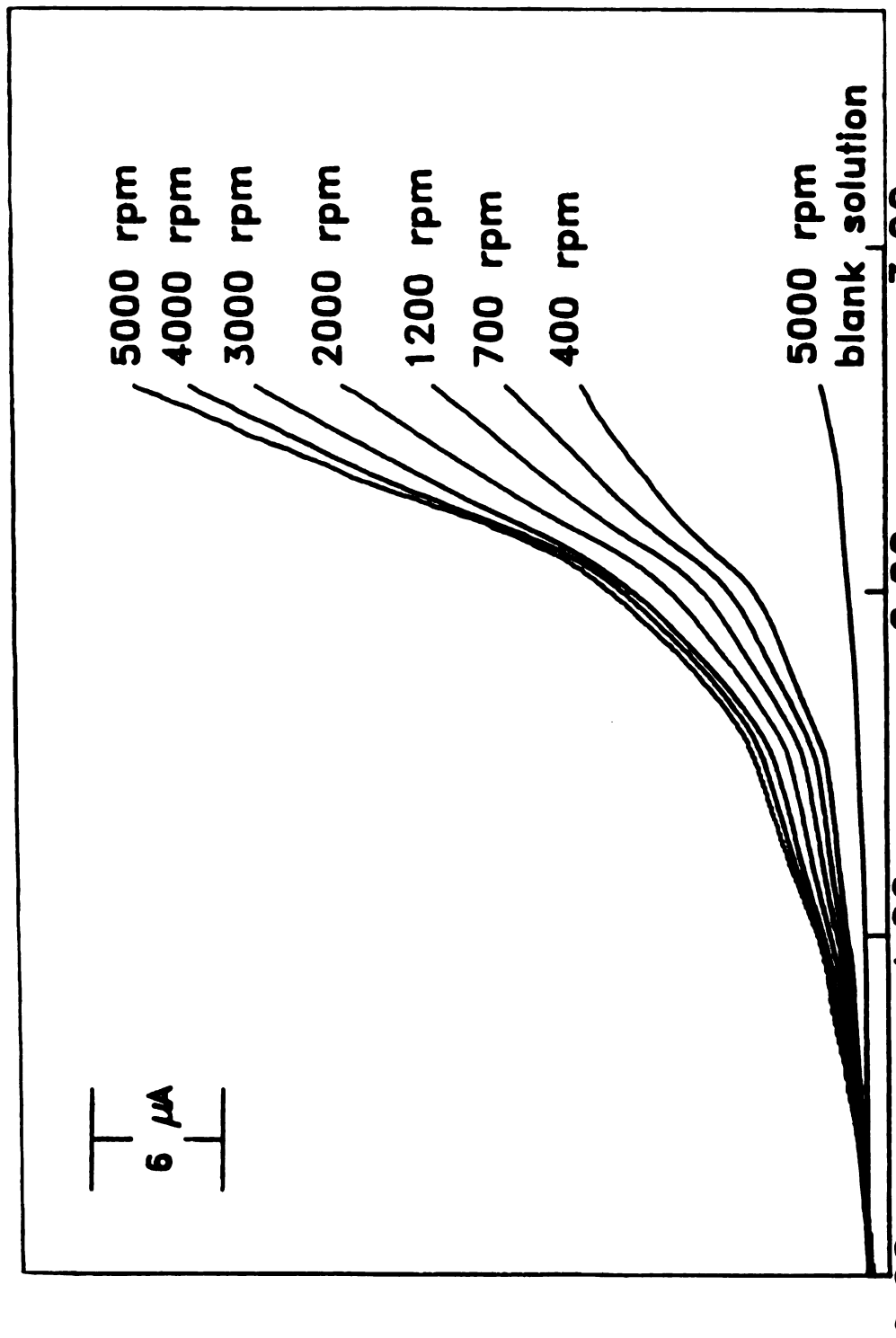
5000 rpm
4000 rpm
3000 rpm
2000 rpm
1200 rpm
700 rpm
400 rpm
5000 rpm
blank solution
6 μA
0.00
-1.00
-2.00
-3.00
potential (volts vs SSCE)

FIGURE 17

Figure 18. Levich plots for the reduction of $[t\text{-}Bu_4PcGeO]_n/TBABF_4$ in THF at various potentials. The % reduction of the listed potentials are as follows: -0.64 V (25% reduction); -0.84 V (37% reduction); -1.04 V (50% reduction); -1.24 V (68% reduction); -1.44 V (98% reduction).

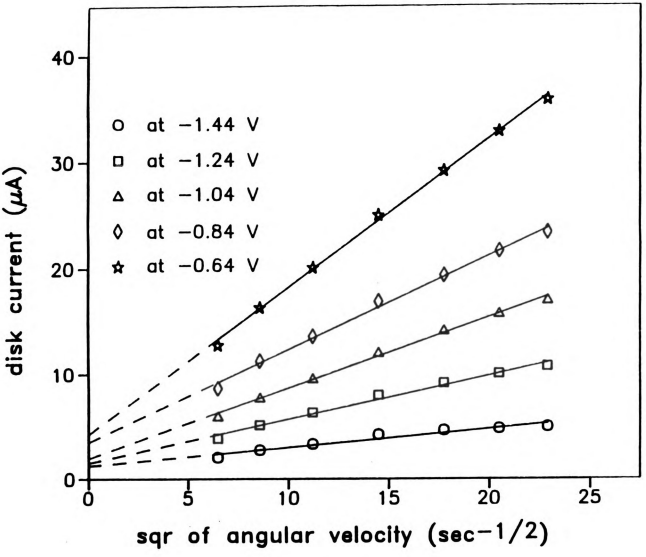
disk current (μA)
sqr of angular velocity (sec−1/2)
at −1.44 V
at −1.24 V
at −1.04 V
at −0.84 V
at −0.64 V
0
10
20
30
40
0
5
10
15
20
25

FIGURE 18

Nernstian process. Shown in Figure 19 is the percent reduction vs potential profile for the germanium within the 1.45 V potential range. The percent reduction, at any potential, is determined by normalizing the RDE current at a given potential to the RDE current at -1.45 V taken as representing 100% reduction and multiplying by 100 (equation 7). This particular potential was chosen based on results of CPC experiments. In this doping profile, the error bars represent the differences in percent reduction calculated from the RDE voltammograms of Figure 17 for the same potential at different rotation rates. As it is observed in Figure 19, the doping profile obtained from RDE data maps out the percent reduction vs potential plot obtained from CPC results. The excellent agreement between coulometric and voltammetric data suggest that the potentials used in CPC and RDE experiments represent the thermodynamic values for which the reduction process occurs. Using a kinematic viscosity value of 6.2 10^{-3} cm^2 sec^{-1} and a disk electrode area value of 0.163 cm^2, a value of 6.6 10^{-6} cm^2 sec^{-1} for the diffusion coefficient of the neutral germanium polymer was obtained from the RDE voltammograms. This value is compatible with that of the silicon analog 3.0 10^{-6} cm^2 sec^{-1} obtained in 1,1,2,2 tetrachloroethane[41], a solvent slightly more viscous than tetrahydrofuran in which the diffusion coefficient of the germanium polymer was measured. Shown in Figure 20a,b,c are a series of RDE, RRE and RRDE voltammograms for the reduction of the germanium polymer over the potential region in which it is stable (0.00 V to -1.45 V). As expected, the RDE and RRDE waves are identical in shape and differ only in magnitude due to the difference in electrode area between that of disk and that of ring-disk. The RRDE data (Figure 20c) represent a continuous shielding-collection experiment in which the disk is held at -1.45 V, resulting in 100% reduction of the polymer and the ring is scanned from -1.45 to 0.00 V.

Figure 19. Degree of partial reduction vs potential determined by rotating disk voltammetry for the reduction of $[t\text{-}Bu_4PcGeO]_n$/TBABF4 in THF. Each point (o) corresponds to the mean value for a reduction/re-oxidation cycle. The mean value is calculated by averaging the current at different rotation rates. The error bars represent the standard deviation.

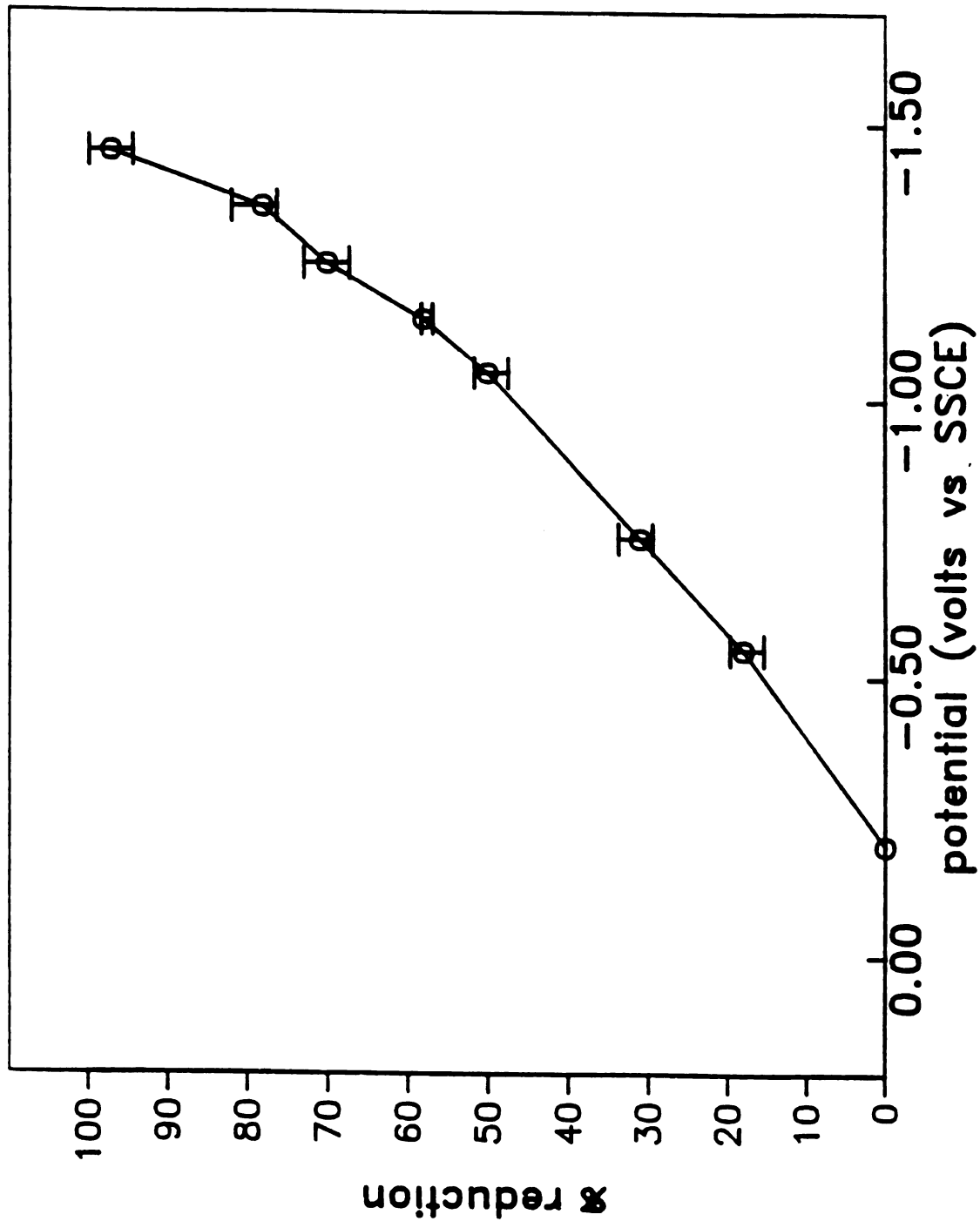
% reduction
100
90
80
70
60
50
40
30
20
10
0
0.00
-0.50
-1.00
-1.50
potential (volts vs SSCE)

FIGURE 19

Figure 20. Experimental (a,b,c) and simulated (d,e,f) rotating disk electrode voltammongrams of a 50.1 μM solution of $[t\text{-}Bu_4PcGeO]_n$/0.2 M $TBABF_4$ in THF. Both the simulation and experimental conditions are identical to the ones of Figure 17. The rotation rate was 4000 rpm.

a,d. disk voltammograms in the absence of the ring

b,e. ring voltammograms in the absence of the disk

c,f. ring voltammograms when the disk is held at -1.45V and the ring is scanned from this potential to the rest potential

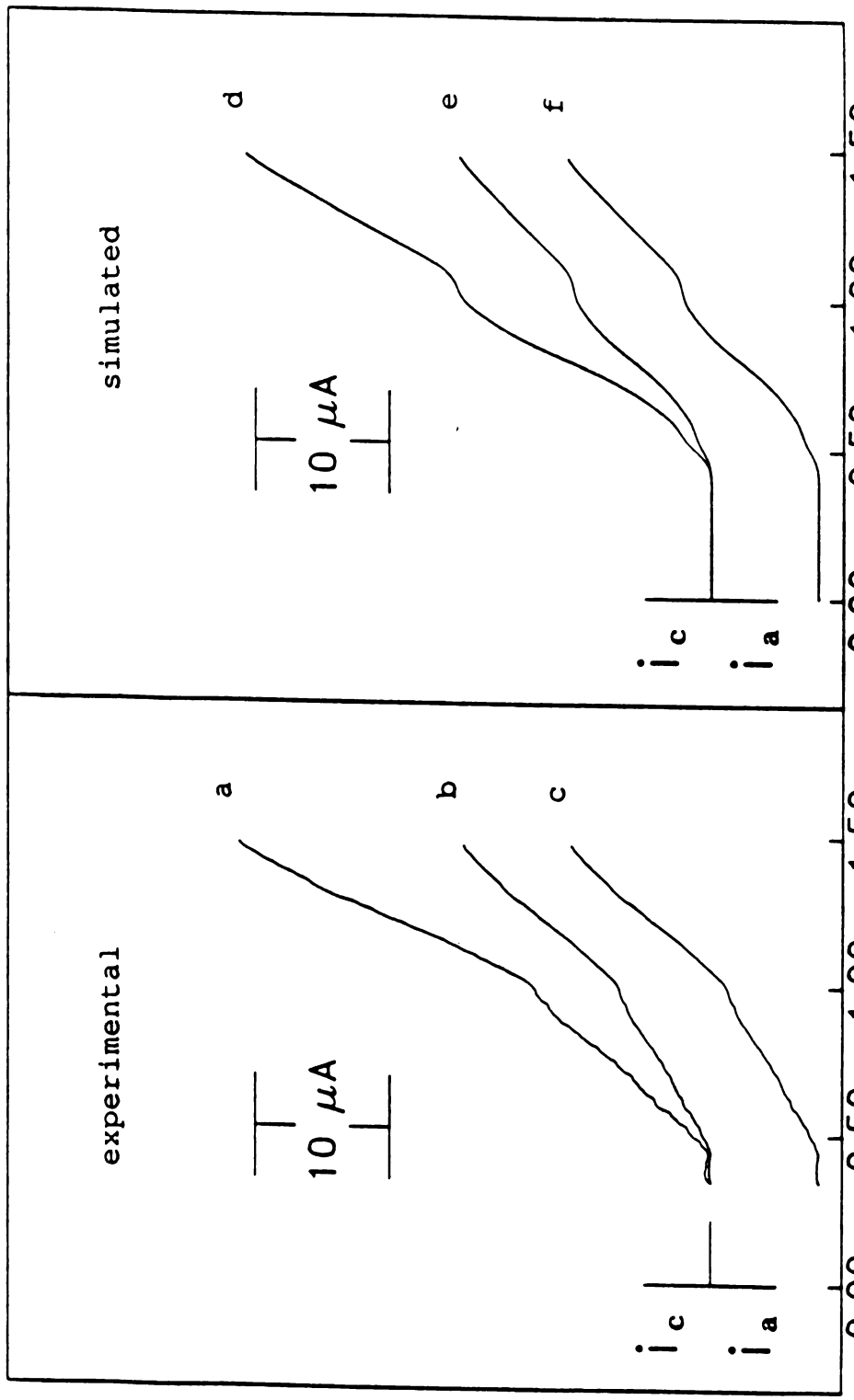
experimental
simulated
a
b
c
d
e
f
10 μA
10 μA
i_c
i_a
i_c
i_a
0.00 -0.50 -1.00 -1.50
0.00 -0.50 -1.00 -1.50
POTENTIAL (volts vs SSCE)

FIGURE 20

Initially, the ring current is cathodic, the ring being shielded by the disk resulting from the reduction of the polymer. As the potential is scanned towards more positive values, the current eventually becomes anodic and reaches a limiting value resulting from the collection (oxidation back to neutral polymer) of the reduced polymer. As predicted by equation 9, the difference between i_R and i_R^0 is a constant at any potential and is equal to i_d * N. These results, shown in Figure 21, represent the $[(i_R - i_R^0)/ i_d]$ - N term vs potential plot. This plot illustrates the applicability and utility of these types of experiments for quickly monitoring the stability of multi-site redox systems. At potentials more negative than -1.45 V, the CV and CPC results suggest that the polymer is unstable upon reduction. Continuous shielding-collection experiments results also suggest this behavior. The RRDE data obtained at disk potentials of -1.64 V and -2.19 V clearly show that the values of $(i_R^0 - i_R) / i_d$ is neither equal to N nor constant over the entire potential range. Only at the limiting potentials, 0.00 V and the value at which the disk is set, is the difference equal to N. The ring current (i_R^0) observed during the RRDE experiments is greater than expected which implies the inclusion of an additional cathodic current from the reductive process. At ring potentials sufficiently positive of the disk potential, near 0.00 V, the values of $(i_R^0 - i_R) / i_d$ again is equal to N, suggesting that all the electroactive material can be collected. This correlates well with the CPC results obtained at -1.65 V and the resulting CV characterization of the decomposed polymer set out in Figure 10c. It supports the assumption that no electroactivity or redox sites are lost, just that the nature of the electroactive species has changed. As will be shown via digital simulations of the RRDE experiments, the mechanism and rates of the homogeneous reactions can be elucidated.

Figure 21. Continuous shielding-collection plots for the reduction of $[t\text{-}Bu_4PcGeO]_n/TBABF_4$ in THF at various disk potentials. The rotation rate is 2000 rpm for all plots. i_{Rc} represents the cathodic ring current when the disk is hold at a particular potential, i_{Rc}^{o} is the cathodic ring current in the absence of reaction at the disk and N is the collection efficiency of the electrode assembly. The % reduction of the listed potentials are as follows: -0.85 V (41%); -1.45 V (100%); -2 V (310%)

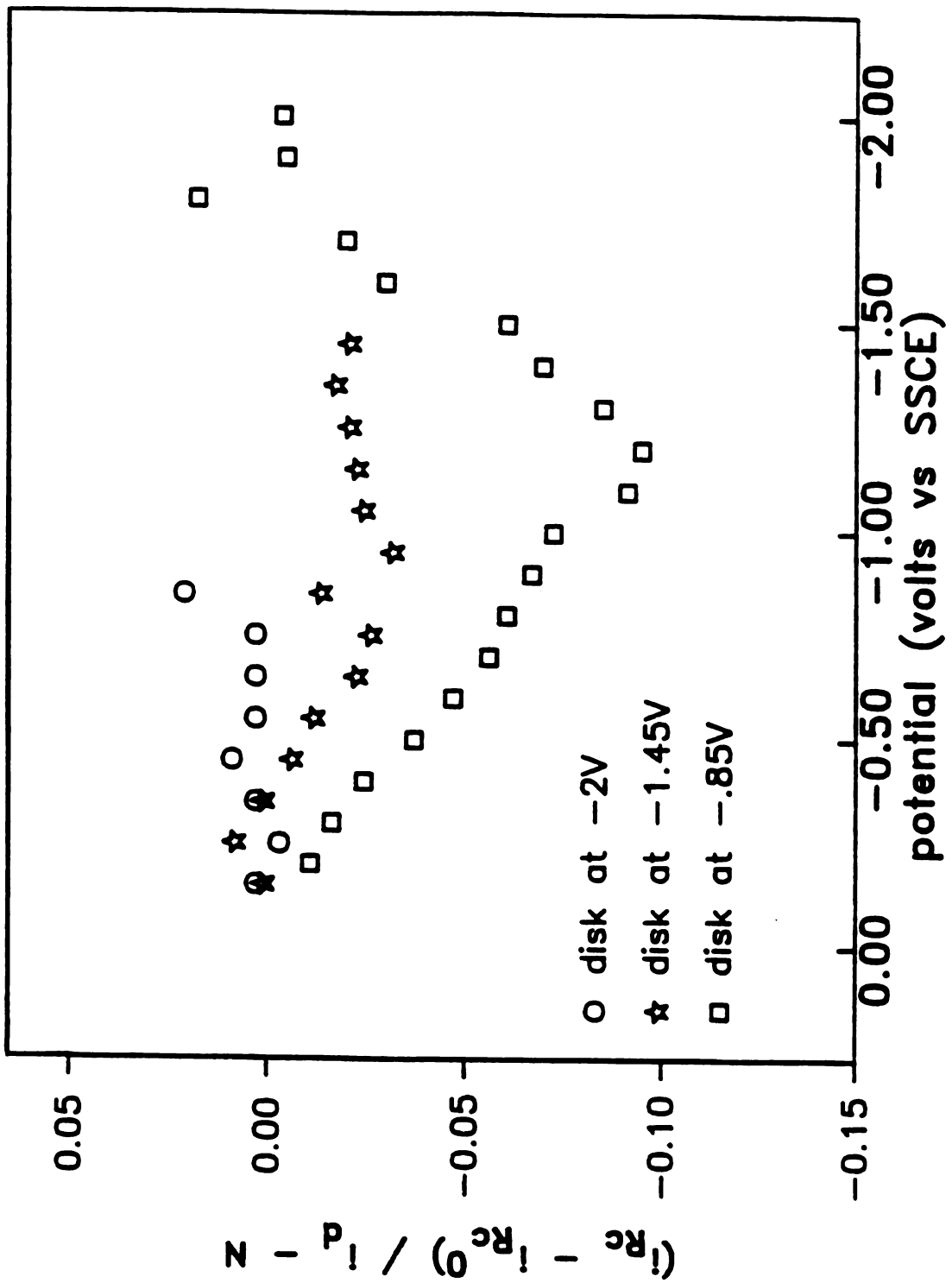
0.05
0.00
−0.05
−0.10
−0.15
0.00
−0.50
−1.00
−1.50
−2.00
potential (volts vs SSCE)
o disk at −2V
☆ disk at −1.45V
□ disk at −.85V

FIGURE 21

3.3.4 Differential pulse voltammetry

The rather featureless responses obtained from the CPC, CV, and RDE experiments have led to use differential pulse voltammetry to more accurately probe the energetics of the doping process. The derivative output of DPV makes it extremely sensitive to small changes in the redox profile of the polymer[42]. Since the pulse sequence employed for DPV effectively performs a pre-electrolysis of the electroactive species near the surface of the electrode before the current is measured, the voltammogram illustrates the ease with which the polymer can go from one oxidation state to another. Shown in Figure 22a is the DPV for the reduction of the polymer over the potential range in which it is stable. The voltammogram represents the conversion of the polymer from neutral material to 1-oxidation state, one electron added per Pc site. The DPV data more clearly show that the reduction of the polymer is not a smooth continuous process but in fact varies greatly depending on potentials. As it will be seen later with the simulated DPV response of the polymer, a large increase in current arises from strong interactions between redox sites within the polymer. This occurs when the standard potentials of redox sites are very close from one another. The large dip observed in current near -1.03 V corresponds to the current plateau seen in the RDE voltammogram. This dip located at approximatively 50% reduction may imply some inherent stability at this particular percent reduction[43]. Theoretical and experimental studies on the silicon analog have suggested such behavior[44]. At potentials more negative than -1.45 V, two additional reduction peaks are observed at -1.79 V and -2.19 V (Figure 22b). The magnitude, shape, and potential of these peaks are not well defined as the response up to -1.45 V. This was expected considering the instability of the polymer at these potentials. The polymer decomposition tends to cause a cumulative depletion of electroactive material near the electrode surface which

Figure 22. Differential pulse voltammograms for the reduction of a 33.4 μM solution of $[t\text{-}Bu_4PcGeO]_n$/0.2 M $TBABF_4$ in THF. The experimental conditions are as follows: pulse amplitude: 50 mV; pulse width: 50 mV sec^{-1}; pulse duration: 1000 msec and scan rate: 4 mV sec^{-1}.

a, b. virgin polymer solution

c. polymer solution after CPC reduction at -1.45 V (98% reduction) and oxidation back at 0.20 V

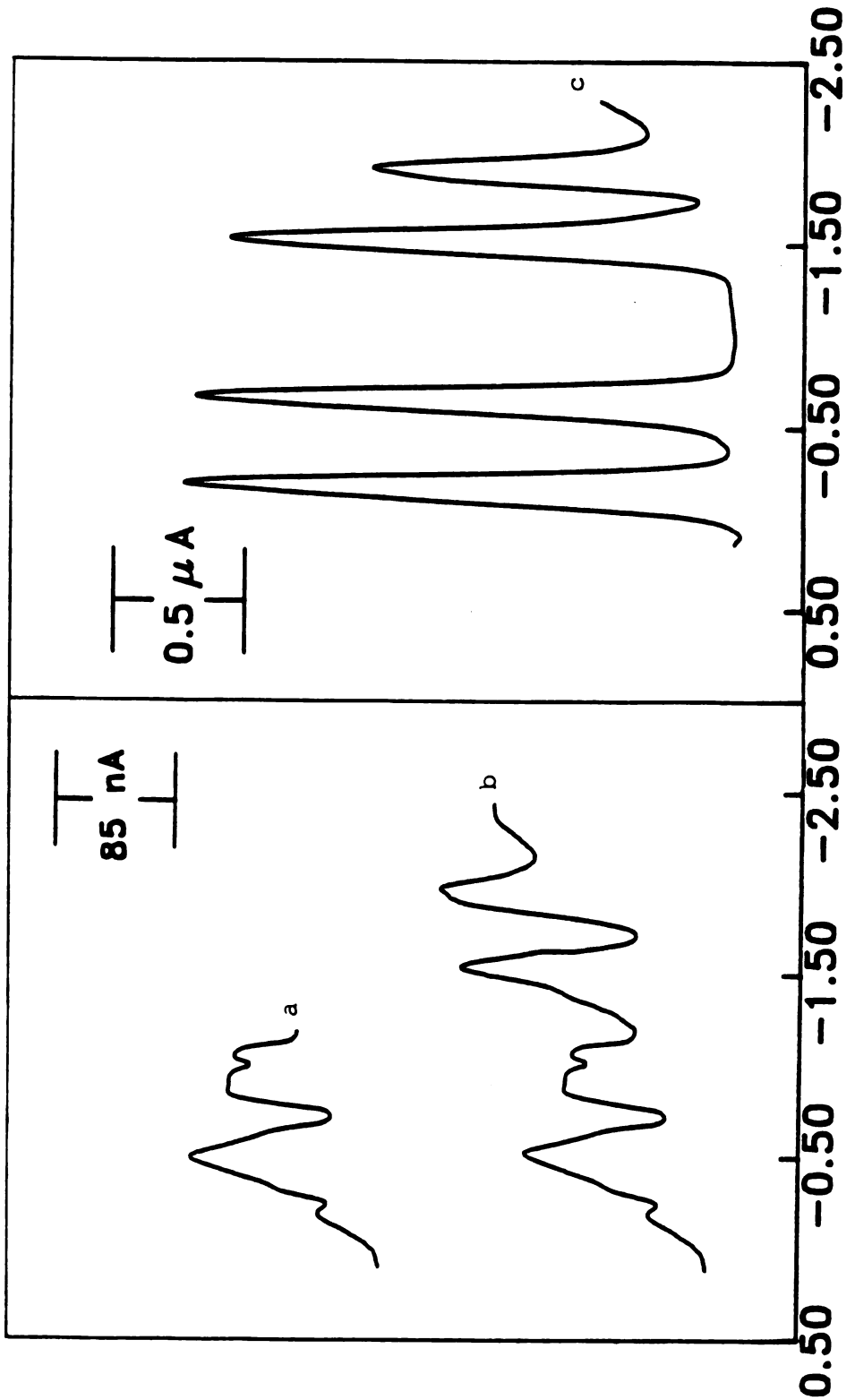
85 nA
0.5 μA
a
b
c
0.50
-0.50
-1.50
-2.50
0.50
-0.50
-1.50
-2.50
potential (volts vs SSCE)

FIGURE 22

severely alters the voltammograms. The two new peaks are believed to arise from the decomposition products and are similar to those observed in the DPV of the dihydroxy(tetra-t-butylphthalocyaninato)germanium monomer. DPV taken after each CPC cycle along the doping profile confirm that the polymer is stable up to -1.45 V and decomposes into monomeric type units at more negative potentials (Figure 22c).

3.4 Electrochemical characterization of dihydroxy(tetra-t-butylphthalo cyaninato)germanium

The decomposition of the polymer upon reduction of more than 100% to monomeric type redox species leads to a detailed investigation of dihydroxy(tetra-t-butylphthalocyaninato)germanium, the monomeric precursor to the polymer. Shown in Figure 23 are the CV and DPV voltammograms for its reduction. The first three peaks at $E_{1/2}$ = -0.29 V, -0.77 V and -1.63 V are characteristic of consecutive one-electron Nernstian reductions. Reversibility of reactions assigned by these peaks and stability of the resulting products are indicated by peak splitting of about 60 mV, peak current ratio of approximate unity and constant $i_{pc} / v^{1/2}$ values for potential scan rates between 50 mV sec^{-1} and 200 mV sec^{-1}. The product of the fourth reduction appears to be unstable on the voltammetric timescale. The oxidation wave following potential reversal is absent for that process. CPC studies also indicate that the polymer can be reduced stepwise to form a stable anion, dianion and trianion. Each process gives a n value of 1.0 + 0.01 for both the initial reduction and oxidation back to the starting material. DPV taken after each CPC cycle (Figure 24) are identical to those of the virgin material (Figure 22b), indicating stability of all four oxidation states (0 to 3-) on the CPC timescale.

Figure 23. Cyclic (a) and differential pulse (b) voltammogram of a 881 μM solution of t-Bu_4PcGe$(OH)_2$/0.2 M $TBABF_4$ in THF. The experimental conditions were the same as above (Figures 10 and 22).

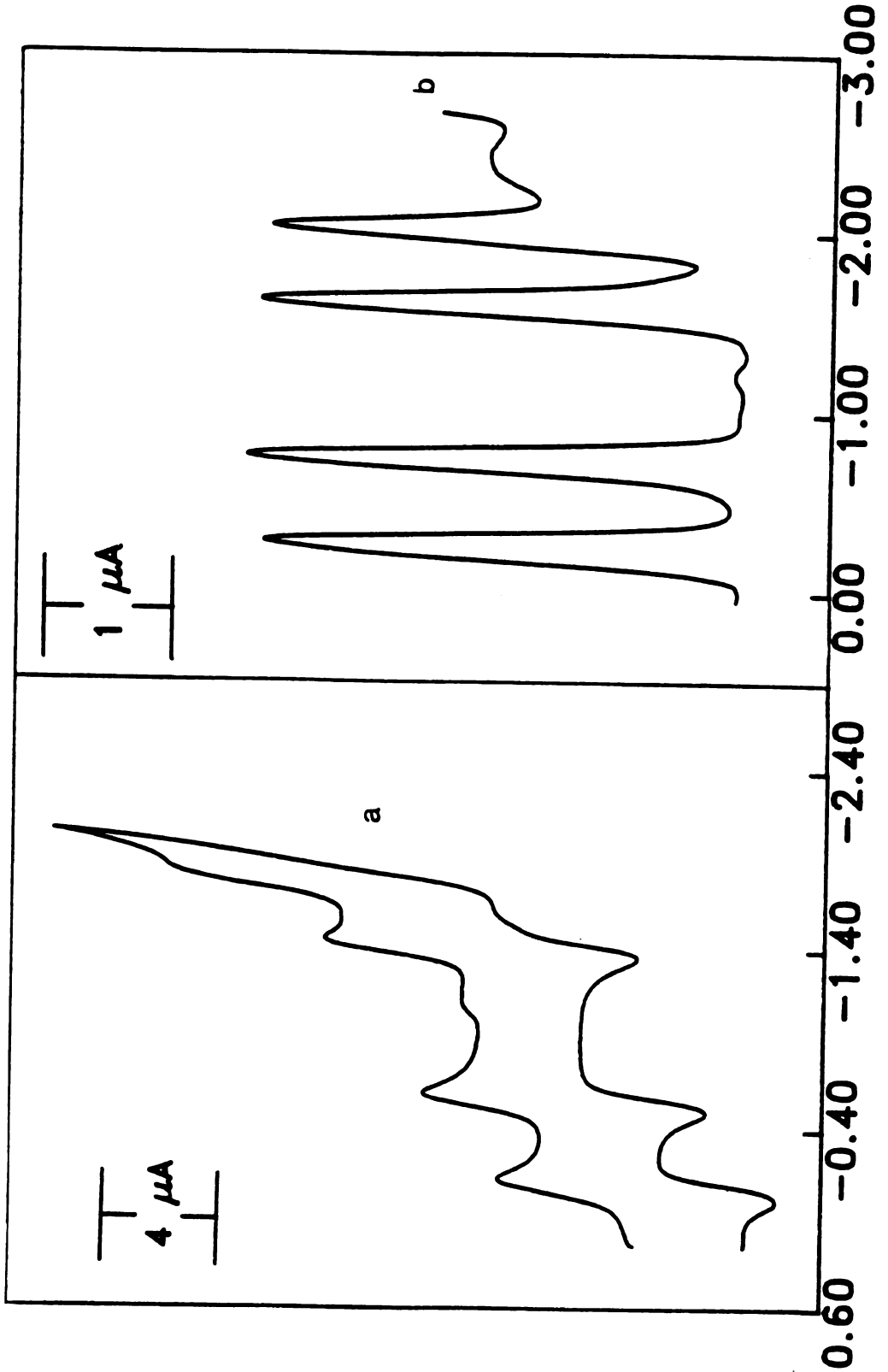
4 μA
a
1 μA
b
0.60
-0.40
-1.40
-2.40
0.00
-1.00
-2.00
-3.00
potential (volts vs SSCE)

FIGURE 23

Figure 24. Differential pulse voltammograms for the reduction of a solution of 881 μM t-$Bu_4PcGe(OH)_2$/0.2 M $TBABF_4$ in THF. The experimental conditions are identical to the ones of Figure 22.

a. virgin monomer solution

b. monomer solution after CPC reduction at -0.50 V and oxidation back at 0.20 V

c. monomer solution after CPC reduction at -1.00 V and oxidation back at 0.20 V

d. monomer solution after CPC reduction at -1.70 V and oxidation back at 0.20 V

e. monomer solution after CPC reduction at -1.85 V and oxidation back at 0.20 V

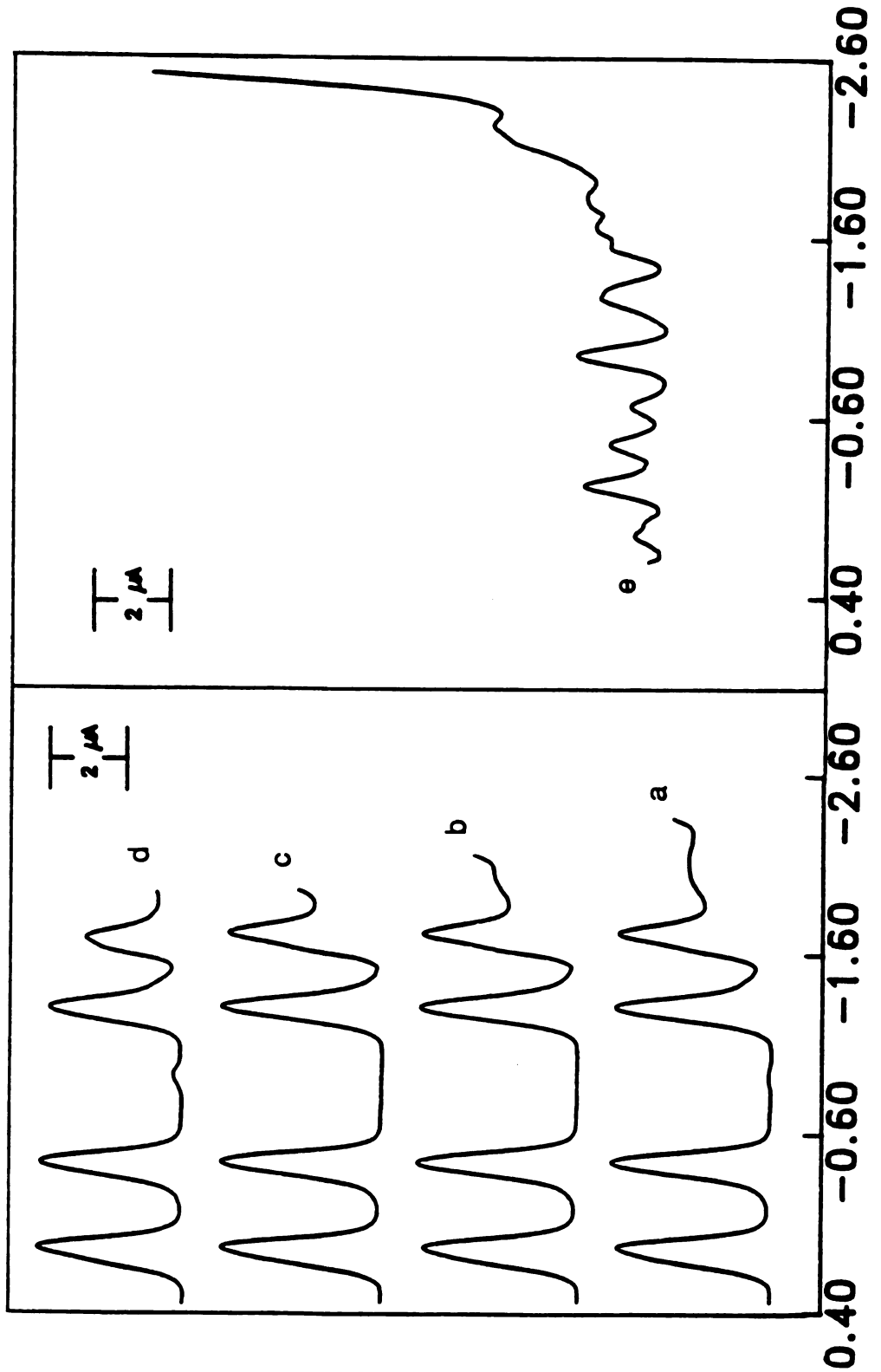
2 μA
d
c
b
a
0.40
-0.60
-1.60
-2.60
2 μA
e
0.40
-0.60
-1.60
-2.60
potential (volts vs SSCE)

FIGURE 24

A diffusion coefficient of 7.5 10^{-7} cm^2 sec^{-1} for the neutral monomer was calculated from its RDE voltammogram. The value is similar to that measured for other monomeric phthalocyanines taking into account differences in solvent viscosities. From the diffusion coefficient of the monomer and that of the corresponding polymer a degree of polymerization of 15 was found for the μ-oxo-(tetra-t-butylphthalocyaninato)germanium. This value of degree of polymerization along with other parameters provided a basis for modelling the current-potential DPV response of the polymer.

3.4 Digital simulations

To help elucidate the complex reductive chemistry of the μ-oxo-(tetra-t-butylphthalocyaninato)germanium, digital simulations of the electrochemical response were undertaken. Controlled potential coulometry and rotating disk voltammetry data suggest that the polymer undergoes Nernstian reduction responses at all potentials over the 1.45 V range in which it is chemically stable and that at -1.45 V each redox site comprising the polymer has undergone a one-electron reduction. Therefore, the reduction of the germanium polymer was modelled as a series of Nernstian one-electron redox couple reactions in equilibrium with one another. Shown in Figure 25b is the simulated differential pulse voltammogram for the reduction of the polymer over which it is stable. The parameters used in the simulations such as the electrode area, concentration of the polymer along with other parameters specific to the technique employed were chosen as identical to the ones used to obtain the experimental data. The degree of polymerization was taken as 15 based on the diffusion coefficient of the polymer. The standard potentials (E_j^0) were carefully chosen to "map out" the experimental response obtained for the reduction of the germanium polymer. The

Figure 25. Experimental (a) and simulated (b) differential pulse voltammongrams of a 50.1 μM solution of $[t\text{-}Bu_4PcGeO]_n$/0.2 M $TBABF_4$ in THF. Both the simulation and experimental conditions are identical to the ones of Figure 22. The standard potentials used to model the system are represented by the vertical lines on the potential axis.

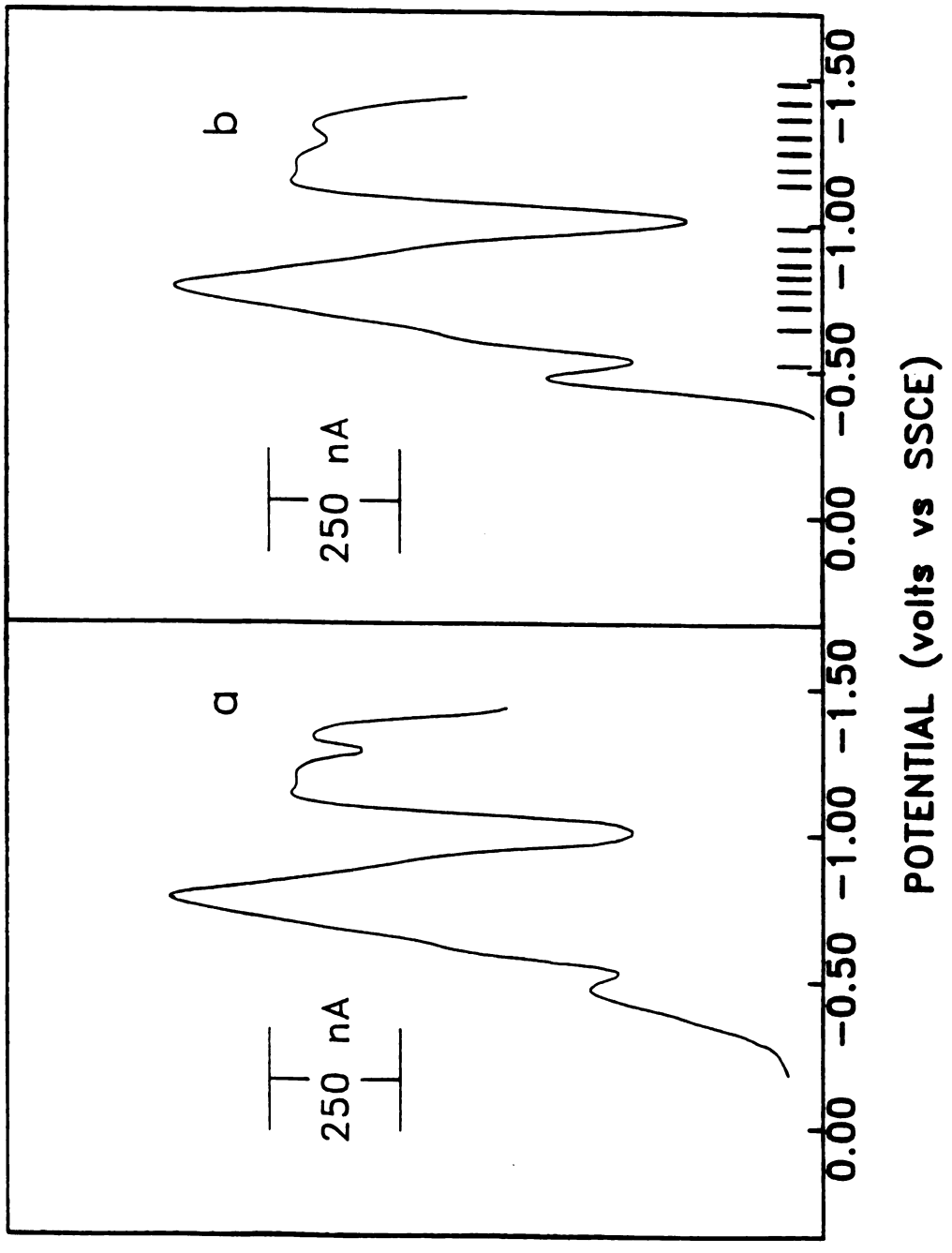
a
b
250 nA
250 nA
0.00
-0.50
-1.00
-1.50
0.00
-0.50
-1.00
-1.50
POTENTIAL (volts vs SSCE)

FIGURE 25

values of these standard potentials are represented as vertical bars on the potential axis. Both the magnitude and the shape of the simulated differential pulse voltammogram are similar with the observed one (Figure 25a). The huge peak seen at -1.65 V appears to be formed by several closely spaced redox centers. It was observed that small variations in the standard potential values caused significent changes in the shape and magnitude of the simulated current response. The fact that the standard potential values are very close to one another indicate the existence of a large amount of interaction between the redox sites. From the simulated differential pulse voltammogram, the percent reduction vs potential profile was determined for the germanium polymer. Simulated data closely match the experimental CPC and RDE results (Figure 26).

Digital simulations of the electrochemical response were also used to determine the mechanism and rate of the decomposition reaction of the germanium polymer. Shown in Figure 20d,e,f are the simulated RDE, RRE and RRDE voltammograms over the potential range in which the polymer is stable. These simulated voltammograms are nearly identical in shape and magnitude with the those obtained experimentally (Figure 20a,b,c). As predicted by equation 9, $(i_R^0 - i_R) / i_d$ is a constant at all potentials over the 1.45 V range and equal to N suggesting that the polymer is chemically stable at potentials positive of -1.45 V (Figure 27a). When including the decomposition process (E_nCEE mechanism) into the simulation program, the $(i_R^0 - i_R) / i_d$ expression deviates from N. Shown in Figure 27b,c is the $[(i_R^0 - i_R) / i_d] - N$ term vs potential plot obtained from the simulated shielding-collection experiments for a decomposition rate constant of 20 sec^{-1} at a disk potential of -1.65 V (216% reduction) and -2.16 V (300% reduction). At -1.65 V, the monomeric anion resulting from the

Figure 26. Degree of partial reduction vs potential determined by controlled potential coulometry, rotating disk voltametry and digital simulation.

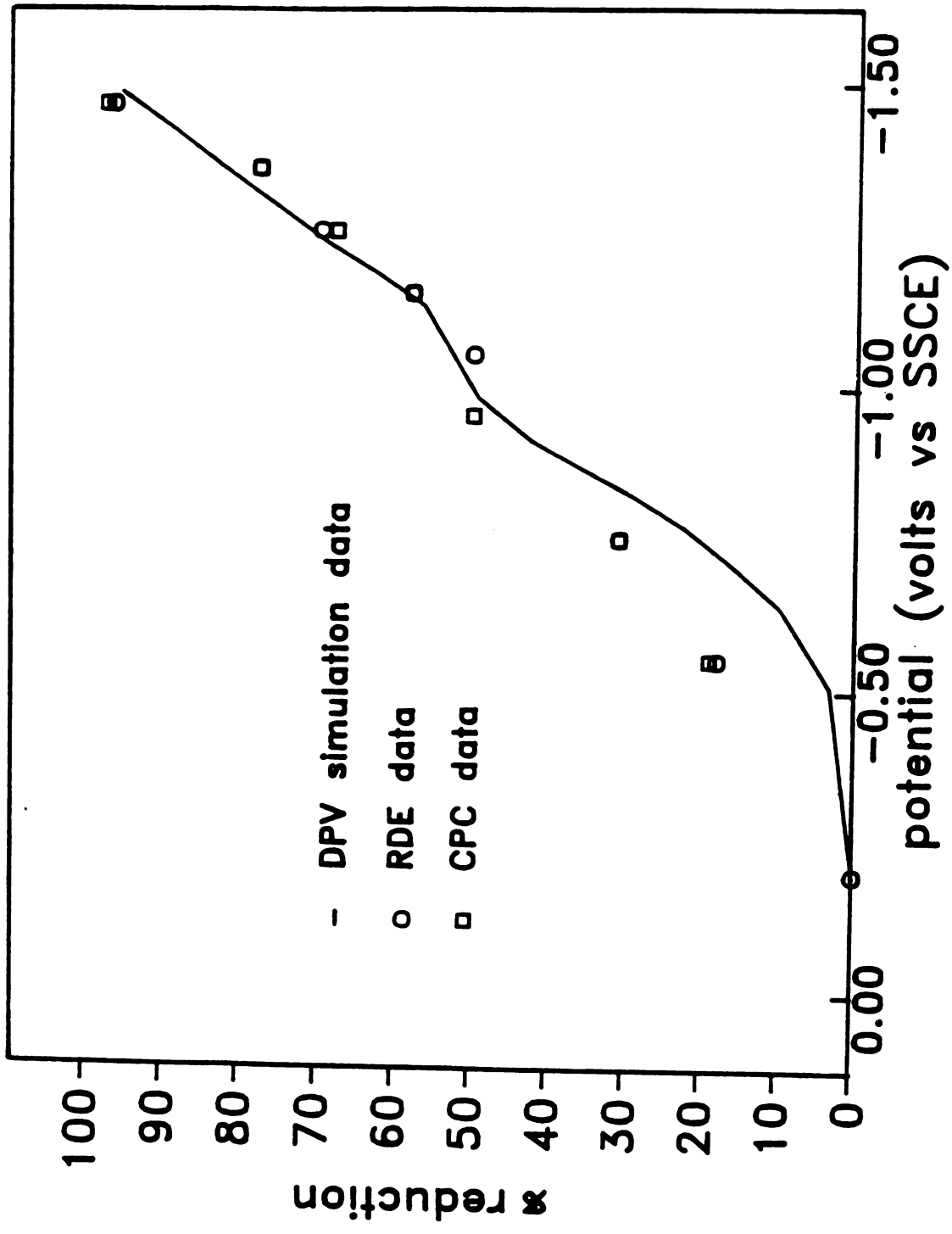
% reduction
100
90
80
70
60
50
40
30
20
10
0
0.00
-0.50
-1.00
-1.50
potential (volts vs SSCE)
DPV simulation data
RDE data
CPC data

FIGURE 26

Figure 27. Simulated continuous shielding-collection plots for the reduction of $[t\text{-}Bu_4PcGeO]_n/TBABF_4$ in THR at various disk potentials. The rotation rate was 2000 rpm. Then simulated data are based on the assumption of the E_nCEE mechanism. The % reduction of the listed potentials are as follows: -1.45V = 100% reduction; -1.64V = 226% reduction and -2.16V = 300% reduction.

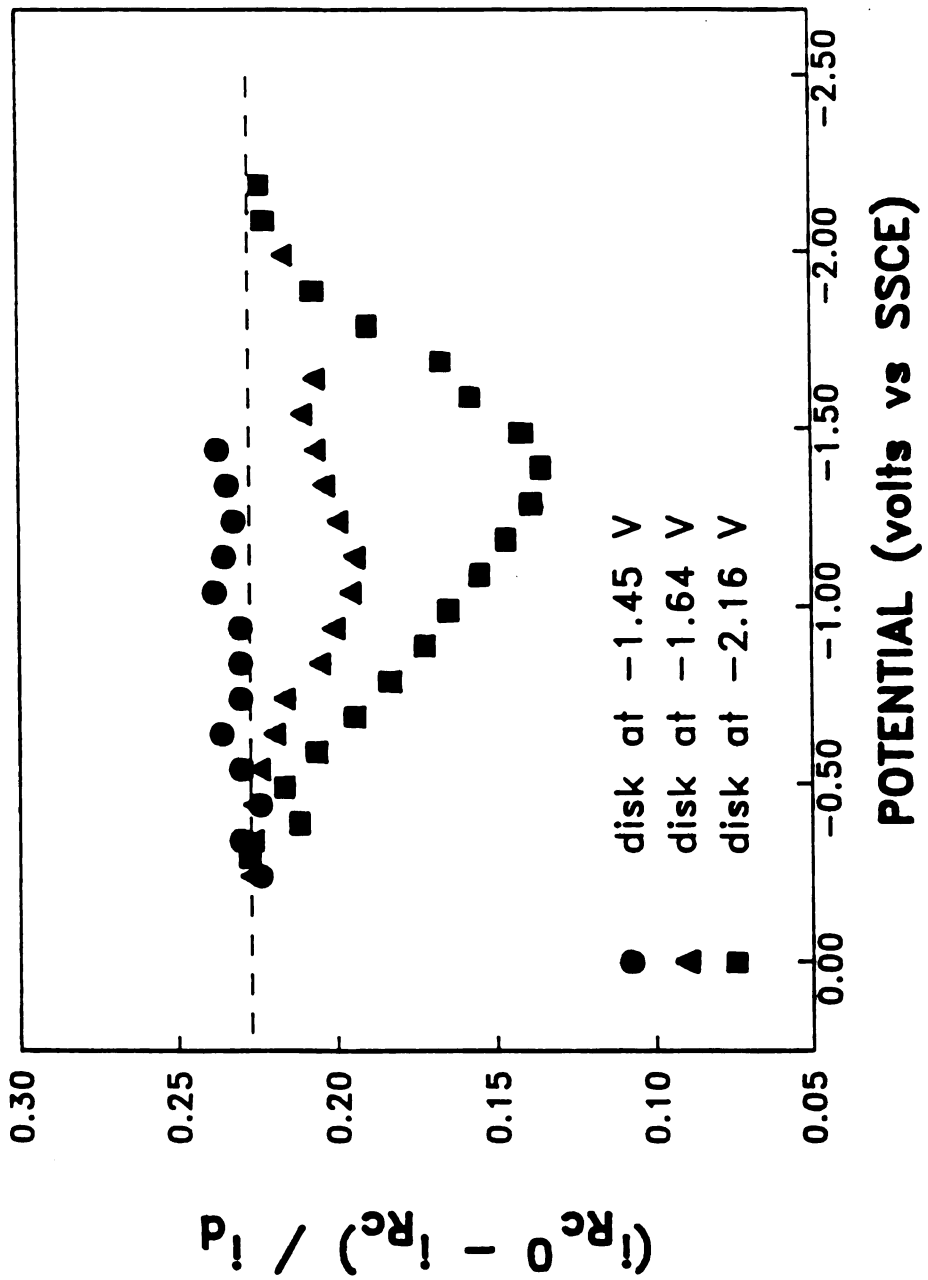
0.30
0.25
0.20
0.15
0.10
0.05
0.00
−0.50
−1.00
−1.50
−2.00
−2.50
POTENTIAL (volts vs SSCE)
disk at −1.45 V
disk at −1.64 V
disk at −2.16 V
(i_RC^0 − i_RC) / i_d

FIGURE 27

decomposition of the polymer is reduced into the dianion and at -2.16 V it is further reduced into the trianion. Good agreement was observed between experimental and simulated results. This allows a better understanding of the reductive chemistry of the μ-oxo-(tetra-t-butylphthalocyaninato)germanium.

4. STUDYING THE ELECTRICAL CONDUCTIVITY AND SPECTROSCOPIC PROPERTIES AS FUNCTION OF BAND FILLING FOR THE SOLUBLE POLY(3,4-DIBUTYLTHIOPHENE)

4.1 Introduction

In our laboratory, we also are interesting in the synthesis and characterization of soluble analogs of conventional conducting organic polymers. Our efforts have focussed on thiophene derivative systems. Polymers of this type have been extensively studied in the solid state[14a,17a-p,45]. The majority of the work has been performed on thin films attached directly to the electrode surface and free-standing films. These materials are generally prepared by simply oxidizing the corresponding monomer. Polymerization occurs via a cation radical coupling mechanism that involves elimination of predominantly α protons. Chain growth is believed to be terminated by either steric hindrance or end group unreactivity[12,14]. The factors dictating the nature of the resulting materials remain poorly understood and largely uncontrolable. In addition, they are significantly influenced by the complications arising from the solid state. Little, if any, influence over the characteristics of these polymers has been possible.

Substituted polythiophenes that are soluble in both aqueous and nonaqueous solvents have recently appeared[17b-q]. Solubility in organic solvents is achieved by the presence of alkyl or substituted alkyl chain on 3-position of the thiophene ring. However, addition of alkyl group on 3-position does not prevent crosslinking polymerization to occur. In order to eliminate this undesirable effect, polydialkylthiophenes have been synthesized. The presence of alkyl groups in 3- and 4-position forces polymerization to occur selectively in 2- and 5-position,

leading to a more structurally regular polymer with mainly α α' linkages. Another way of to enhance the selectivity of these α α' linkages consists in synthesizing polydisubstitutedthiophenes by polymerization of β-disubstituted oligomeric thiophene instead of the common monomer. The presence of the alkyl groups in 3- and 4-position also improves the solubility of these polymers, allowing them to be studied in solution. In this study, the redox properties of poly(3,4-dibutylthiophene) will be investigated. Since this new polymer is soluble both in its oxidized and neutral (undoped) form, the study will be performed in solution using a variety of conventional analytical techniques. Electrochemical techniques (CV, DPV, and CPC) will be employed to characterize this polymer when it is oxidized to various degrees. Unlike doping performed on thin films where the degree of band-filling is influenced or limited by the structure of the material, this soluble polymer may be able to be oxidized to any level ranging from 0 to 100%. Electrical and optical measurements will be used to investigate how the collective properties of this conducting polymer vary as function of band-filling. Optical absorption studies have proven useful in characterizing the basic electronic structure and the nature of the charge carriers of conducting organic polymers. The appearance of mid-bandgap transitions as degree of band-filling is varied will provide direct evidence for polarons and/or bipolarons. Conductivity also will be performed when varying the degree of band-filling. Information on chemical stability upon doping will be provided using a combination of electrochemical and spectroscopic techniques. It will be the first time that the same probe system will be simultaneously investigated in solution and on an electrode surface. Finally, comparison with other derivative thiophene systems such as poly(3',4'-dibutyl-α-terthiophene) and poly(3",4"-dibutylquinquethiophene) which differ in the number of thiophenes present in the repeat unit will help in searching for new conducting materials with predictable and tunable properties.

4.2 Synthesis

Synthesis of monomeric and polymeric 3,4-dibutylthiophene

3,4-Dibutylthiophene was prepared according to the method described by Kumada et al[46]. The stepwise synthesis is outlined in Scheme 2. Commercially available thiophene was easily brominated and then selectively debrominated to form 3,4-dibromothiophene[47]. This halothiophene, in the presence of catalytic amounts of a nickel-phosphine complex was readily alkylated vith butyl magnesium bromide (Grignard reagent) resulting in the formation of the 3,4-dibutylthiophene, the basic building block of the polymer.

Scheme II. Chemical preparation of 3,4-dibutylthiophene

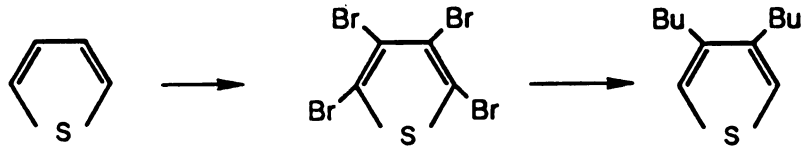

a. $Br_2/CHCl_3$

b. $nBuLi/Et_2O$

c. 2 $BuMgBr/Ni(dppp)Cl_2$ (dppp = 1,3-bis(diphenylphosphino)propane)

Very pure 3,4-dibutylthiophene was obtained by following this route. The ^1H-NMR spectrum of this compound shows peaks at 0.94, 1.40, and 1.61 ppm which were assigned to the methyl and methylene groups of the butyl substituent. A peak much further downfield at 7.00 ppm assigned to the aromatic hydrogen located at the α-positions of the thiophene (Figure 28).

The synthesis of poly(3,4-dibutylthiophene) was achieved by electrochemical oxidative polymerization of the above described monomer. The

Figure 28. ^{1} H-NMR spectrum of 3.4 Dibutylthiophene in CD_3COCD_3. The peak at 2.04 ppm is due to the residual solvent.

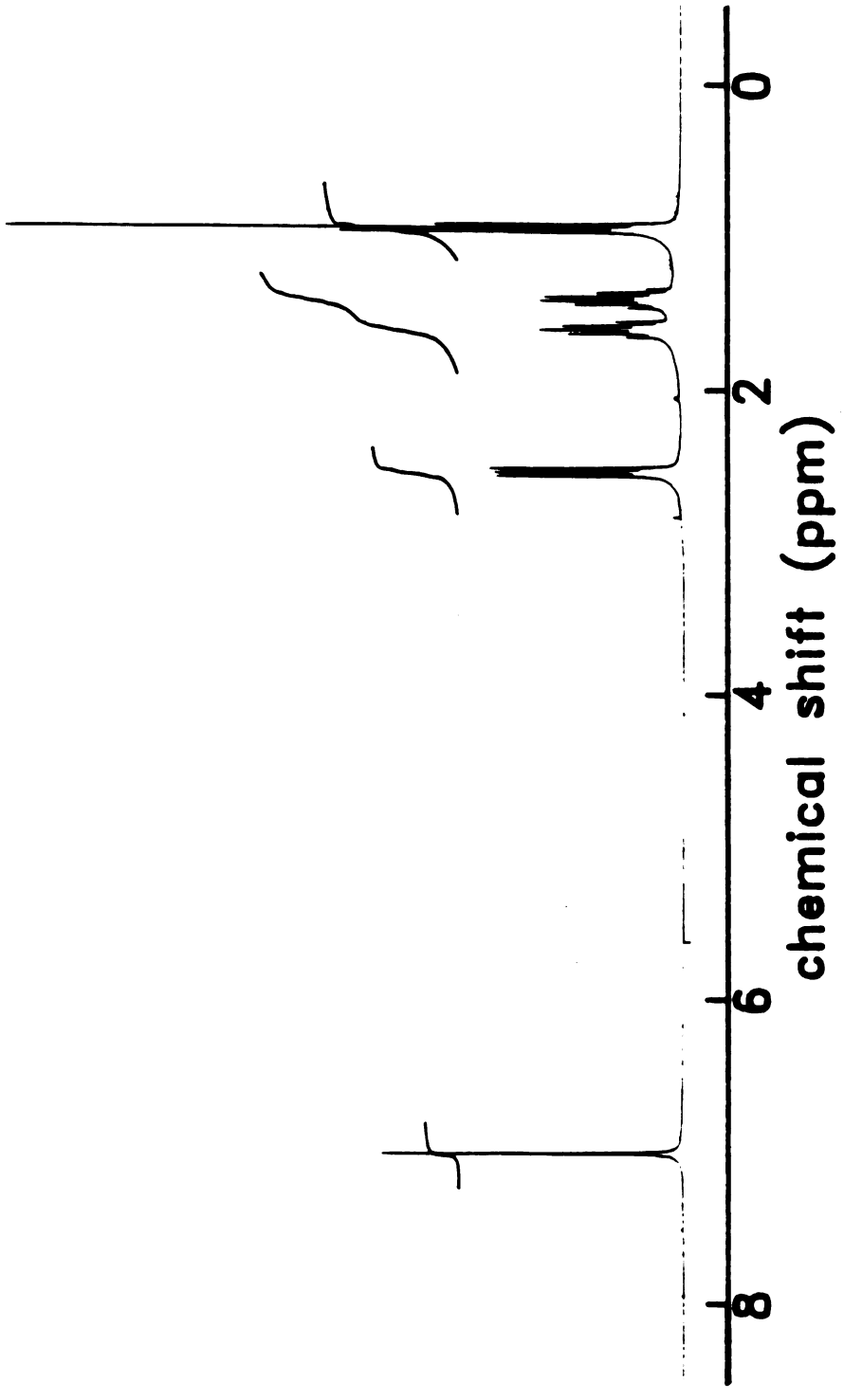

FIGURE 28

electrochemical approach was preferred over the synthetic one because of its simpler and cleaner method of preparation. With chemical synthesis, low molecular weight polymers, structural defects, and/or impurities are generally obtained. The mechanism proposed for the disubstituted thiophene polymerization is a general scheme for the electrochemical process of heterocycles (Scheme 3)[22]. The coupling step of two identical, monomer radical cations produces an intermediate dication which, upon loss of two protons, yields the neutral dimer (step 2). The high concentration of the monomer radical cation maintained near the electrode surface allows for the continued coupling with the oligomer radical cation (step 3 and 4). The overall reaction is referred to as an $E(CE)_n$ type mechanism, i.e., an electron transfer reaction (E) followed by a cascade of chemical (C) and electron transfer (E) reactions. Poly(3,4-dibutylthiophene) was electrochemically generated in nitromethane containing 2.5 10^{-2} M monomer and 2.5 10^{-2} M supporting electrolyte ($TBABF_4$). The reaction vessel was a one-compartment cell as described previously using a platinum flag electrode as working electrode. A potential sweep technique (CV) was used for the anodic film growth. The growth of the disubstituted polythiophene film is illustrated through a series of repetitive cyclic voltammograms (Figure 29). During the first sweep, a broad, irreversible oxidation peak which corresponds to the formation of the monomer radical cation is observed at E_{pa} = 1.77 V. The amount of energy required for the oxidation of the β-disubstituted thiophene is about the same as that for the oxidation of the unsubstituted thiophene, but much higher than that for the oxidation of the β-monosubstituted thiophene[48]. In other words, the steric hindrance effect is more important than the electronic effect for β-disubstituted thiophene, thus rendering polymerization more difficult[49]. The fact that the peak is irreversible suggests that the intermediate species was unstable and rather reactive[50]. At a

Scheme III. Mechanism of the electrochemical polymerization reaction for thiophene deriviatives.

1) 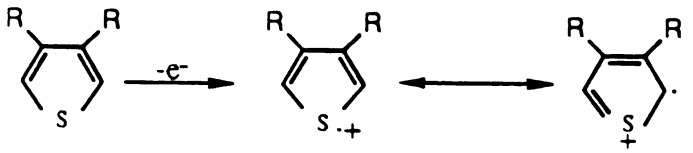

2) 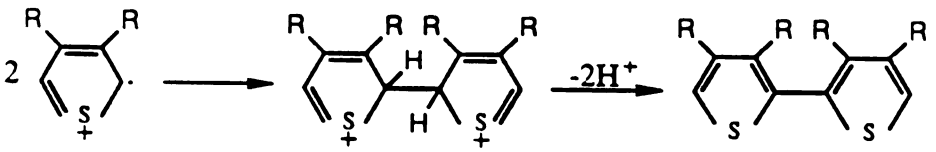

3) 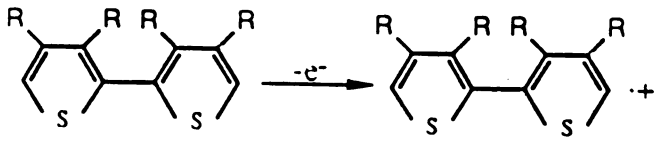

4) 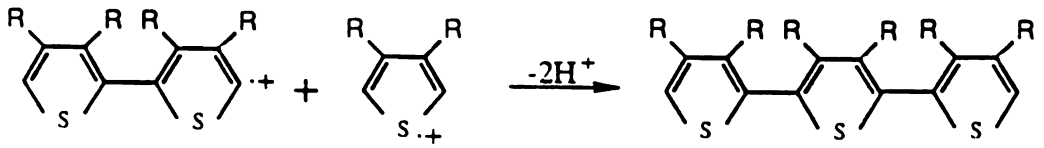

overall reaction

(x) 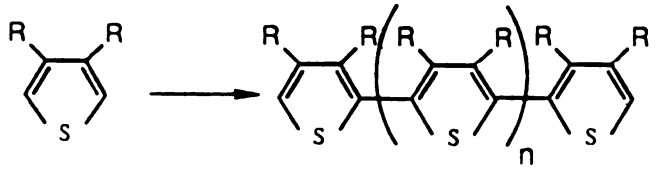

SCHEME III

Figure 29. Repetitive cyclic voltammograms for the polymerization of a 25 mM solution of 3,4-Dibutylthiophene/0.02M $TBAGF_4$ in CH_3NO_2 at a sweep rate of 50 mV sec^{-1}.

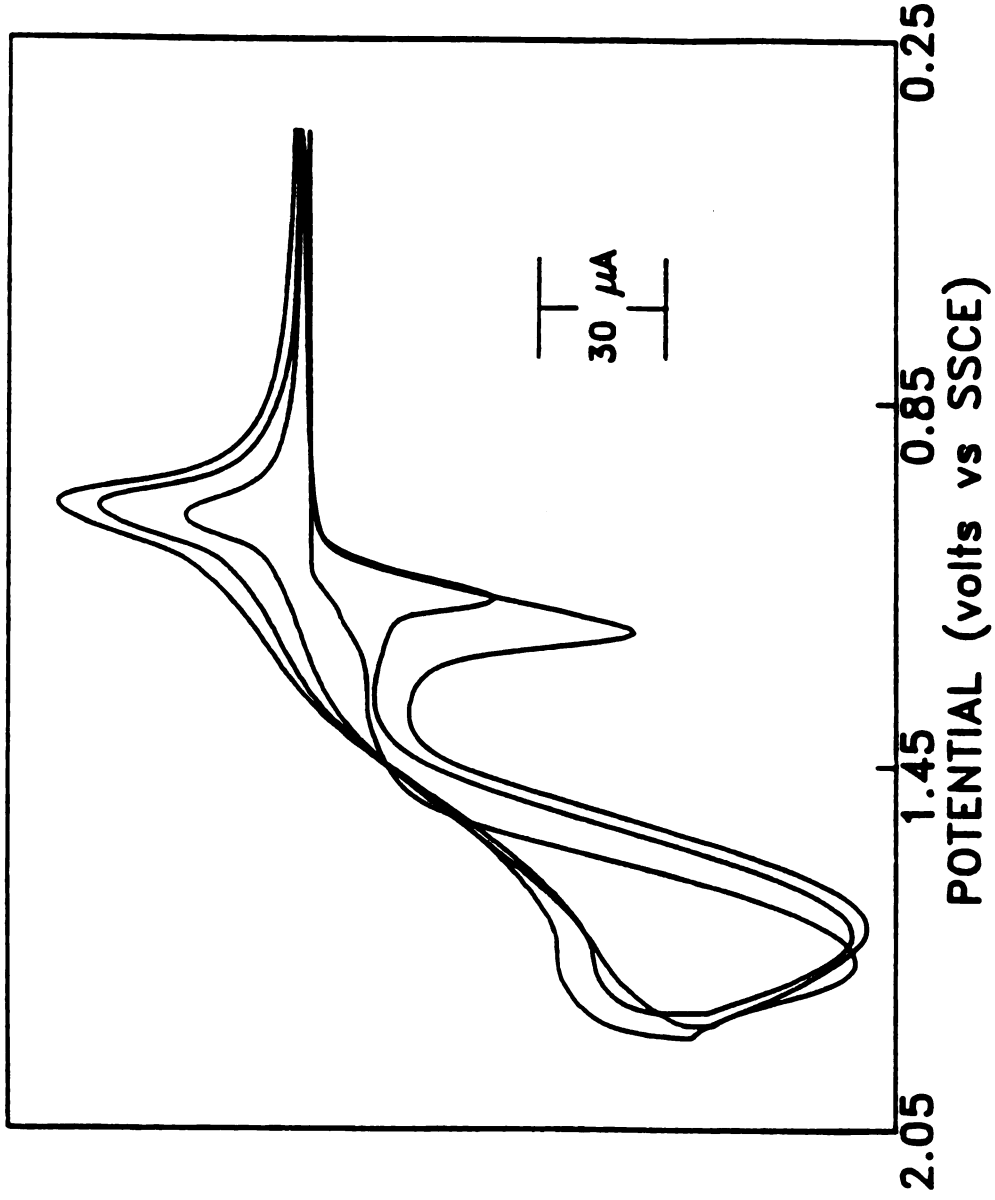

FIGURE 29

few millivolts more anodic than the oxidation potential of the monomer, the potential scan was reversed, and a reduction peak assigned to the reduction of the oxidized polymer is observed at $E_{pc} = 1.04$ V. In successive cyclic voltammograms, the intensities of the reduction and corresponding oxidation peaks of the polymer regularly increase with the number of cycles revealing the continuous growth of the polymer film without any loss in electroactivity. This was confirmed by observing the electrode surface which became progressively covered with thicker and thicker polymer films. Good quality film and high conductivity were obtained for polymer film thickness in the 1-3 μm range as measured using a profiler. The redox process occurring during the electropolymerization was accompanied by a reversible change in color. The polymer, yellowish in its neutral form, turned transparent dark blue when oxidized. This is due to a solvatochromic effect involving a conformational change of the polymer backbone during the charging/discharging process[24c]. In the charging step, the molecular chain with its twisted units becomes less planar, and after discharging, the system returns to its original state of ordered twisting. After electrochemical synthesis, the polymer was peeled from the electrode and washed with acetonitrile to remove any residual monomer, small size oligomers, or supporting electrolyte and then dried under high vacuum at room temperature for several hours. The resulting polymer was characterized by its FTIR and NMR spectra (Figures 30 and 31). It appears to have a regular linear structure with predominant α α' linkages. This hypothesis was supported by the lack of polymerization in 3- and 4-position due to the blockage of these two positions by butyl groups which would require too much energy for the C-C bond between the thiophene and the butyl group to be broken. The addition of the butyl substituents on the thiophene ring mainly served in improving the solubility of the polythiophenes. Poly(3,4-dibutylthiophene) was found to be soluble in a large

Figure 30. Fourier transformed infra-red spectrum of poly (3,4-Dibutylthiophene) on KBr pressed pellet.

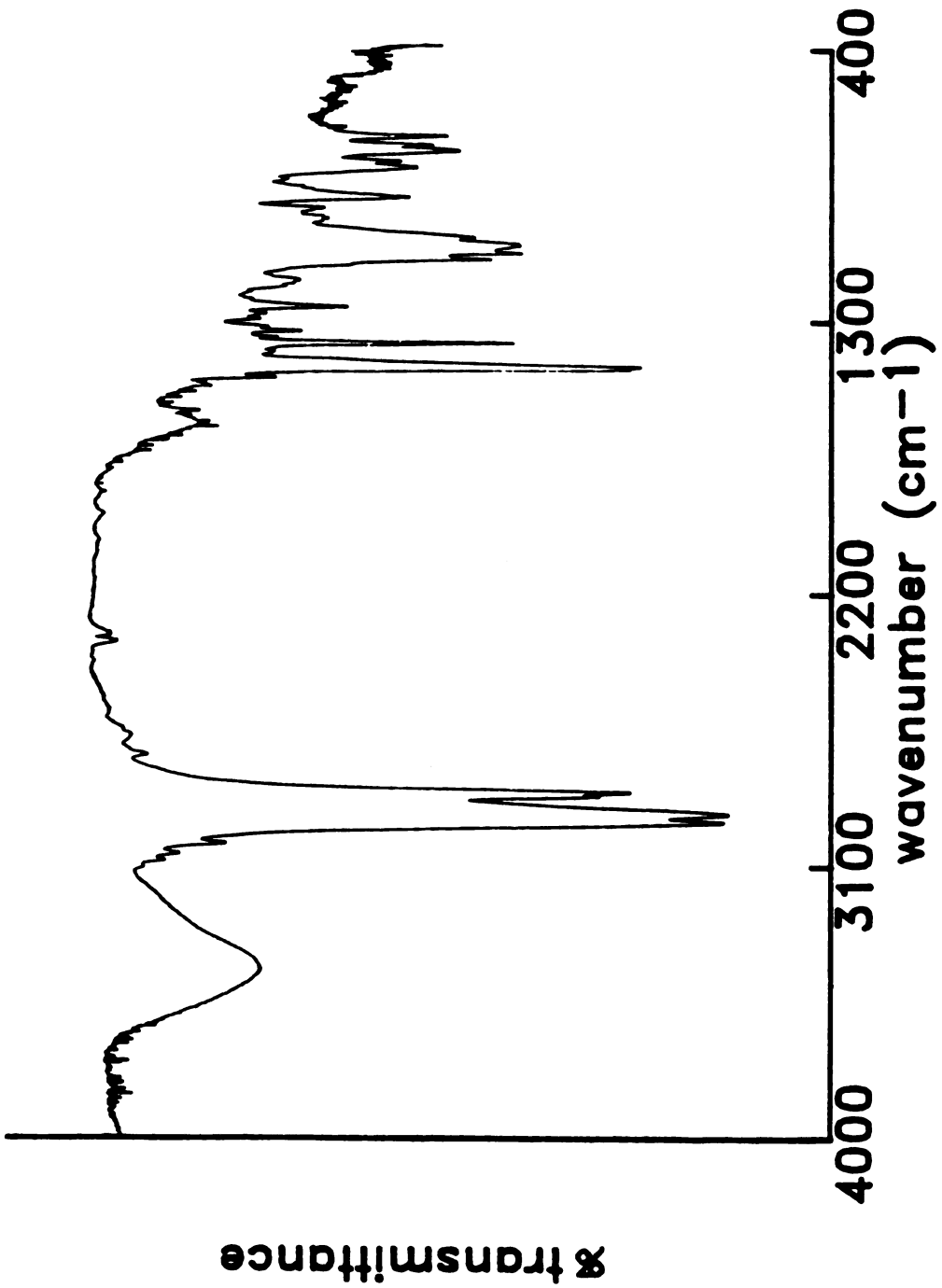

FIGURE 30

Figure 31. ^{1}H-NMR spectrum of poly(3,4-dibutylthiophene) in $CDCl_3$. The peak at 7.24 ppm is due to the solvent.

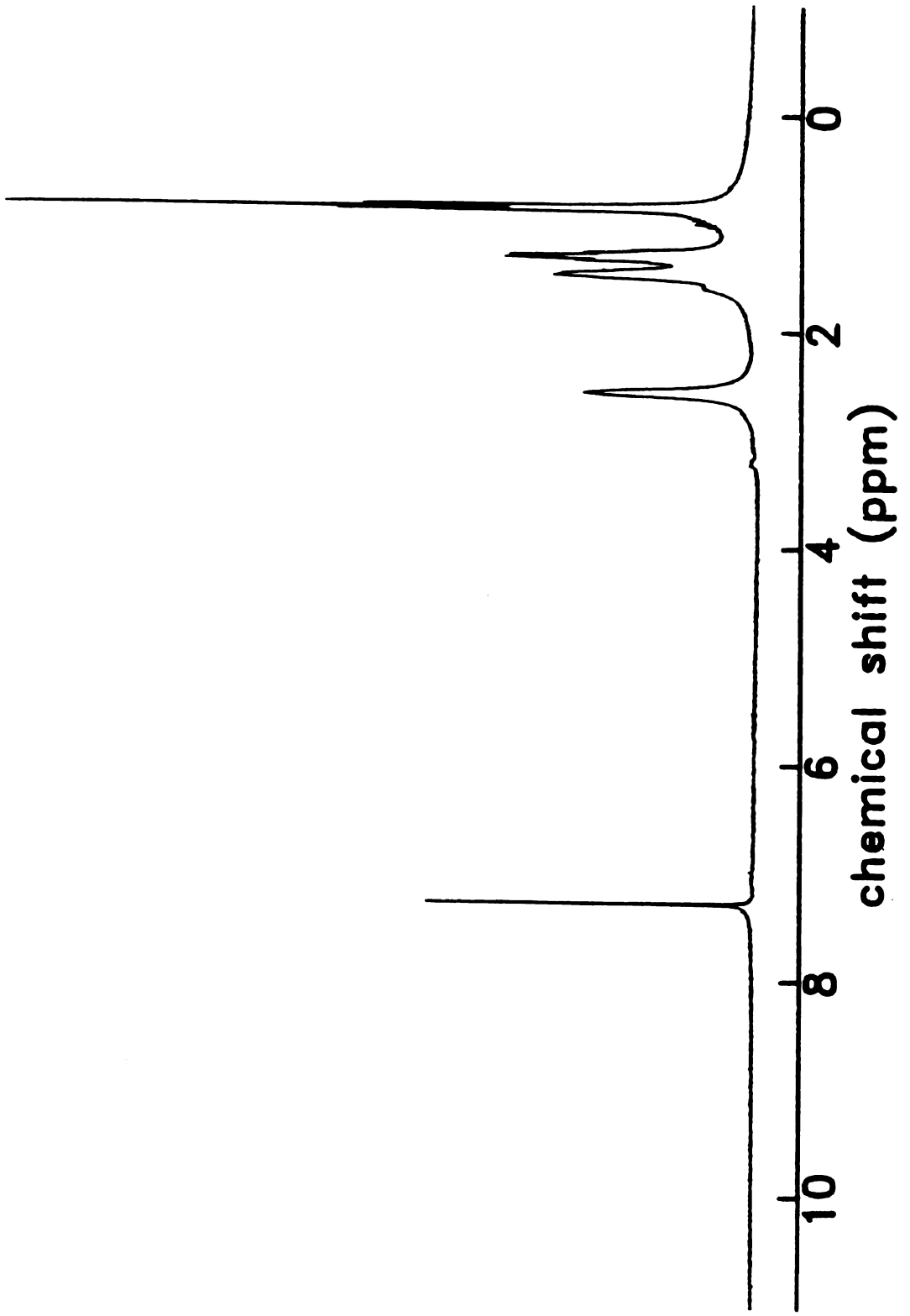

FIGURE 31

variety of organic solvents such as toluene, acetone, methylene chloride, and tetrahydrofuran, thus rendering possible the study of the electrical and physicochemical properties of this polymer in solution. Determination of the molecular weight of this electrochemically synthesized polymer by gel permeation chromatography using THF as eluent gave a mean value of 2000 against polystyrene standard which corresponds to a polymer of 10 units length (Figure 32). The sharpness of the chromatographic peak suggests that the synthesized poly(3,4-dibutylthiophene) has a narrow molecular weight distribution.

Figure 32. Gel permeation chromatogram of the poly(3,4-dibutyl thiophene) in THF. The flow rate is 1.5 ml min^{-1}.

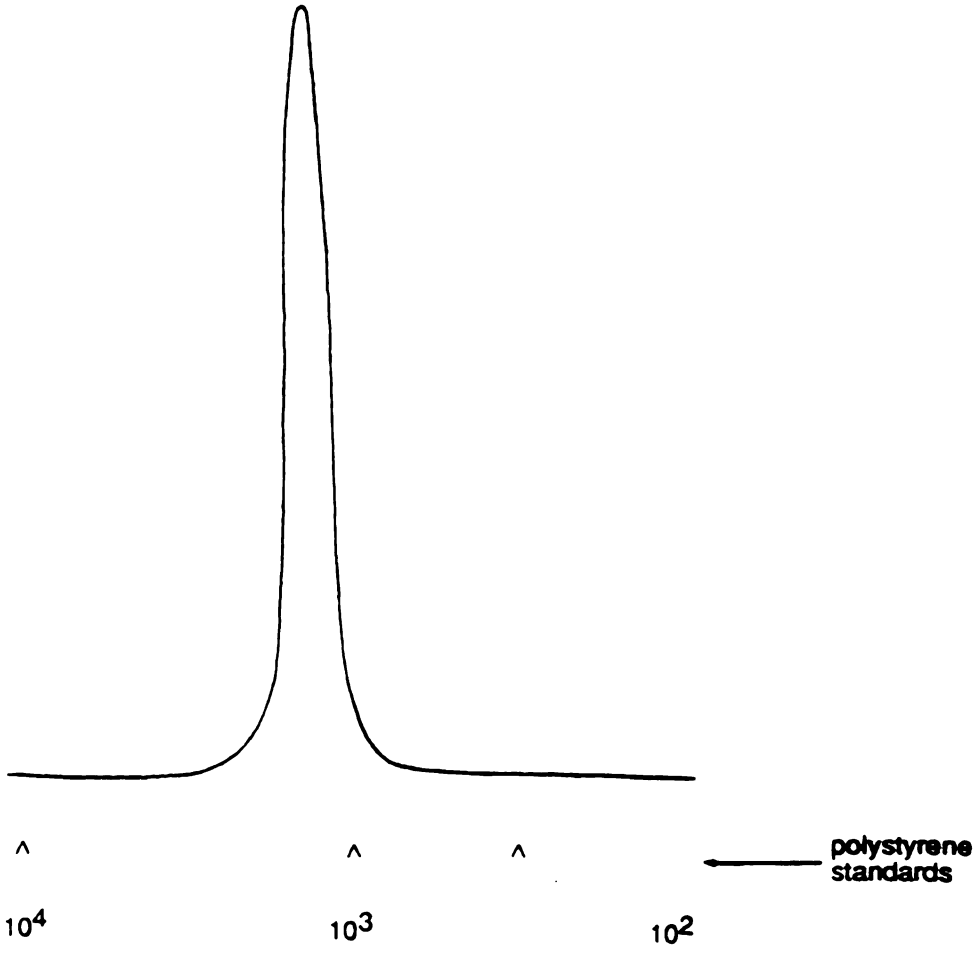

Synthesis of oligomeric and polymeric 3',4'-dibutyl-α-terthiophene

3',4'-Dibutyl-α-terthiophene was prepared following a method developed in our laboratory by M. Benz. 3,4-dibutylthiophene was first brominated using tetramethyl ammonium tribromide (TMAT). The resulting brominated thiophene reacted with two equivalents of thienyl magnesium bromide in presence of a nickel based catalysis to form 3',4'-dibutyl-α-terthiophene (Scheme 4).

Scheme IV. Chemical preparation of 3',4'-dibutyl-α-terthiophene

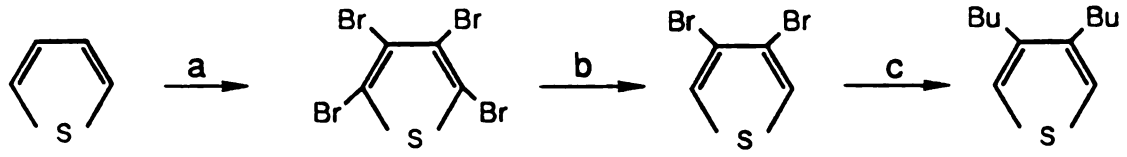

a. $TMAT/CH_3CO_2H/CH_2Cl_2$

b. $2\ C_4H_3SMgBr/Pd(dppp)Cl_2/Et_2O$

Electrochemical polymerization of 3',4'-dibutyl-α-terthiophene was carried out in acetonitrile using $5\ 10^{-3}$ M monomer and $2.5\ 10^{-2}$ M supporting electrolyte ($TBABF_4$). Figure 33 represents the successive cyclic voltammograms obtained in the course of the polymerization process. A comparison with the cyclic voltammograms obtained during the polymerization of the monomeric disubstituted thiophene shows a similar shape. As expected, the oxidation peak of the starting material is broader for longer chain length oligomers. This could be explained by the closeness of the E^0 values of the disubstituted and unsubstituted thiophenes. It also could be explained by a poor swelling of the material in acetonitrile. In addition, a decrease in the E_{pa} value of the starting material is observed. This indicates that polymerization of longer chain length oligomers is energetically favored. The polymerization process also was

Figure 33. Repetitive cyclic voltammograms for the polymerization of a 25 mM solution of 3',4'-Dibutyl-α-lerthiophene/0.02 M $TBABF_4$ in CH_3CN at a sweep rate of 50 mV sec^{-1}.

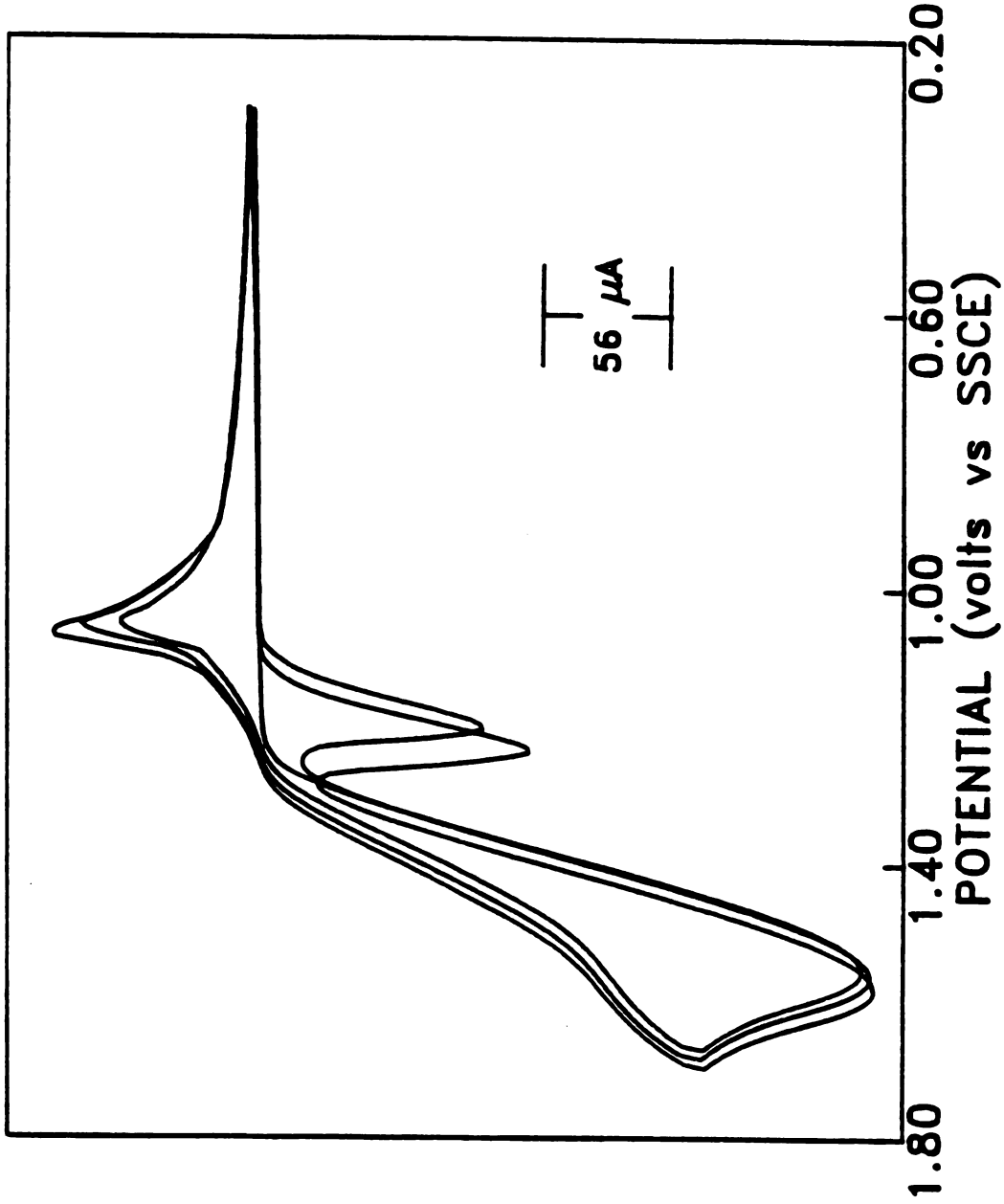

FIGURE 33

accompanied by a change in color from a bright red in the neutral state to a dark green in the oxidized state.

Synthesis of oligomeric and polymeric 3",4"-dibutylquinquethiophene

The last compounds studied in the disubstituted thiophene series were 3",4"-dibutylquinquethiophene and its corresponding polymer. 3",4"-dibutylquinquethiophene was synthesized following the same procedure as that employed for the preparation of 3',4'-dibutyl-α-terthiophene. This latter oligomer served as starting material. The electropolymerization of 3",4"-dibutylquinquethiophene also was performed in acetonitrile using 10^{-3} M monomer and 2.5 10^{-2} M supporting electrolyte ($TBABF_4$). Contrary to the cyclic voltammograms obtained during the polymerization of the substituted terthiophene, three distinctive oxidation waves accompanied with the corresponding, but not as well defined, reduction waves are observed (Figure 34). These waves are indicative of different redox processes. As expected, the oxidation of this oligomer started at a lower potential than those of smaller size oligomers. This confirms the idea that longer oligomers are easier to oxidize. The resulting polymer exhibits a reversible electrochromic behavior as it was cycled between a bright red color in the neutral state and a dark green color in the oxidized state.

4.3 Electrochemical characterization

The synthesized poly(3',4'-dibutylthiophene) film was characterized by its cyclic voltammogram (Figure 35a). A sharp intensive anodic wave is observed at 1.39 V, followed in the reverse scan by a broad peak potential-shift cathodic wave of low peak current height. The peak height of the anodic and

Figure 34. Repetitive cyclic volammogrames for the polymerization of a 2.5 mM solution of 3",4"-dibutylquinquethiophene/0.02M $TBABF_4$ in CH_3CN at a sweep rate of 50 mV sec^{-1}.

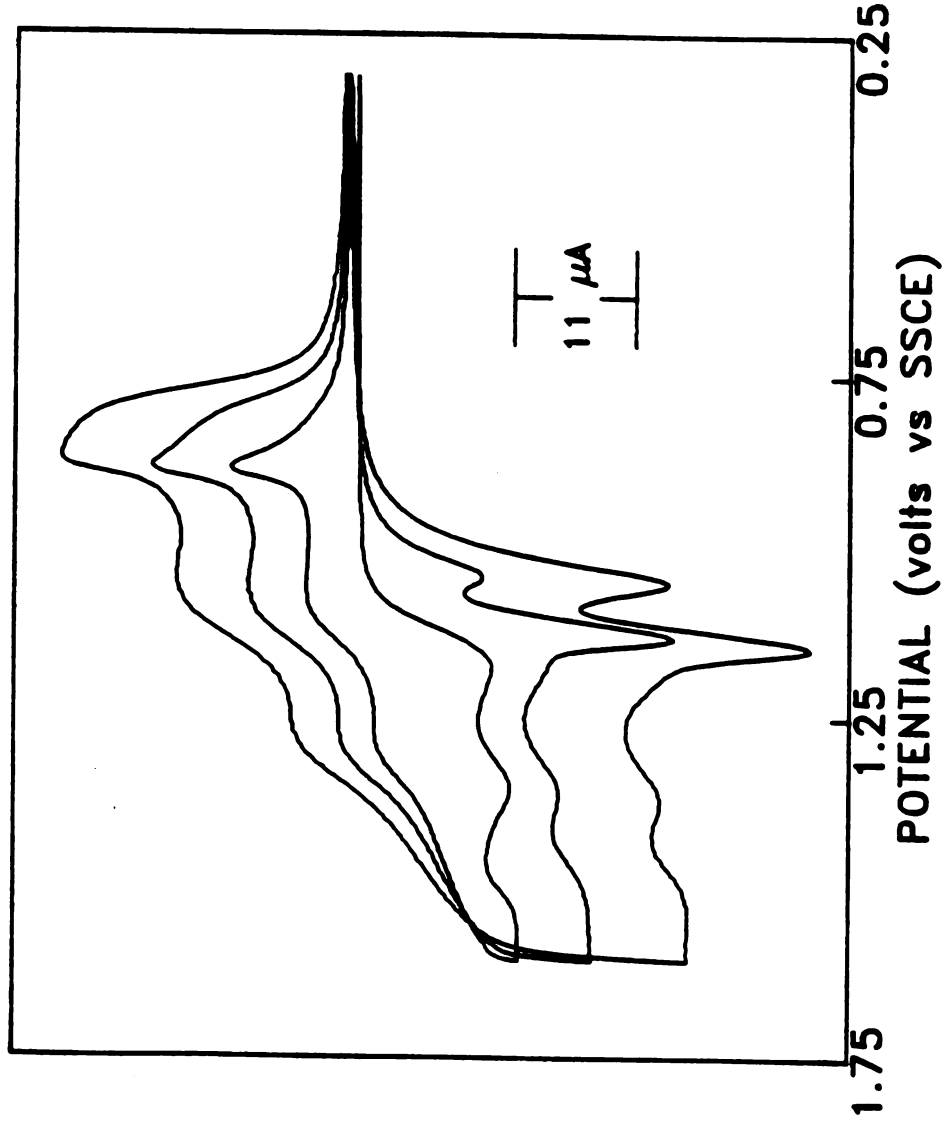

FIGURE 34

Figure 35. Cyclic voltammograms of poly (3,4-Dibutylthiophene) (a), poly (3',4'-Dibutyl-α-tethiophene) (b) and poly 3",4"-Dibutyloquinquethiophene) (c) as synthesized films in $CH_3CN/TBABF_4$. The sweep rate was 50 mV sec^{-1}.

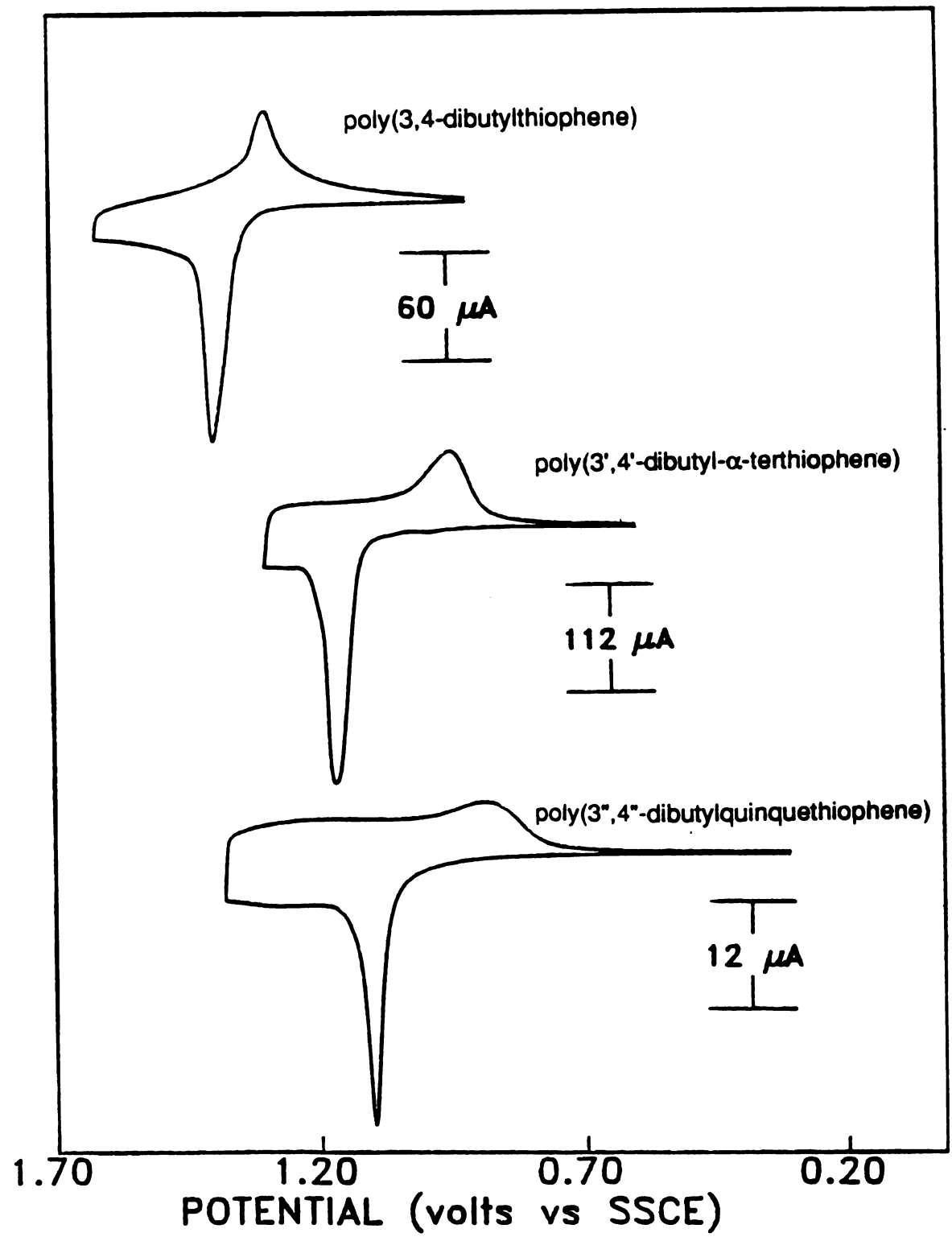
poly(3,4-dibutylthiophene)
60 μA
poly(3',4'-dibutyl-α-terthiophene)
112 μA
poly(3",4"-dibutylquinquethiophene)
12 μA
1.70
1.20
0.70
0.20
POTENTIAL (volts vs SSCE)

FIGURE 35

cathodic waves are proportional to the sweep rate (v). This is characteristic of a thin cell behavior[34a]. It is less common than the linear i_p vs $v^{1/2}$ relationship observed for electroactive ions freely diffusing in homogeneous solution. Deviation from $\Delta E = 0$ was interpreted as the result of nonequilibrium between reduced and oxidized state caused by either uncompensated film resistance or, more probably, steric effects leading to conformational changes during the charging and discharging processes[51]. Cyclic voltammograms of poly(3',4'-dibutyl-α-terthiophene) and poly(3",4"-dibutylquinquethiophene) exhibit similar shapes (Figures 35b and c). The addition of the broad anodic tail in these voltammograms was interpreted as a pure capacitance current due to large inner surfaces of these polymers[24c,52]. Consequently, this increase in the charging current induces a higher reactivity of the system. As already observed for the oligomers compared with the monomeric disubstituted thiophene, partially disubstituted thiophene polymers having longer repeat units are easier to oxidize when coated as thin film on the electrode surface.

Since poly(3,4-dibutylthiophene) is soluble in common organic solvents in both its oxidized and neutral form, the electrochemical behavior of this polymer also was studied in solution. Shown in Figure 36 are the cyclic and differential pulse voltammograms of this virgin polymer in methylene chloride. Only the oxidative properties will be investigated since no reduction process is seen in the negative potential window of the solvent. The polymer exhibits a broad continuous oxidation process over a 1000 mV range. This is characteristic of a band-type electronic structure material having a large amount of interaction between the redox sites comprising the assembly of the polymer[30a,35]. The shape of its cyclic voltammogram does not change when varying the sweep rate and the peak heights of the anodic and cathodic waves are proportional to $v^{1/2}$

Figure 36. Cylic and differential pulse voltammograms of a 273 μM solution of poly (3,4-dibutylthiophene)/0.2 M $TBABF_4$ in CH_2Cl_2. The experimental conditions for differential pulse voltammetry were: pulse amplitude: 50 mV; pulse width: 50 mV sec^{-1}; pulse duration = 1000 mV sec^{-1} and scan rate = 4 mV sec^{-1}. for cyclic voltammetry, the sweep rate was 50 mV sec^{-1}.

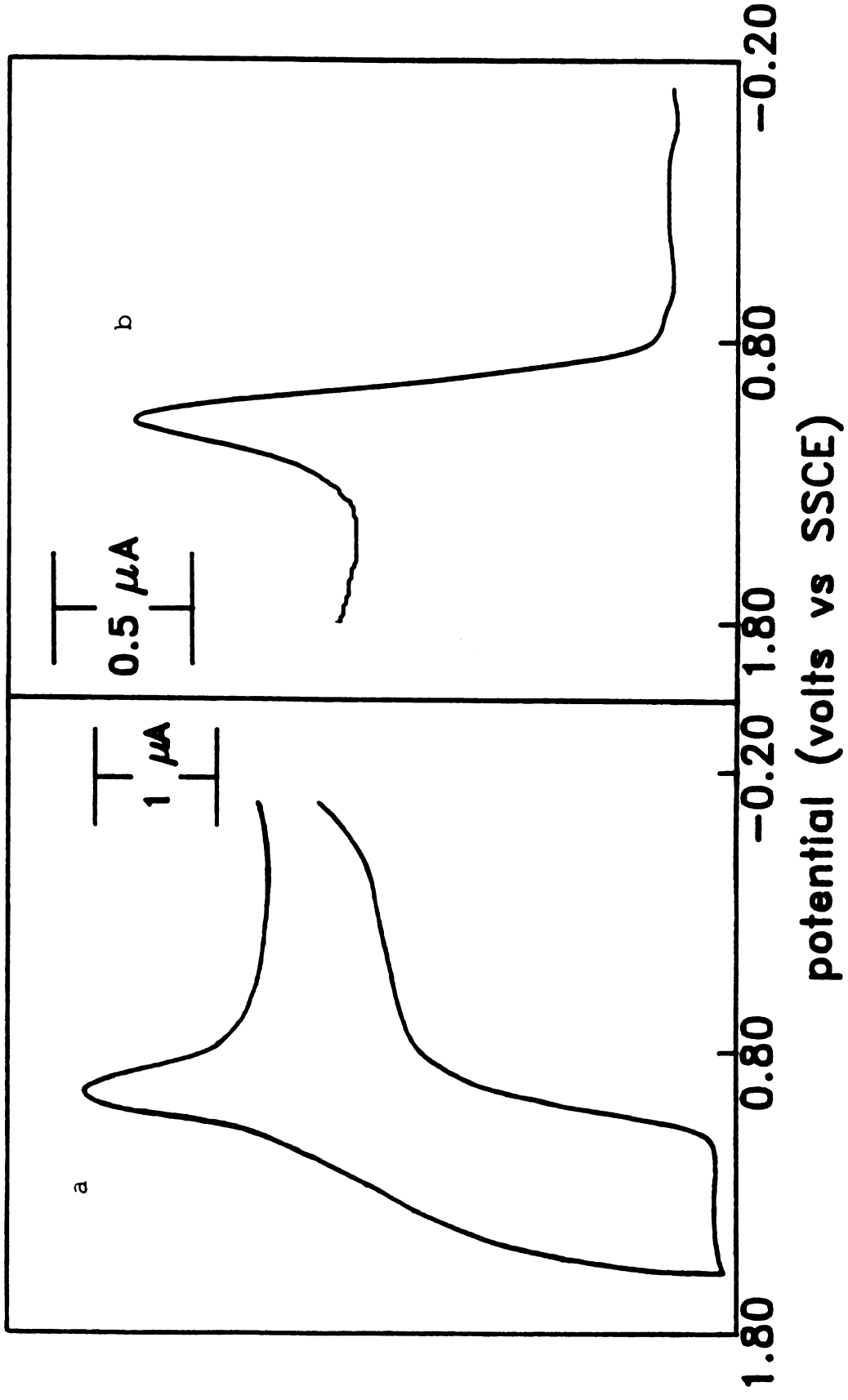

FIGURE 36

suggesting a diffusional behavior contrary to the one observed in the solid state. The polymer also can be cycled repeatedly between the oxidized and the neutral state with no appreciable decomposition of the material rendering possible the study of the redox properties of the poly(3,4-dibutylthiophene) in the solution chemistry.

4.4 Redox properties

Previous studies on the soluble polyalkylthiophenes have shown that these polymers, when coated as thin films on the electrode surface, usually can be oxidized from 0 to 30%[22]. The maximum doping level attained in the solid state can vary significantly, depending on the nature of the counterion and structural properties of the film[13a,22,48]. In solution, these complications do not occur, thus rendering possible the doping of these polymers at higher levels. In order to determine the doping profile as function of potential for poly(3,4-dibutylthiophene) in solution, a series of controlled potential coulometry experiments was performed in methylene chloride. As was expected from theory[49], current curves which decay exponentially with time to the background current value were obtained except for the curve of the re-reduction of the 34% oxidized solution. In this case, the polymer remains partially oxidized. It can not be fully re-reduced even after several hours of the undoping process. The percent oxidation-potential plot determined from this series of CPC experiments for the poly(3,4-dibutylthiophene) is shown in Figure 37. Each point of the graph represents the percent oxidation determined by averaging the amount of charge passed for the oxidation of the neutral polymer and the reduction back to its neutral state both in solution and in the solid state. The error bars depict the differences between these values. A smooth doping profile is seen, suggesting that there is a continuum or band into which charge can be added. The

Figure 37. Degree of partial oxidation vs. potential determined by controlled potential coulometry for poly(3,4-dibutylthiophene)/$TBABF_4$ in CH_2Cl_2 solution and as film. Each point ( ) corresponds to the mean value for an oxidation/re-reduction cycle. The error bars represent the difference between the oxidation and re-reduciton.

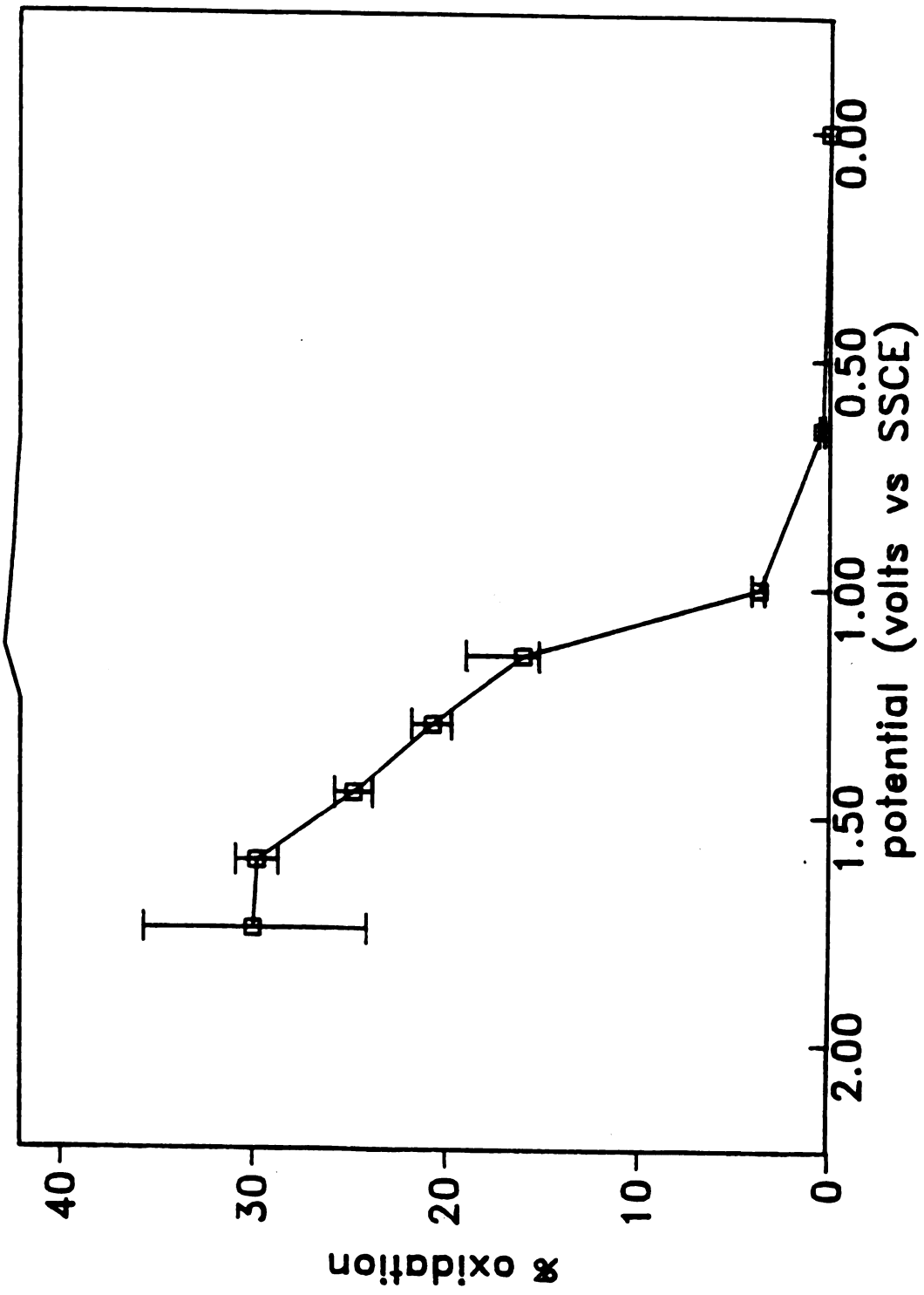
% oxidation
40
30
20
10
0
2.00
1.50
1.00
0.50
0.00
potential (volts vs SSCE)

FIGURE 37

differences in the percent oxidation at a given potential indicate that the polymer is stable up to a value of 30% and, that above this level, some instability inherent to the polymer is observed. This was proved by looking at the number of coulombs passed for the oxidation which differs largely from that for the re-reduction. It appears that the reduction of the doped polymer, when it is more than 30% oxidized, is not complete. In other words, access to the bipolaron band for external electrons is more difficult. Similar behavior was found for poly(3,4-dibutylthiophene) film. Tourillon and Garnier observed the same phenomenon and concluded that the doping process is more difficult to achieve for polydialkylthiophenes because of the steric hindrance effect of the bulky substituents on the thiophene ring[49].

4.5 Optical properties

Figure 38 represents the visible absorption spectra of both the solution and film of the oxidized and reduced state of poly(3,4-dibutylthiophene). In both cases, the neutral (undoped) polymer has a strong absorption band in the 320 nm region which corresponds to the π - π^* transition from the valence band to the conduction band. Another common feature of the polymer film and its solution is that upon doping, the interband transition decreases and simultaneously a new absorption peak appears at higher energy. These similarities in absorption spectra suggest that the electronic structure of poly(3,4-dibutylthiophene) is unchanged after dissolution. The shift of the absorption band corresponding to the interband transition implies a conformational change in solution, presumably to a more disordered conformation.

Figure 38. In-situ optical absorption spectra of poly(3,4-dibutylthiophene) as synthesized film and solution in both its neutral (undoped) and oxidized form.

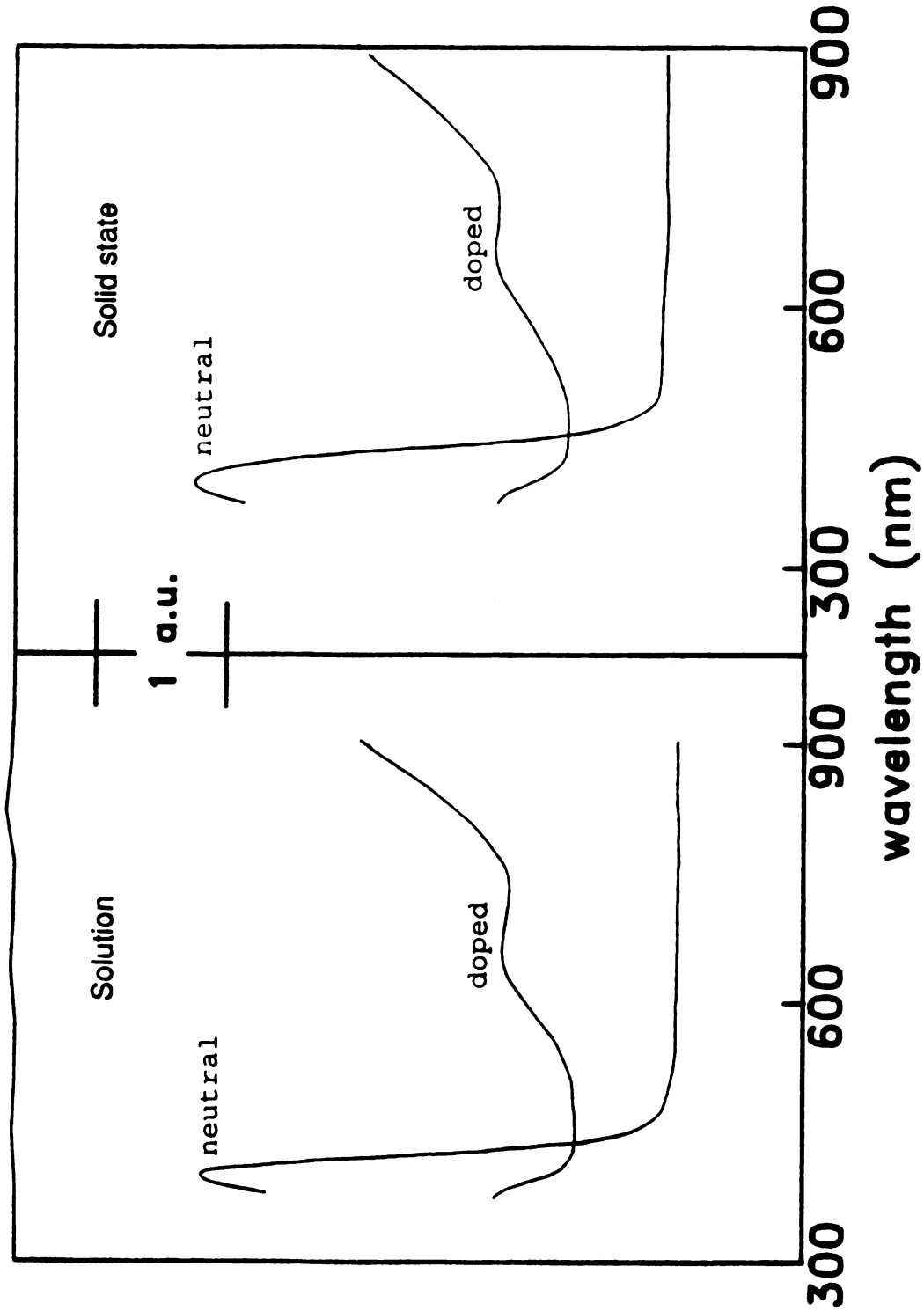
Solution
Solid state
neutral
doped
neutral
doped
1 a.u.
300
600
900
300
600
900
wavelength (nm)

FIGURE 38

In order to determine the nature of the charge-storage species in the polymer chain during the doping process, a series of electronic absorption spectra of the poly(3,4-dibutylthiophene) in dilute methylene chloride solution was obtained at various doping levels (y) (Figure 39). In the neutral state, a peak corresponding to the interband transition is observed at 3.9 eV. Upon doping, ($0.04 \leq y \leq 0.34$), a defined peak is observed at 3.9 eV along with two broad peaks at 2 and 1 eV. This is consistent with the concept of doping through bipolaron. As the doping level increases, the subgap absorptions grow at the expense of the interband transition. The high dopant level data were consistent with previously reported optical spectra of heavily doped polythiophenes and their derivatives[17h,k,l,33f,g]. This suggests that, at high doping levels, charge is predominantly stored in bipolaron.

It is well known that the existence of π-conjugation in conducting polymers is implied by their optical spectra. In order to evaluate the amount of conjugation in polydisubstitutedthiophenes, the absorption spectra of the neutral poly(3,4-dibutylthiophene), poly(3',4'-dibutyl-α-terthiophene) and poly(3",4"-dibutylquinquethiophene) films were recorded and compared (Figure 40). These spectra reveal a slight shift of the absorption maximum of poly(3',4'-dibutyl-α-terthiophene) compared with poly(3,4-dibutylthiophene) towards lower wavelength, indicating a lower conjugation for the latter polymer. This shift is even more strongly marked in the case of poly(3",4"-dibutylquinquethiophene). The displacement of the absorption maxima indicates that the conjugation in these polymers increases when increasing chain length of the starting oligomer with unsubstituted thiophene units. As a result, a better conducting polymer is formed. Further support for this conclusion will be provided by the conductivity data of these polydisubstitutedthiophenes.

Figure 39. In-situ electronic absorption spectra of a 273 μM solution of poly(3,4-dibutylthiophene)/0.2 M $TBABF_4$ oxidized at various degrees in CH_2Cl_2.

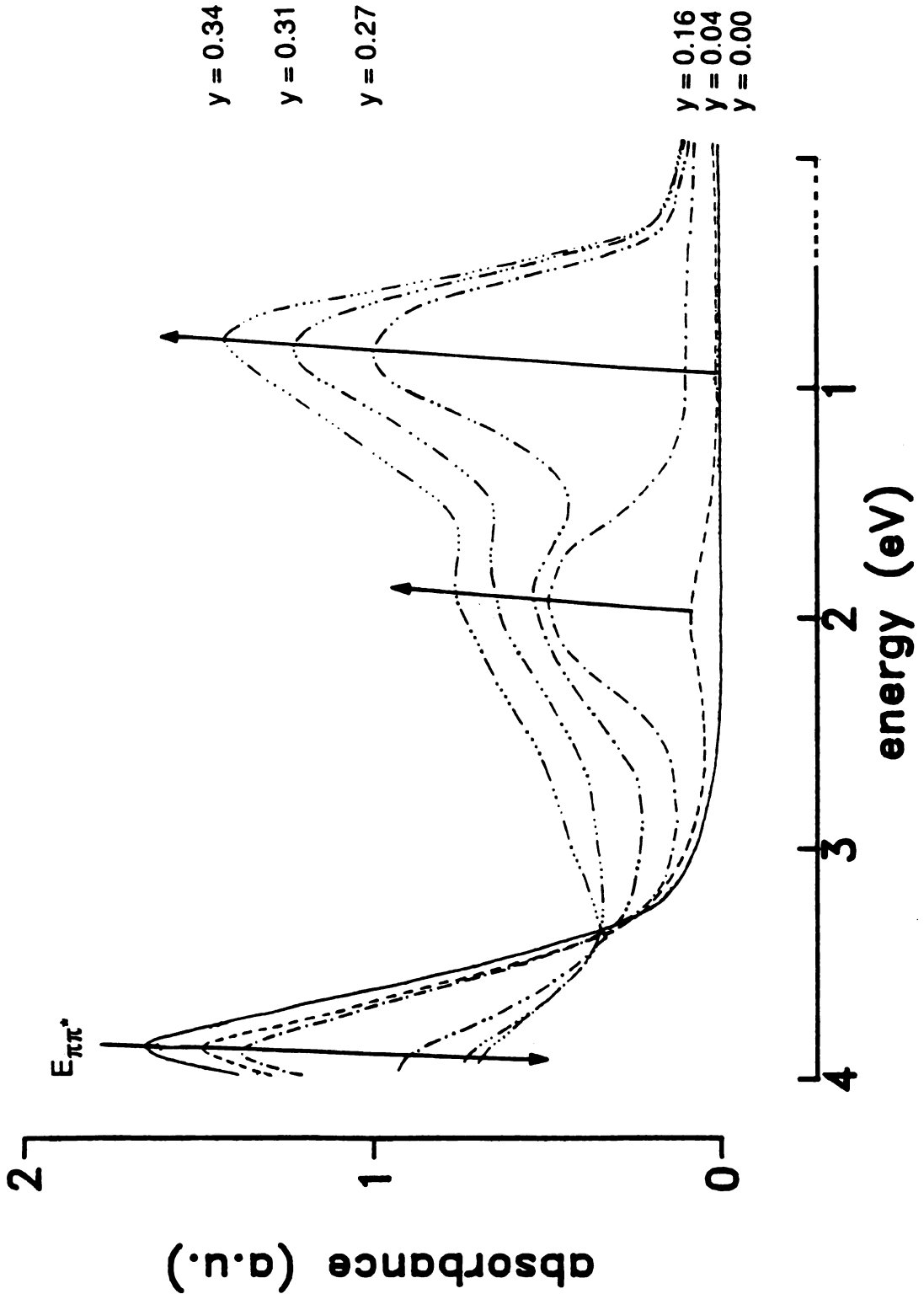
y = 0.34
y = 0.31
y = 0.27
y = 0.16
y = 0.04
y = 0.00
$E_{\pi\pi^*}$
absorbance (a.u.)
0
1
2
energy (eV)
1
2
3
4

FIGURE 39

Figure 40. Optical absorption spectra of poly(3,4-dibutylthiophene), poly(3'4'-dibutyl-α-terthiophene), and poly(3",4"-dibutylquinque thiophene) as synthesized films.

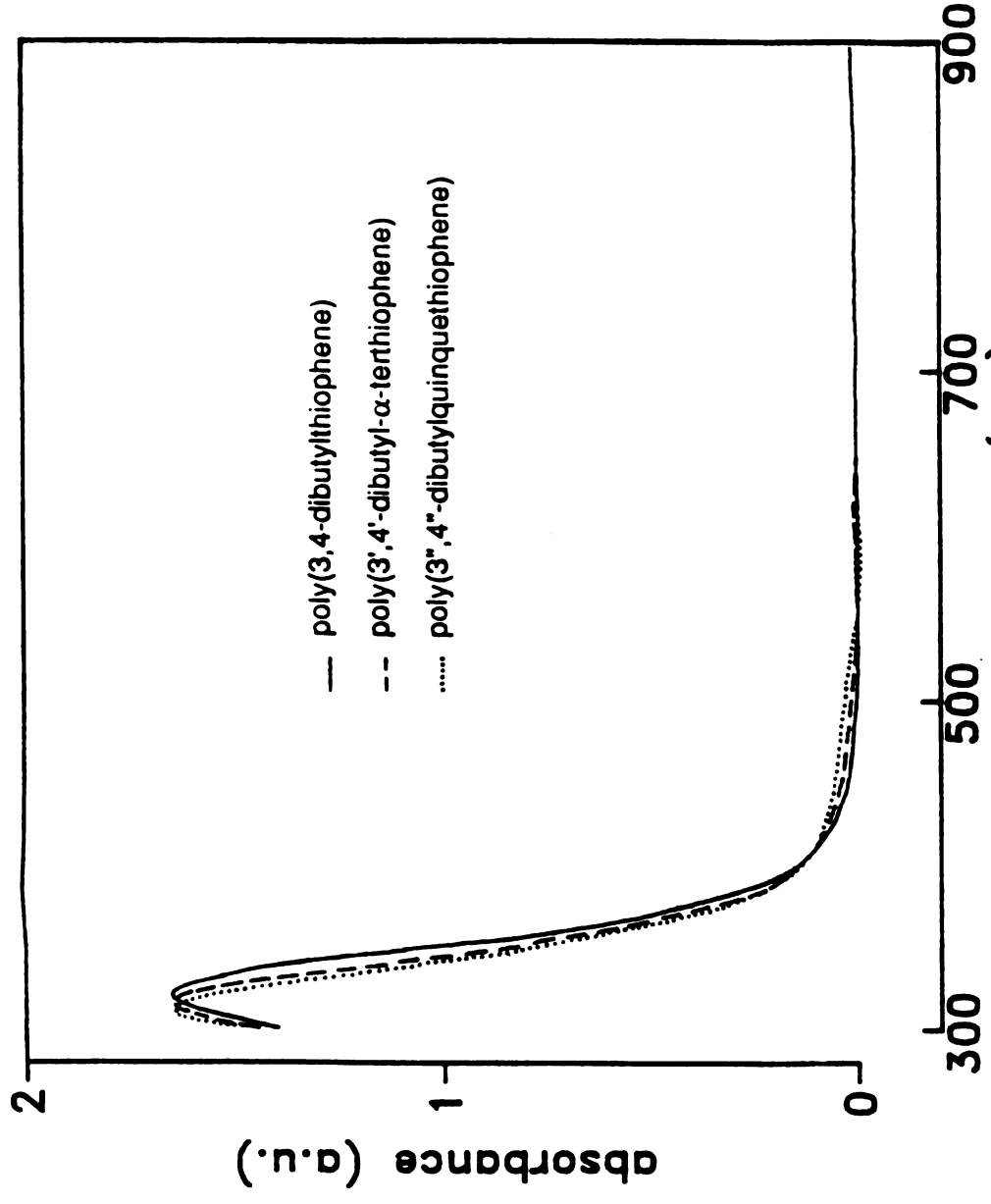
poly(3,4-dibutylthiophene)
poly(3',4'-dibutyl-α-terthiophene)
poly(3",4"-dibutylquinquethiophene)
absorbance (a.u.)
0
1
2
300
500
700
900
wavelength (nm)

FIGURE 40

4.6 Conductivity

The study of the electrical properties of poly(3,4-dibutylthiophene) has been carried out as function of the doping level (y). The results of the electrical conductivity data at room temperature (σ_{RT}) are summarized in Figure 41. The conductivity increases dramatically with doping in a manner typical of conducting polymers, i.e., the profile of conductivity upon doping corresponds to a smooth, continuous process. The polymer is insulating in its neutral form. Upon doping, conductivity increases up to 9 orders of magnitude. The highest conductivity of 1 S cm^{-1} was obtained for a maximum doping level of 0.34. The comparison of the conductivity values of highly doped poly(3,4-dibutylthiophene) with other derivative polythiophenes in Table 5 allows some comments to be made. Contrary to what could be expected, polyalkylthiophenes and polydialkylthiophenes have, in general, lower electrical conductivity (except for poly(3-methylthiophene)) than the parent polythiophene in their oxidized state. This can be explained by the fact that, when bulky groups are substituted on β-carbon atoms in the thiophene unit, steric hindrance forcing adjacent rings to twist out of coplanarity increases, leading to less conjugation in the polymeric chain and lower conductivity on doping. This effect is even greater for polydialkylthiophenes possessing large substitutent groups. Another interesting observation concerns polythiophene and their derivatives synthesized from oligomers of different chain lengths instead of the usual monomer. When going from polythiophene to polytrithiophene, the conductivity decreases upon doping[24a,c]. In other words, the use of oligomers of increasing chain length as starting materials for the polymerization of unsubstituted polythiophenes leads to less conducting polymers with a lower degree of conjugation. However, if the starting material contains both unsubstituted and substituted thiophene units, the conductivity increases with the number of thiophene units toward the value

Figure 41. Electrical conductivity vs. degree of partial oxidation at room temperature for the poly(3,4-dibutylthiophene).

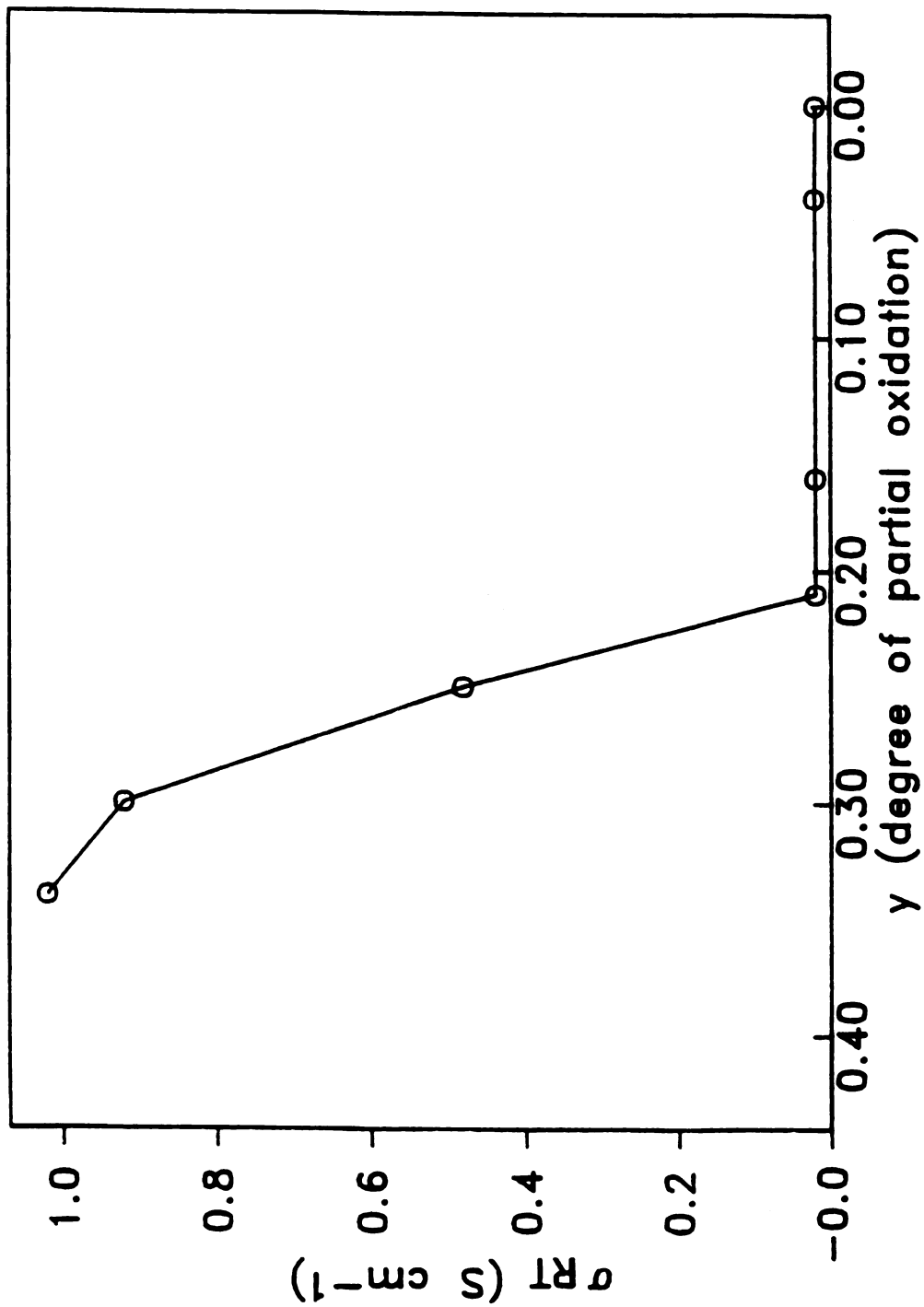
1.0
0.8
0.6
0.4
0.2
-0.0
σRT (S cm⁻¹)
0.40
0.30
0.20
0.10
0.00
y (degree of partial oxidation)

FIGURE 41

Table 5. Room temperature electrical conducitivity data for β-mono and -disubstituted thiophene derivatives.

TABLE 5

Polymer	Composition	Conductivity (s cm^{-1})
polythiophene	$[(C_4H_2S)(ClO_4)_{0.30}]_n$	90[171]
poly(3-methylthiophene)	$[(C_5H_4S)(ClO_4)_{0.35}]_n$	750[17g]
poly(3-butylthiophene)	$[(C_8H_{10}S)(PF_6)_{0.19}]_n$	40[17g]
poly(3,4-dimethylthiophene)	$[(C_6H_6S)(SO_3CF_3)_{0.30}]_n$	50[14h]
poly(3,4-dibutylthiophene)	$[(C_{12}H_{18}S)(BF_4)_{0.34}]_n$	1
poly(2,2'-bithiophene)	unknown	2.8[10d]
poly(2,2',2"-terthiophene)	unknown	0.14[10d]
poly(3',4'-dibutyl-α-terthiophene)	$[(C_{20}H_{22}S)(BF_4)_{0.35}]_n$	30
poly(3",4"-dibutylquinquethiophene)	$[(C_{28}H_{26}S)(BF_4)_{0.37}]_n$	50

obtained for the unsubstituted polythiophene, synthesized from the monomer. Similar behavior was observed for copolymers based on polyalkylthiophene and polythiophene[17h]. Plots of conductivity as function of doping for the poly(3',4'-dibutyl-α-terthiophene) and poly(3",4"-dibutylquinquethiophene) indicate that these polythiophenes also have a smooth continuous conductivity-doping profile starting at 17% and levelling off around 30% (Figure 42). A higher conductivity value is reached at lower doping levels. Compared with that of the parent thiophene, the conductivity increases by more than 10-fold, even at low doping levels.

Figure 42. Electrical conductivity vs degree of partial oxidation at room temperature for poly(3,4-dibutylthiophene), poly(3',4'-dibutyl-α-terthiophene), and poly(3"4"-dibutylquinquethiophene).

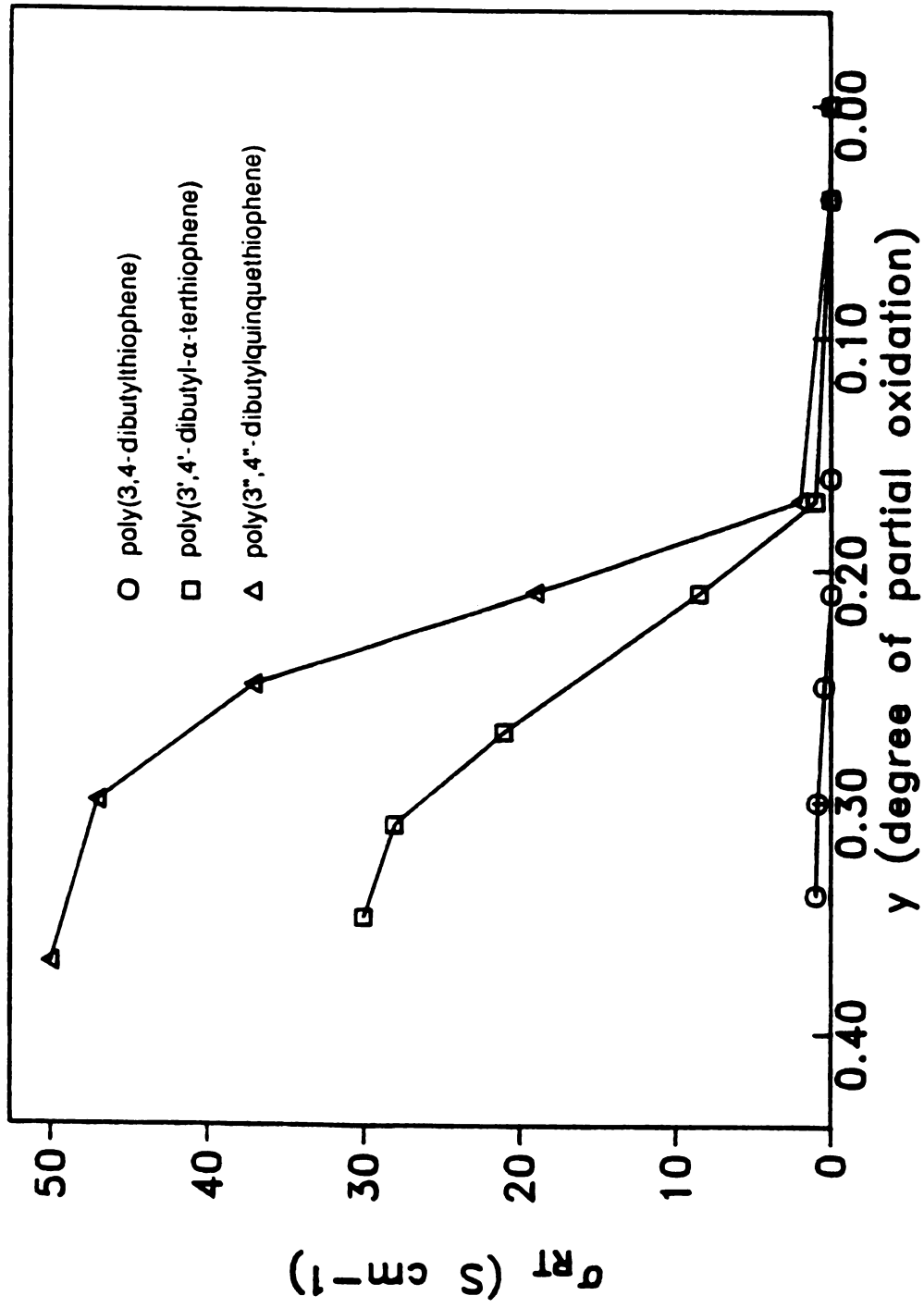
poly(3,4-dibutylthiophene)
poly(3',4'-dibutyl-α-terthiophene)
poly(3",4"-dibutylquinquethiophene)
σRT (S cm−1)
0
10
20
30
40
50
0.40
0.30
0.20
0.10
0.00
y (degree of partial oxidation)

FIGURE 42

5. CONCLUSION

Conventional and unconventional electrochemical techniques can be used to characterize soluble conducting polymers. Contrary to the electrochemical response observed for conventional electroactive compounds, conducting polymers exhibit a broad, continuous response in solution. This behavior is characteristic of a material having a large amount of interaction between its redox centers. Despite the complications accompanying the electrochemical study of such systems, it has been possible to accurately probe the redox properties of these conducting materials to a sophisticated level never attempted before.

The partial reduction of the μ-oxo-(tetra-t-butylphthalocyaninato) germanium can be accurately and systematically varied to any specific level, ranging from 0 to 1- by simply changing the potential of the working electrode. The reduction process can be described as a simple charge-transfer reaction occurring at the electrode surface, only limited by the mass transport of the material to the electrode. The germanium polymer is chemically stable at all degrees of partial reduction and remains stable upon repeating reduction/re-oxidation cycles. At greater than 100% reduction, the polymer quantitatively fragments into electroactive monomeric species. This decomposition can be easily, quickly, and precisely monitored using modified rotating ring-disk voltammetry technique. Besides the advantages of easiness, rapidity, and precision offered by this technique, the solution remains intact during the entire experiment. Digital simulations of the electrochemical responses indicate that the

reduction of the germanium polymer can be modeled as a series of reversible redox couples in equilibrium undergoing sequential one-electron transfers. From the simulations of the conventional voltammetry response, the standard potentials of the redox sites comprising the polymer are determined along with an estimation of the amount of interaction between the redox sites. From the simulations of the unconventional voltammetry responses, the mechanism of the decomposition is elucidated and the rate constant of the decomposition measured.

In a fashion similar to the μ-oxo-(tetra-t-butylphthalocyaninato) germanium, soluble poly(3,4-dibutylthiophene) can be oxidized to any level between 0 and 0.34 and remains chemically stable. Similar behavior is observed for the corresponding film. It is the first time that the same probe has been investigated simultaneously in solution and in the solid state. Conductivity measurements of the polythiophene derivative oxidized to various degrees are directly related to potential, thus allowing the determination of the conductivity profile as function of band-filling. The optical properties of this polymer as function of band-filling are studied, using in-situ experiment combining electrochemical and spectroscopic techniques. Information on the nature of the charge carriers during the redox process is provided in this experiment.

Such study is valuable in the long term goal for developing new material with predictable properties.

APPENDIX 1

The digital simulation models employed for both differential pulse and rotating ring-disk voltammetry techniques are based on the method of finite-differences[32]. The solution near the electrode surface is divided into volume elements of equal size. The movement of species between adjacent volumes is used to mimique diffusion. Parameters are handled in dimensionless form in accordance with standard procedure. The main difference between this model and the others discussed in the literature are the equations used to describe the surface boundary conditions and the dimensionless current for a multi-component system such as the conducting polymer.

In these models, it is assumed that each phtalocyanine ring (Pc) is an active redox site having its own and unique standard potential (E_j^0) in equilibrium with the other sites comprising the assembly of the polymer[54]. Based on the CPC and RDE data (Nernstian one electron transfer, one electron removed per Pc site at 100% reduction), the reduction of the polymer can be viewed as a system undergoing sequential Nernstian one-electron transfer:

$$R_n + e^- \Longleftrightarrow R_{n-1}O_1 \quad E_1^0$$

$$R_{n-1}O_1 + e^- \Longleftrightarrow R_{n-2}O_2 \quad E_2^0$$

$$R_{n-2}O_2 + e^- \Longleftrightarrow R_{n-3}O_3 \quad E_3^0$$

etc...

where :

R = neutral species

O = oxidized species

n = length of the polymer

The polymer was found to be comprised of 15 redox sites, based on the results obtained from the RDE voltammetry experiments. To generalize the computational process, the concentration of any form of the polymer, regardless of what redox state it is in, is normalized with respect to the initial concentration. Since the system is reversible, the concentration at the electrode surface is governed by the Nernst equation.

The fractional concentration of each species at a given potential is derived from the potential-dependent equilibrium constant describing each redox reaction. The equilibrium constants (K_n) of each redox site are :

$$K_1 = \frac{[R_{n-1}\ O_1]}{[R_n]} = \exp\ (E - E_1^0) * \frac{RT}{n_1 F}$$

$$K_2 = \frac{[R_{n-2}\ O_2]}{[R_n]} = \exp\ (E - E_2^0) * \frac{RT}{n_2 F}$$

$$K_3 = \frac{[R_{n-3}\ O_3]}{[R_n]} = \exp\ (E - E_3^0) * \frac{RT}{n_3 F}$$

etc...

The initial bulk concentration $[O_n]_0$ calculated from the mass balance is :

$$[R_n]_0 = [R_n] + [R_{n-1}\ O_1] + [R_{n-2}\ O_2] + [R_{n-3}\ O_3] + .. + [O_n]$$

Using this new expression for $[R_n]_0$ and including the equilibrium constants in the expression of concentrations, the fractional concentrations (α_n) of each species at the electrode surface are :

$$\alpha_0 = \frac{[R_n]}{[R_n]_0} = \frac{1}{1+K_1+K_1K_2+K_1K_2K_3+...+K_1K_2K_3...K_n}$$

$$\alpha_1 = \frac{[R_{n-1}\ O_1]}{[R_n]_0} = \frac{K_1}{1+K_1+K_1K_2+K_1K_2K_3+...+K_1K_2K_3...K_n}$$

$$\alpha_2 = \frac{[R_{n-2}\,O_2]}{[R_n]_0} = \frac{K_1K_2}{1+K_1+K_1K_2+K_1K_2K_3+...+K_1K_2K_3...K_n}$$

etc...

with $\alpha_0+\alpha_1+\alpha_2+...+\alpha_n = 1$

This model is analogous to the one used for the dissociation of a polyfunctional acid or base[30b]. The real modifications made in the DPV and RRDE simulation programs concern the flux expression used in the determination of current. It is important to note here that, even if the DPV and RRDE simulation programs are constructed following the same scheme, these two techniques will be treated separatively due to their different modes of mass transfer. In DPV, mass transfer occurs only by diffusion, linear in character. In RRDE, a radial term is added to the linear component of the diffusion and a convection term is added to the diffusion one in the mass transfer equation. For an easy understanding, the simulation program of DPV is described first, below, and in detail and will serve as a basis for the more complicated RRDE simulation program.

Assuming that diffusion is the only mode of mass transfer and that diffusion is linear, the general expression for the flux of species j (F_j) at the electrode surface is the following:

$$F_j = \frac{-i}{n_jFA} = -D_j \left[\frac{\delta C_j(x,t)}{\delta x}\right]_{x=0}$$

where:

i	= current
n_j	= number of electrons transferred
F	= Faraday's constant

A = area of the electrode

D_j = diffusion coefficient

$\left[\frac{\delta C_j(x,t)}{\delta x}\right]_{x=0}$ = concentration gradient at the electrode surface

In simulation term, the flux expression (F_j) becomes:

$F_j = DM_j [C(j+1,t) - C(j,t)]$

where:

DM_j = dimensionless diffusion current of species j

C(j,t) = concentration of species j in the j volume element

C(j+1,t) = concentration of species j+1 in the j+1 volume element

For the model that has been developed in this study, the expression for the individual flux (F_j) can be written as:

$F_j = DM_j [C(j+1,t) - \alpha_j(t)]$

From the flux, the dimensionless current is calculated. It is the sum of the individual flux terms scaled to some proportionality constant depending only on the electrochemical technique used.

dimensionless current = $\sum_{j=1}^{n} \sum_{k=1}^{j} (n+1-k) * F_j(k) * c_j$

where:

n = number of redox sites

C = simulation constant (DM_j, Δx, Δt)

Likewise the percent of charge transfer at a given potential is:

$\sum_{j=1}^{n} \frac{[R_{n-j}\ O_j]}{[R_n]_o} \sum_{k=1}^{j} n_k * 100$

where:

n_k = total number of electrons involved in the j redox step

The other variables are defined as before.

A problem encountered with the computation of the flux terms is that, as the number of sites increases and/or the the difference between the standard potential of each redox couple becomes large, the common dominator used to calculate the individual fluxes becomes unmangeable. For a standard potential more negative than the applied potential, the equilibrium constant quickly becomes extremely small. Conversely, for a standard potential more positive than the applied potential, the equilibrium constant becomes exceedingly large. When the number of sites is large, the product of the equilibrium constants used to calculate the fractional concentrations at the electrode surface becomes difficult to handle. To alleviate this problem, a "sliding potential window" is used to determine which equilibrium constants are needed to describe the entire system. If the applied potential is 300 mV more negative than the E^0 value, the redox reaction is assumed to have gone to completion and the fractional concentration of all species needed to generate that component are set to zero. Likewise, if the applied potential is 300 mV more positive than the E^0 value, the species of interest has not been formed yet, and again its fractional concentration is set to zero. A value of 300 mV was chosen since it represents, for a one-electron process, a ratio of 10^{-5} for one form of the couple over the other ($0.3RT/F = \log (Ox/Red)$). This procedure has the additional benefit to effectively cutting down the number of equilibrium constants that are needed to characterize the entire system, resulting in shorter processing time.

For the RRDE, the following model is used. The solution is divided into thin parallel layers and each layer into a cylindrical box and a series of concentric annular boxes. In this model, several regions are considered: the disk, the insulating gap between the disk and the ring, the ring and the outer insulation. Unlike previous work, the number of boxes assigned to the disk or ring is no

longer a constant, but depends on the diameter of the electrode considered. For each region the flux is first calculated from the mass transfer equation which includes terms of diffusion and convection. Then the disk and ring currents are calculated in a manner similar to the one described earlier. The ring current also is calculated when the disk is held at a certain potential. Finally the decompsition of the germanium is monitored by simulation of the continuous shielding-collection experiments. The decompositon is considered as a first order homogeneous chemical reaction, i.e., the polymer decomposes totally into the corresponding monomeric type units, in anion form which are further reduced into dianions and trianions. This decomposition is part of the E_nCEE mechanism described earlier. Thus, a new set of fractional concentrations taking into account the decomposition process are calculated from which the flux and current are derived. From this simulation, a rate constant of 20 sec^{-1} was obtained for the decompostion of the germanium polymer.

REFERENCES

1. (a) Skotheim, T.A., Ed. "Handbook of Conducting Polymers", (Dekker, New York, 1986) Vols. 1-2.
   (b) Ferraro, J.R.; Williams, J.M. "Introduction to Synthetic Electrical Conductors", (Academic Press, New York, 1987).
   (c) Skotheim, T.A., Ed. "Electroresponsive Molecular and Polymeric Systems", (Dekker, New York, 1988) Vol. 1.
   (d) Miller, J.S., Ed. "Extended Linear Chain Compounds", (Plenum Press, New York, 1982) Vols. 1-3.
   (e) Ward, M.W. "Electroanalytical Chemistry"; Bard, A.J., Ed. (Dekker, NY, 1989) Vol. 16, 181-312.
   (f) Miller, J.S.; Epstein, A.J. "Progress in Inorganic Chemistry"; Lippard, S.J. Ed. (Wiley, New York, 1976) Vol. 20, 1-151.
   (g) Proceedings of the International Conference on Science and Technology of Synthetic Metals (ICSM '86), *Synth. Met.*, **1987**, 17.
   (h) Proceedings of the International Conference on Science and Technology of Synthetic Metals (ICSM '88), *Synth. Met.*, **1988-1989**, 27-29.
   (i) Epstein, A.J.; Conwell, E.M. Eds. "Proceedings of the International Conference on Low-Dimensional Conductors", Boulder Colorado, August 9-16, 1981, *Mol. Cryst. Liq. Cryst.*,77, 79, 83, 85, 86, Parts A-F (**1981-1982**).

2. (a) Chiang, C.K.; Fincher, C.R. Jr.; Park, Y.W.; Heeger, A.J.; Shirakawa, H.; Louis, E.J.; Gau, S.C.; MacDiarmid, A.G. *Phys. Rev. Lett.*, **1977**, 39, 1098-1101.
   (b) Shirakawa, H.; Louis, E.J.; MacDiarmid, A.G.; Chiang, C.K.; Heeger, A.J. *J. Chem. Soc. Chem. Commun.*, **1977**, 578-580.
   (c) Chiang, C.K.; Druy, M.A.; Gau, S.C.; Heeger, A.J.; Louis, E.J.; MacDiarmid, A.G.; Park, Y.W. *J. Am. Chem. Soc.*, **1978**, 100, 1013-1015.
   (d) Chiang, C.K.; Park, Y.W.; Heeger, A.J.; Shirakawa, H.; Louis, E.J., MacDiarmid, A.G. *J. Chem. Phys.*, **1978**, 69, 5098-5104.

3. (a) Albery, W.J.; Bartlett, P.N.; Cass, A.E.G.; Craston, D.H.; Haygett, B.G.D. *J. Chem. Soc. Faraday Trans. I*, **1986**, 82, 1033-1050.
   (b) Heeger, A.J.; Moseo, D.; Sinclair, M. *Synth. Met.*, **1986**, 15, 95-104.
   (c) Alper, J. *Science*, **1989**, 246, 208-210.
   (d) Duke, C.B. *Synth. Met.*, **1987**, 21, 5-12.
   (e) Inganos, O.; Lundstrom, I. *Synth. Met.*, **1987**, 21, 13-19.
   (f) MacDiarmid, A.G. *Synth. Met.*, **1987**, 21, 79-83.

4. (a) Cowan, D.O.; Wiygul, F.M. *chem. Eng. News*, **1986**, 64, 28-45.
   (b) Bryce, M. R.; Murphy, L.C. *Nature*, **1984**, 309, 119-126.
   (c) Wudl, F. *Acc. Chem. Res.*, **1984**, 17, 227-232.

5. (a) Scrosati, B. *Prog. Solid State Chem.*, **1988**, 18, 1-77.
   (b) Wegner, G. *Angew. Chem. Int. Ed. Eng.*, **1981**, 20, 361-381.
   (c) Reynolds, J.R. *Chemtech.*, **1988**, 18, 440-447.

(d) Heinze, J.; Storzbach, M.; Mortensen *J. Ber. Bungsenges. Phys. Chem.*, **1987**, 91, 960-961.
(e) Heinze, J. *Top. Curr. Chem.*, **1990**, 152, 1-47.

6. Greene, R.L.; Street, G.B. *Science*, **1984**, 226, 651-656.

7. (a) Hoffmann, R. *Angew. Chem. Int. Ed. Eng.*, **1987**, 26, 846.
(b) Duke, B.J.; O'leary, B. *J. Chem. Ed.*, **1988**, 65, 319-321.
(c) Duke, B.J.; O'leary, B. *J. Chem. Ed.*, **1988**, 65, 379-383.

8. (a) Marks, T.J. *Science*, **1985**, 227, 881-889.
(b) Marks, T.J. *Angew. Chem. Int. Ed. Eng.*, **1990**, 29, 857-890.

9. Whangbo, M.-H. *Acc. Chem. Res.*, **1983**, 16, 95-101.

10. (a) Sato, M.; Tanaka, S.; Kaeriyama, K. *J. Chem. Soc. Chem. Commun.*, **1985**, 713-714.
(b) Satoh, M.; Kaneto, K.; Yoshino, K. *Jpn. J. Appl. Phys.*, **1985**, 24, L423-450.
(c) Roneali, J.; Garnier, F. *Nouv. J. Chim.*, **1986**, 10, 237-240.
(d) Roneali, J.; Garnier, F.; Lemaire, M.; Garreau, R. *Synth. Met.*, **1986**, 15, 323-331.
(e) Grant, P.M. *Phys. Rev. B.: Conden. Matter*, **1982**, 26, 6888-6895.
(f) Grant, P.M. *Bull. Am. Phys. Soc.*, **1981**, 26, 213-217.
(g) Weger, M.; Kaveh, M.; Gutfreund, H. *Solid State Commun.*, **1981**, 37, 421-426.
(h) Gutfreund, H.; Hartstein, C.; Weger, M. *Solid State Commun.*, **1980**, 36, 647-651.
(i) Conwell, E.M. *Phys. Rev. B: Condens. Matter*, **1980**, 22, 1761-1779.
(j) Epstein, A.J.; Conwell, E.M.; Miller, J.S. *Ann. N.Y. Acad. Sci.*, **1978**, 313, 183-209.

11. (a) Mizutari, F.; Iijima, S.; Tanabe, Y.; Tsuda, K. *J. Chem. Soc. Chem. Commun.*, **1985**, 1728-1729.
(b) Fan, F.-R.; Bard, A.J. *J. Electrochem. Soc.*, **1986**, 133, 301-309.
(c) Penner, R.M.; Martin, C.R., *J. Electrochem. Soc.*, **1986**, 133, 310-315.
(d) Iyoda, T.; Ohtani, A., Shimidzu, T.; Honda, K. *Chem. Lett.*, **1986**, 687-690.

12. Chung, T.C.; MacDiarmid, A.G.; Feldblum A.; Heeger, A.J. *J. Chem. Phys.*, **1981**, 74, 5504-5507.

13. (a) Diaz, A.F.; Lacroix, J.C. *New J. Chem.*, **1988**, 12, 171-180.
(b) Wudl, F. *Isreal J. Chem.*, **1986**, 27, 289-292.

14. (a) Diaz, A.F.; Logan, A.J. *J. Electroanal. Chem.*, **1980**, 111, 111-114.
(b) Diaz, A.F.; Clark, T.C. *J. Electroanal. Chem.*, **1980**, 111, 115-117.
(c) Diaz, A.F.; Castillo, J.I.; Logan, J.A.; Lee, W.Y. *J. Electroanal. Chem.*, **1981**, 129, 115-132.
(d) Diaz, A.F.; Martinez, A.; Kanazawa, K.K. *J. Electroanal. Chem.*, **1981**, 130, 181-187.

(e) Bull, R.A.; Fan, F.-R. F.; Bard, A.J.; Castillo, J; Kanazawa, K.K.; Logan, J.A. *J. electroanal. Chem.*, **1982**, 129, 1009-1015.
(f) Diaz, A.F.; Castillo, J.; Kanazawa, K.K.; Logan, J.A. *J. Electroanal. Chem.*, **1982**, 133, 233-239.
(g) Tourillon, G.; Garnier, F. *J. Electroanal. Chem.*, **1982**, 135, 173-178.
(h) Garnier, F.; Tourillon, G.; Gazard, M.; Dubois, J.C. *J. Electroanal. Chem.*, **1983**, 148, 299.
(i) Genies, E.M.; Bidan, G.; Diaz, A.F. *J. Electroanal. Chem.*, **1983**, 149, 101-113.
(j) Waltman, R.J.; Bargon, J.; Diaz, A.F. *J. Phys. chem.*, **1983**, 87, 1459-1463.

15. (a) Feldberg, S.W. *J. Am. Chem. Soc.*, **1984**, 106, 4671-4674 and references therein.
(b) Murray, R.W. "Electroanalytical Chemistry"; Bard, A.J. Ed., (Dekker, NY, 1986) Vol. 13.
(c) Chung, T.C.; MacDiarmid, A.G.; Feldblum, A.; Heeger, A.J. *J. Chem. Phys.*, **1981**, 74, 5504-5507.

16. (a) Gaudiello, J.; Marcy, H.O.; McCarthy, W.J.; Moguel, M.K.; Kannewurf, C.R.; Marks, T.J. *Synth. Met.*, **1986**, 15, 115-128.
(b) Gaudiello, J.; Almeida, M.; Marks, T.J.; McCarthy, W.J.; Butler, J.C.; Kannewurf, C.R. *J. Phys. chem.*, **1985**, 90, 4917-4920.
(c) Almeida, M.; Gaudiello, J.; Butler, J.C.; Marcy, H.O.; Kannewurf, C.R.; Marks, T.J. *Synth. Met*, **1988**, 27, 261-266.
(d) Kellogg, G.E.; Gaudiello, J.; Schlueter, J.A.; Tetrick, S.M.; Marks. T.J.; Marcy, H.O.; McCarthy, W.J.; Kannewurf, C.R. *Synth. Met.*, **1989**, 29, F15-F24.
(e) Gaudiello, J.W.; Kellogg, G.E.; Tetrick, S.M.; Marks, T.J. *J. Am. Chem. Soc.*, **1989**, 111, 5259-52271.
(f) Almeida, M.; Gaudiello, J.G.; Kellogg, E.K.; Tetrick. S.M.; Marcy, H.O.; McCarthy, W.J.; Butter, J.C.; Kannewurf, C.R.; Marks, T.J. *J. Am. Chem. Soc.*, **1989**, 111, 5271-5284.

17. (a) Frommer, J.E. *Acc. Chem. Res.*, **1986**, 19, 2-9.
(b) Li, S.; Cao, Y.; Xue, Z. *Synth. Met.*, **1987**, 20, 141-149.
(c) Jiang, R.; Dong. S. *Synth. Met.*, **1988**, 24, 255-265.
(d) Elsenbaumer, R.L.; Jen, K.Y.; Ododi, R. *synth. Met.*, **1986**, 15, 169-174.
(e) Elsenbaumer, R.L.; Jen, K.Y.; Miller, G.G.; Shacklelte, L.W. *Synth. Met.*, **1987**, 18, 277-282.
(f) Patil, A.D.; Ikenove, Y.; Basecu, N.; Colaneci, N.; Chen, J.; Wudl, F.; Heeger, A.J. *Synth. Met.*, **1987**, 20, 151-159.
(g) Hotta, S. *Synth. Met.*, **1987**, 22, 103-113.
(h) Hotta, S.; Soga, M.; Sonada, N. *Synth. Met.*, **1988**, 16, 267-279.
(i) Ruiz, J.P.; Nayak, K.; Marynick, D.S.; Reynolds, J.R. *Macromolecules*, **1989**, 22, 1231-1238.
(j) Rughooputh, S.D.D.V.; Novak, M.; Hotta, S.; Heeger, A.J.; Wudl, F. *Synth. Met.*, **1987**, 21, 41-50.
(k) Sato, M.-A.; Tanaka, S.; Rughooputh, S.D.D.V.; Heeger, A.J.; Wudl, F. *Macromolecules*, **1987**, 20, 212-215.
(l) Roncoli, J.; Garreau, R.; Yassar, A.; Marque, P.; Garnier, F.; Lemaire, M. *J. Phys. Chem.*, **1987**, 91, 6706-6714.

(m) Nalwa, H.S. *Synth. Met.*, **1990**, 35, 387-391.
(n) Patil, A.D.; Ikenove, Y; Wudl, F.; Heeger, A.J. *J. Am. Chem. Soc.*, **1987**, 109, 1858-1859.
(o) Patil, A.D.; Ikenove, Y.; Wudl, F.; Heeger, A.J.; *Synth. Met.*, **1987**, 20, 151-159 and references therein.
(p) Metz, J.; Pawlowowski, G.; Hanack, M. *Z Naturforsch.*, **1983**, 386, 378-382.
(q) Hanack, M.; Datz, A.; Faye, R.; Fischer, K.; Keppeler, V.; Kach, J.; Metz, J.; Mezger, M.; Schneider, O.; Schulze, H. "Handbook of Conducting Polymers"; Skelheim, T.A., Ed., (Dekker, NY, 1986) Vol. 1 and references therein.
(r) Hanack, M.; Vermehren, P. *Synth. Met.*, **1989**, 32, 257-261.

18. (a) Hanack, M.; Mitulla, K.; Pawlowski, G.; Subramanian, L.R. *J. Organometal. Chem.*, **1981**, 204, 315-325.
(b) Hanack, M. *Mol. Cryst. Liq. Cryst.*, **1988**, 160, 133-137.
(c) Hanack, M.; Lange, A.; Rein, M.; Babnisch, R.; renz, G.; Leverenz, A. *Synth. Met.*, **1989**, 29, 71-78.

19. (a) Diel, B.D.; Inabe, T.; Lyding, J.W.; Schoch, Jr., K.F.; Kannewurf, C.R.; Marks, T.J. *J. Am. Chem. Soc.*, **1983**, 105, 1551-1567.
(b) Petersen, J.L.; Schramm, C.S.; Stojakovic, D.,R.; Hoffman, B.M.; Marks, T.J. *J. Am. Chem. Soc.*, **1977**, 99, 286-288.
(c) Schramm, C.S.; Scaringe, R.P.; Skojakovic, D.R.; Hoffman, B.M.; Ibers, J.A.; Marks, T.J. *J. Am Chem. Soc.*, **1980**, 102, 6702-6713.
(d) Diel, B.D.; Inake, T.; Jaggi, N.K.; Lyding, J.W.; Schneider, D.; Hannack, M.; Kannewurf, C.R.; Marks, T.J., Schwartz L.H. *J. Am. Chem. Soc.*, **1984**, 106, 3207-3214.
(e) Inabe, T.; Gaudiello, J.G.; Moguel, M.K.; Lyding, J.W.; Burton, R.L.; McCarthy, W.J.; Kannewurf, C.R.; Marks, T.J. *J. Am. Chem. Soc.*, **1986**, 108, 7595-7608.
(f) Marks, T.J.; Schoch, K.F. Jr.; Kundalkar, B.R. *Synth. Met.*, **1979-1980**, 1, 337-347.
(g) Brant, P; Nohr, R.S.; Wynne, K.J.; Weber, D.C. *Mol. Cryst.*, **1982**, 81, 255-263.
(h) Dirk, C.W.; Inabe, T.; Schoch Jr., K.F.; Marks, T.J. *J. Am. Chem. Soc.*, **1983**, 105, 1539-1550.
(i) Dirk, C.W.; Marks, T.J. *Inorg. Chem.*, **1984**, 23, 4325-4332.

20. (a) Sugimoto, R.; Takeda, S.; Gu, M.B.; Yoshino, K. *Chem. Express*, **1986**, 1, 635-642.
(b) Barker, J.; Huddleston, P.R.; Wood, M.L. *Syn. Commun.*, **1975**, 5, 59-62.
(c) Kobayashi, M.; Chen, J.; Moraes, T.-C.; Heeger, A.J.; Wudl, F. *Synth. Met.*, **1984**, 9, 77-86.
(d) Yen, K.Y.; Miller, G.G.; Elsenbaumer, R.L. *J. Chem. Soc. Chem. Commun.*, **1986**, 1346-1347.

21. (a) Genies, E.M.; Bidan, G.; Diaz, A.F. *J. Electroanal. Chem. Interfacial Electrochem.*, **1983**, 149, 101-113.
(b) Fuyimoto, H.; Nagashima, V.; Inokrechi, H.; Scki, K.; Nakahara, H.; Hakayana, J.; Hoshino, M.; Fukudo, K. *J. Chem. Phys.*, **1988**, 89, 1198-1199.

22. Watman, R.J.; Baugen, J. *Can. J. chem.*, **1986**, 64, 76-95.

23. Sato, M.-A.; Tanaka, S.; Kaeriyama, K. *Synth. Met.*, **1987**, 18, 229-232.

24. (a) Roncalier, J.; Garnier, F. *Synth. Met.*, **1986**, 15, 323-331.
(b) Krische, I.; Zagorska, M. *Synth. Met.*, **1989**, 33, 257-267.
(c) Heinze, J.; Martensen, J.; Hinkelmann, K. *Synth. Met.*, **1987**, 21, 209-214.
(d) Kulszewicz-Bajer, I.; Zagorska, M.; Genoud, F.; Kruszka, J.; Stocka, K.; Pron, A.; Nechtschein, M. *Synth. Met.*, **1990**, 35, 129-133.
(e) Funt, L.; Lowen, S.V. *Synth. Met.*, **1985**, 11, 129-137.

25. Schriver, D.E. "The Manipulation of Air-Sensitive Compounds", (McGraw-Hill, New York, NY 1969).

26. Smith, W.H.; Bard, A.J. *J. Am. Chem. Soc.*, **1975**, 97, 5203-5210.

27. Adams, R.N. "Electrochemistry at Solid Electrodes", (Marcel Dekker, NY, 1969) and references therein.

28. (a) Genies, E.M.; Hany, P.; Lapkowski, M.; Santier, Ch.; Olmedo, L. *Synth. Met.*, **1988**, 25, 29-37.
(b) Olmedo, L.; Chanteloube, I.; Germain, A.; Petit, M. *Synth. Met.*, **1989**, 30, 159-172.

29. (a) Bard, A.J.; Faulkner, C.R., "Electrochemical Methods", (Wiley, New York, 1980).
(b) Rieger, P.H., "Electrochemistry", (Prentice-Hill, Englewood Cliffs, New Jersey 1987).
(c) Kissenger, P.T.; Heiniman, W.R., Eds. "Laboratory Techniques in electroanalytical Chemistry", (Marcel Dekker, New York, 1984).
(d) Harrar, J.E. "Electroanalytical Chemistry"; Bard, A.J. Ed., (Dekker, NY, 1975) Vol. 8, 1-167.
(e) Bard, A.J.; Santhanam, K.S. "Electroanalytical Chemistry" A.J. Bard, Ed. (Marcel Dekker, NY, 1979) Vol. 4, 215-315.

30. (a) Flanagan, J.B.; Margel, S.; Bard, A.J.; Anson, F.C. *J. Am. Chem. Soc.*, **1979**, 100, 6248-6253.
(b) Tanford, C., "Physical Chemistry of Macromolecules", (Wiley, New York, 1961).

31. (a) Janson, T.R.; Kane, A.R.; sullivan, J.F.; Knox, K.; Kenney, M.E. *J. Am. Chem. Soc.*, **1969**, 91, 5210-5214.
(b) Kane, A.R.; Sullivan, J.F.; Kenney, D.H.; Kenney, M.E. *Inorg. Chem.*, **1970**, 9, 1445-1448.
(c) Hush, N.S.; Woolsey, I.S. *Molecular Phys.*, **1971**, 21, 465-474.
(d) Mooney, J.R.; Choy, C.K.; Knox, K.; Kenney, M.E. *J. Am. Chem. Soc.*, **1975**, 97, 3033-3038.
(e) Ciliberto, E.; Doris, K.A.; Pietro, W.J.; Reisner, G.M.; Ellis, D.E.; Fragala, I.; Herbstein, F.M.; Ratner, M.A.; Marks, T.J. *J. Am. Chem. Soc.*, **1984**, 106, 7748-7761.
(f) Simiic-Glavaski, B.; Tanaka, A.A.; Kenney, M.E.; Yeager, F. *J. Electroanal. Chem.*, **1987**, 229, 285-296.

(g) Mezza, T.M.; Armstrong, N.R.; Ritter, G.W.; Iafalice, J.P.; Kenney, M.E. *J. Electroanal. Chem.*, **1982**, *137*, 227-237.
(h) DeWulf, D.W.; Leland, J.K.; Wheeler, B.L.; Bard, A.J.; Batzel, D.A.; Dinninny, D.R.; Kenney, M.E. *Inorg. Chem.*, **1987**, *26*, 266.
(i) Doris, K.A.; Ciliberto, E.; Fragala, I.; Ratner, M.A.; Marks, T.J. *Isreal J. Chem.*, **1986**, *27*, 337-346.

32. (a) Feldberg, S.W. "Electroanalytical Chemistry"; Bard, A.J. ed., (Marcel Dekker, New York, 1964) Vol. 3, 271.
(b) Prater, K. B. "Computers in Chemistry and Instrumentation"; Mattson J.S.; Mark, H.B.; MacDonald, H.C. Eds., (Marcel Dekker, New York, 1972) Vol. 2.
(c) Malloy, J.T. "Laboratory Techniques in Electroanalytical Chemistry", Kissinger, P.T.; Heineman, W.R., Eds., (Marcel Dekker, New York, 1984).
(d) Britz, D. "Digital Simulations in Electrochemistry, lecture notes in chemistry", (Springer-Veilaz, Heidleberg, 1981).

33. (a) Bredas, J.L.; Street, G.B. *Acc. Chem. Res.*, **1985**, *18*, 309-315.
(b) Bredas, J.L.; Themans, B.; Andre, J.M.; Chance, R.R.; Silbey R. *Synth. Met.*, **1984**, *9*, 265-276.
(c) Su, W.P.; Schrieffer, J.R.; Heeger, A.J. *Phys. Rev. Letts.*, **1979**, *42*, 1698-1701.
(d) Sato, M.; Tanaka, S.; Kaeriyama, K. *J. Chem. Soc., Chem. Commun.*, **1985**, 713-715; *Synth. Mat.*, **1986**, *14*, 279-288.
(e) Bertho, D.; Jouanin, C. *Synth. Met.*, **1988**, *24*, 179-182.
(f) Patil, A.D.; Heeger, A.J.; Wudl, F. *chem. Rev.*, **1988**, *88*, 183-200.
(g) Novak, M.; Rughooputh, S.O.O.V.; Hotta, S.; Heeger, A.J. *Macromolecules*, **1987**, *20*, 965-968.
(h) Nowak, M.J.; Spiegel, D.; Hotta, S.; Heeger, A.J.; Pincus, P.A. *Macromolecules*, **1989**, *22*, 2917-2926.
(i) Colaneiri, N.; Newak, M.J.; Spiegel, D.; Hotta, S.; Heeger, A.J. *J. Phys. Rev. B*, **1987**, *36*, 7966-7968.
(j) Scott, J.C.; Bredas, J.L.; Yakuski, K.; Pfluger, P.; Street, G.B. *Synth. Met.*, **1984**, *9*, 165-172.

34. (a) Murray, R.W. "Electroanalytical Chemistry", Bard, A.J. Ed. (Dekker, New York, 1984) Vol. 13 and references therein.
(b) Morrison, Jr., W.H.; Krogsrud, S.; Hendrickson, D.N. *Inorg. Chem.*, **1973**, *12*, 1998-2004.
(c) Brown, G.M.; Meyer, T.J.; Cowan, D.O.; LeVanda, C.; Kaufman, E.; Roling, P.V.; Rausch, M.D. *Inorg. Chem.*, **1975**, *14*, 506-511.
(d) LeVanda, C.; Bechgard, K.; Cowan, D.O.; Rausch, M.D. *J. Am. Chem. Soc.*, **1977**, *99*, 2964-2967.
(e) Debois, M.H.; Astruc, D.; Guillin, J.; Maroit, J.P.; Varret, F. *J. Am. Chem. Soc.*, **1985**, *107*, 5280-5282 and references therein.
(f) Van Order, Jr., N.; Gergei, W.E.; Bitterwolf, T.E.; Rheingold, A.L. *J. Am. Chem. Soc*, **1987**, *109*, 5680-5690 and references therein.

35. Yap, W.T.; Durst, R.A. *J. Electroanal. Chem.*, **1981**, *30*, 3-8.

36. For preparing the precursors of this polymer, see: Hanack, M.; Metz, J.; Pawlowski, G. *Chem. Ber.*, **1982**, *115*, 2836-2853.

37. Marks T.J., private communication.

38. Ammar, F.; Saveant, J.M. *J. Electroanal. Chem.*, **1973**, 47, 215-221.

39. Nicholson, R.S.; Chain, I. *Anal. Chem.*, **1961**, 36, 706-723.

40. Karp, S.; Meites, L. *J. Electroanal. Chem.*, **1968**, 17, 253-265.

41. Levich, V.G. "Physicochemical Hydrodynamics", (Prentice-Hill, Englewood Cliffs, NJ 1962).

42. Gale, D.C.; Gaudiello, J.G. *J. Am. Chem. Soc.*, submitted for publication.

43. Parry, E.P.; Osteryoung, R.A. *Anal. Chem.*, **1965**, 37, 1634-1637.

44. (a) Su, W.P.; Schrieffer, J.R.; Heeger, A.J. *Phys. Rev. Lett.*, **1979**, 42, 1698-1701.
(b) Rice, M.J. *Phys. Lett.*, **1979**, A-71, 152.
(c) Schrieffer, J.R. *Mol. Cryst. Liq. Cryst.*, **1981**, 77, 201-207.

45. Gale, D.C., Master Dissertation, Michigan State University (1989).

46. (a) Thackeray, J.W.; White, H.S.; Wrighton, M.S. *J. Phys. Chem.*, **1985**, 89, 5133-5140.
(b) Mallouk, T.E.; Cammarata, V.; Crayston, J.A.; Wrighton, M.S. *J. Phys. Chem.*, **1986**, 90, 2150-2156.
(c) Tackeray, J.W.; Wrighton, M.S. *J. Phys. Chem.*, **1986**, 90, 6674-6679.
(d) Wrighton, M.S. Comments *Inorg. Chem.*, **1985**, 4, 269-294.
(e) White, N.S.; Kittlesen, G.P.; Wrighton, M.S. *J. Am. Chem. Soc.*, **1984**, 106, 5375-5377.
(f) Kittlesen, H.; White, S.; Wrighton, M.S. *J. Am. Chem. Soc.*, **1984**, 106, 7389-7396.
(g) Paul, E.W.; Ricco, A.J.; Wrighton, M.S. *J. Phys. Chem.*, **1985**, II89, 1441-1447.
(h) Kittlesen, G.P.; White, H.S.; Wrighton, M.S. *J. Am. Chem. Soc.*, **1985**, 107, 7373-7377.
(i) Ofer, D.; Wrighton, M.S. *J. Am. Chem. Soc.*, **1988**, 10, 6667-6668.
(j) Crooks, R.M.; Chyan, O.M.R.; Wrighton, M.S. *Chem. Maker*, **1989**, 1, 2-4.

47. Tamao, K.; Kodama, S.; Nakajima, I.; Minata, A.; Suzuki, K.; Kumada, M. *Tetrahedron*, **1982**, 38, 3347-3354.

48. For preparing the precursors of this monomer see:
(a) Janda, M.; Srogl, J.; Shbor, I.; Nemec, M.; Vopatrna, P. *Synthesis*, **1972**, 10, 545-547.
(b) Lawesson, S.A. *Arkiv Kemi*, **1957**, 1, 325-336.
(c) Aiello, E.; Dattolo, G.; Cirrincione, G.; Almerico, A.M.; Asdia, D. *J. Heterocyclic Chem.*, **1982**, 19, 977-979.

49. Tourillon, G. "Handbook of Conducting Polymers", Skotheim, T.A. Ed., (Dekker, NY, 1986) Vol. 1 and references therein.

50 Tourillon, G.; Garnier, F. *J. Electroanal. Chem.*, **1984**, *161*, 51-58.

51. Dian, G.; Barley, G.; Decroix, B. *Synth. Met.*, **1986**, *13*, 281-289.

52. (a) Daum, P.; Murray, R.W. *J. Phys. Chem.*, **1981**, *85*, 389-396.
(b) Perce, P.J.; Bard, A.J. *J. Electroanal. Chem.*, **1980**, *114*, 89-115.
(c) Deronzier, A.; Latour, J.M. *J. Electroanal. Chem.*,**1987**, *224*, 295-301.
(d) Abruna, H.D.; Meyer, T.J.; Murray, R.W. *Inorg. Chem.*, **1979**, *11*, 3233-3240.

53. Feldberg, S.W. *J. Am. Chem. Soc.*, **1984**, *106*, 4671-4674.

54. (a) Mezza, T.M.; Armstrong, N.R.; Ritter, G.W.; Iafalice, J.P.; Kenney, M.E. *J. Electroanal. Chem.*, **1982**, *37*, 227-237.
(b) Wheeler, B.L.; Nagasubramanian, G.; Bard, A.J.; Schechtman, L.A.; Dininny, D.R.; Kenney, M.E. *J. Am. Chem. Soc.*, **1984**, *106*, 7404-7410.
(c) Dewulf, D.W.; Leland, J.K.; Wheeler, B.L.; Bard, A.J.; Batzel, D.A.; Dininny, D.R.; Kenney, M.E. *Inorg. Chem.*, **1987**, *261*, 260-270.
(d) Simic-Glavaoki, B.; Tanaka, A.A.; Kenney, M.E.; Yeager, E. *J. Electroanal. Chem.*, **1987**, *229*, 285-296.